



**CRITICAL FLARE RATES FOR W-BEAM GUARDRAIL –  
DETERMINING MAXIMUM CAPACITY USING  
COMPUTER SIMULATION**

**NCHRP 17-20(3)**

Submitted by

Beau D. Kuipers, B.S.M.E., E.I.T.  
Graduate Research Assistant

Ronald K. Faller, Ph.D., P.E.  
Research Assistant Professor

John D. Reid, Ph.D.  
Professor

**MIDWEST ROADSIDE SAFETY FACILITY**

University of Nebraska-Lincoln  
527 Nebraska Hall  
Lincoln, Nebraska 68588-0529  
(402) 472-6864

MwRSF Research Report No. TRP-03-157-04

January 24, 2005

## TECHNICAL REPORT DOCUMENTATION PAGE

1. Report No. <b>TRP-03-157-04</b>	2.	3. Recipient's Accession No.	
4. Title and Subtitle <b>Critical Flare Rates for W-beam Guardrail – Determining Maximum Capacity using Computer Simulation</b>		5. Report Date <b>January 24, 2005</b>	
		6.	
7. Author(s) <b>Kuipers, B.D., Faller, R.K. and Reid, J.D.</b>		8. Performing Organization Report No. <b>TRP-03-157-04</b>	
9. Performing Organization Name and Address <b>Midwest Roadside Safety Facility (MwRSF) University of Nebraska-Lincoln 527 Nebraska Hall Lincoln, Nebraska 68588-0529</b>		10. Project/Task/Work Unit No.	
		11. Contract © or Grant (G) No.	
12. Sponsoring Organization Name and Address <b>National Academy of Sciences National Cooperative Highway Research Program 500 5th Street NW Washington, DC 20001</b>		13. Type of Report and Period Covered <b>Final Report, 2003-2005</b>	
		14. Sponsoring Agency Code <b>NCHRP 17-20(3)</b>	
15. Supplementary Notes			
16. Abstract (Limit: 200 words)  <p>Strong-post, W-beam guardrail systems are allowed to be installed with a flare rate up to 15:1. By increasing the flare rate, there is a possibility that overall costs can be reduced, while safety is improved. Thus, the Midwest Roadside Safety Facility has begun a multi-phase project to study flare rates. The portion of the overall project described in this report determines the maximum capacity (i.e., critical flare rate) for both the G4(1S) system and Midwest Guardrail System (MGS).</p> <p>A literature review on flare rates and relevant W-beam crash testing is provided, followed by detailed analysis, using BARRIER VII computer simulation, to determine critical flare rates. During the simulation process, it was deemed necessary to evaluate two possible scenarios for the MGS system: (1) using baseline post properties and (2) using early release post properties resulting from an increased impact severity. The early release post properties were deemed to be the worst case scenario.</p> <p>A critical flare rate of 13:1 was determined for both the MGS and modified G4(1S) system. Barrier deflection and wheel-to-post overlap (i.e., wheel snag) were the primary criteria used to determine the critical flare rates. For both systems, the critical impact point was determined to be 9.375 in. upstream of post no. 12.</p>			
17. Document Analysis/Descriptors <b>Highway Safety, Flare Rates, W-beam, Computer Simulation</b>		18. Availability Statement <b>No restrictions.</b>	
19. Security Class (this report) <b>Unclassified</b>	20. Security Class (this page) <b>Unclassified</b>	21. No. of Pages <b>165</b>	22. Price

## **DISCLAIMER STATEMENT**

The contents of this report reflect the views of the authors who are responsible for the facts and the accuracy of the data presented herein. The contents do not necessarily reflect the official views or policies of neither the Federal Highway Administration nor State Highway Departments participating in the Midwest States Regional Pooled Fund. This report does not constitute a standard, specification, or regulation.

## **ACKNOWLEDGMENTS**

The authors wish to acknowledge the National Cooperative Research Project for sponsoring this project. In addition, the authors wish to acknowledge the Midwest State's Regional Pooled Fund Program for sponsoring other portions of the overall flare rate project.

Acknowledgment is also given to the following individuals who made a contribution to the completion of this research project.

### **Midwest Roadside Safety Facility**

D.L. Sicking, Ph.D., P.E., MwRSF Director and Professor

J.R. Rohde, Ph.D., P.E., Associate Professor

J.C. Holloway, M.S.C.E., E.I.T., Research Associate Engineer

K.A. Polivka, M.S.M.E., E.I.T., Research Associate Engineer

R.W. Bielenberg, M.S.M.E., E.I.T., Research Associate Engineer

Undergraduate and Graduate Assistants

## EXECUTIVE SUMMARY

NCHRP Report 350 defines crash testing standards that hardware must satisfy in order to be approved for installation on the NHS. In the case of strong-post, W-beam guardrail systems this does not mean, however, that the installation of the guardrail must be identical to the crash testing conditions. For example, such guardrail systems are allowed to be installed with a flare up to a rate of 15:1; as opposed to the tangent installations used for crash testing. This flare rate is justified because of an overall reduction in crash frequency due to the flare. Reducing the number of crashes can offset modest increases in crash severity, such that total accident costs, measured in terms of injuries and fatalities, go down.

The 15:1 flare rate justification was performed many years ago, before sophisticated computer simulation and analysis programs were available, and before extensive crash testing experience had been gained with current testing requirements. Further, this flare rate was based to some degree on the engineering judgment of FHWA engineers.

Thus, with the support of the Midwest States Pooled Fund Program and NCHRP Project 17-20(3), the Midwest Roadside Safety Facility (MwRSF) began a project to update the recommendations for flare rate installations of strong-post, W-beam guardrail systems. The flare rate project has been divided into two phases, with the first phase having two parts:

Phase 1. Determine the capacity of strong post, W-beam guardrail systems.

Part 1 – Determine the critical flare rate using computer simulation. (Sponsored by NCHRP 17-20(3).)

Part 2 – Using Part 1 results as an initial guide, perform crash testing to determine the maximum flare rate that can meet NCHRP 350 requirements. (Sponsored by Midwest States.)

Phase 2. Using the information from Phase 1, determine from a cost-benefit analysis a maximum recommended flare rate for installation. (Currently unfunded.)

This report covers Part 1 of Phase 1 and includes the detailed background of flare rates. Two different strong-post, W-beam guardrail systems are investigated: the modified G4(1S) system and the Midwest Guardrail System (MGS). Justification for investigating these two systems is provided in the report.

After extensive computer analysis using BARRIER VII, it was determined that the critical flare rate appears to be 13:1 for both systems investigated. Note that the critical flare rate is the maximum rate at which the guardrail system is capable of passing NCHRP 350 criteria; it is not the recommended installation flare rate. Determining that rate is the objective of Phase 2.

The next step in the project is Part 2 of Phase 1. During that portion of the project, the researchers at MwRSF, with input from the Midwest States, will determine which of the guardrail systems to crash test.

## TABLE OF CONTENTS

<b>TECHNICAL REPORT DOCUMENTATION PAGE.....</b>	<b>ii</b>
<b>DISCLAIMER STATEMENT .....</b>	<b>iii</b>
<b>ACKNOWLEDGMENTS .....</b>	<b>iii</b>
<b>EXECUTIVE SUMMARY .....</b>	<b>iv</b>
<b>TABLE OF CONTENTS .....</b>	<b>vi</b>
List of Figures.....	ix
List of Tables .....	xi
<b>1. INTRODUCTION.....</b>	<b>1</b>
1.1. Examination of Flare Rates.....	1
1.2. Objective.....	4
1.3. Research Plan.....	5
<b>2. LITERATURE REVIEW .....</b>	<b>7</b>
2.1. Background.....	7
2.2. Previous Standards and Suggestions.....	12
2.3. Current Standards .....	16
<b>3. RELEVANT CRASH TESTING .....</b>	<b>18</b>
3.1. Introduction.....	18
3.2. Standard Strong-Post, W-beam Guardrail Systems.....	19
3.2.1. <i>G4(2W) – Wood Post/Wood Blockout</i> .....	19
3.2.2. <i>G4(1S) – Steel Post/Steel Blockout</i> .....	20
3.2.3. <i>Discussion – G4(2W) versus G4(1S)</i> .....	22
3.2.4. <i>Modified G4(1S) – Steel Post/Routed Wood Blockout</i> .....	23
3.2.5. <i>System Differences – G4(1S) versus Modified G4(1S)</i> .....	24
3.3. Additional Strong-Post W-Beam (G4) Testing .....	25
3.3.1. <i>Wood Post, Wood Blockout, W-Beam Guardrail System - MwRSF</i> .....	25
3.3.2. <i>Michigan Type B - Steel Post/Wood Blockout</i> .....	26
3.4. Conclusion for Standard, Strong-Post, W-Beam Guardrail System.....	28
3.5. Midwest Guardrail System .....	30
3.6. Comparison and Conclusion for Midwest Guardrail System .....	32
<b>4. BARRIER VII BASELINE MODEL DEVELOPMENT .....</b>	<b>33</b>
4.1. Midwest Guardrail System .....	33
4.1.1. <i>Introduction</i> .....	33
4.1.2. <i>Development of the MGS Model</i> .....	33

4.1.3. Calibration of the MGS Model .....	34
4.1.4. Validation of the MGS Model .....	35
4.1.5. Further Analysis of the MGS Model .....	43
4.1.6. Conclusions for the MGS Model .....	54
4.1.7. The MGS Baseline Model .....	55
4.2. The Standard NCHRP 350 Strong-Post, W-Beam BARRIER VII Model .....	55
4.2.1. Introduction .....	55
4.2.2. Development of the Modified G4(1S) Model .....	56
4.2.3. Calibration of the Modified G4(1S) Model .....	57
4.2.4. Validation of the Modified G4(1S) Model .....	57
4.2.5. Further Analysis of the Modified G4(1S) Model .....	62
4.2.6. Conclusions for the Modified G4(1S) Model .....	72
4.2.7. The Standard NCHRP 350 Strong-Post, W-Beam BARRIER VII Baseline Model .....	72
4.3. Additional BARRIER VII Modeling – Anchor Calibration .....	73
4.3.1. Introduction .....	73
4.3.2. Test Description .....	73
4.3.3. MGS Baseline Model .....	74
4.3.4. Calibration of the MGS Model to Test No. 22-14MG-1 .....	74
4.3.5. Validation of the MGS Model to Test No. 22-14MG-1 .....	77
4.3.6. Conclusions for Test No. 22-14MG-1 .....	84
<b>5. CRITICAL IMPACT POINT SIMULATIONS .....</b>	<b>86</b>
5.1. Introduction .....	86
5.2. CIP Analysis .....	87
5.2.1. Parallel Time .....	89
5.2.2. Maximum Dynamic Rail Deflection .....	89
5.2.3. Maximum Rail Tension Forces .....	91
5.2.4. Vehicle Pocketing .....	91
5.2.5. Wheel Snag .....	91
5.3. MGS Baseline Post Property CIP Simulation Results .....	92
5.4. MGS Early Post Release Property CIP Simulation Results .....	96
5.5. Modified G4(1S) CIP Simulation Results .....	97
5.6. CIP Simulation Conclusions .....	101
<b>6. MGS CRITICAL FLARE RATE IDENTIFICAION .....</b>	<b>102</b>
6.1. Introduction .....	102
6.2. BARRIER VII Simulation Scenarios .....	102
6.2.1. Baseline Post Property Simulation Scenario .....	103
6.2.2. Early Release Post Property Simulation Scenario .....	108
6.3. Conclusions .....	112
<b>7. MODIFIED G4(1S) CRITICAL FLARE RATE IDENTIFICAION .....</b>	<b>113</b>
7.1. Introduction .....	113
7.2. Modified G4(1S) CIP Simulation Comparison .....	113
7.2.1. Parallel Time .....	114

7.2.2. <i>Maximum Rail Deflection</i> .....	114
7.2.3. <i>Maximum Rail Tension Forces</i> .....	115
7.2.4. <i>Wheel Snag</i> .....	116
7.2.5. <i>Vehicle Vaulting</i> .....	116
7.2.6. <i>Vehicle Pocketing</i> .....	116
7.2.7. <i>Energy Balance</i> .....	117
7.3. <i>Conclusions</i> .....	118
<b>8. ADDITIONAL SIMULATION USING LS-DYNA.....</b>	<b>119</b>
8.1. <i>Introduction</i> .....	119
8.2. <i>Baseline Model Development</i> .....	120
8.3. <i>Flared Impact Simulation</i> .....	127
8.3.1. <i>Rail Tension Forces</i> .....	129
8.4. <i>Conclusion for LS-DYNA Simulations</i> .....	131
<b>9. SUMMARY AND FUTURE WORK.....</b>	<b>132</b>
9.1. <i>Summary</i> .....	132
9.2. <i>Future Work</i> .....	133
<b>9. REFERENCES.....</b>	<b>135</b>
<b>APPENDIX A – MGS Calibration/Validation BARRIER VII Input Deck .....</b>	<b>138</b>
<b>APPENDIX B– G4(1S) Calibration/Validation BARRIER VII Input Deck.....</b>	<b>144</b>
<b>APPENDIX C– 22-14MG-1 Calibration/Validation BARRIER VII Input Deck.....</b>	<b>150</b>

## List of Figures

	Page
Figure 1. Comparison of Overall Flared Guardrail Lengths (distances in meters) .....	2
Figure 2. Relationship between Lateral Displacement and Lane Width [3] .....	9
Figure 3. Relationship between Lateral Displacement and Offset Distance [4].....	11
Figure 4. Relationship between Lateral Displacement and Vehicle Speed [4].....	11
Figure 5. Relationship of Vehicle Speed and Distance from Object at which Displacement Began [4] .....	12
Figure 6. Parameters and Results for TTI Test 471470-26 [14] .....	20
Figure 7. Parameters and Results for TTI Test 471470-27 [14] .....	22
Figure 8. Parameters and Results for TTI Test 405421-1 [15] .....	24
Figure 9. Parameters and Results for MwRSF Test MIW-2 [17].....	28
Figure 10. Parameters and Results for MwRSF Test NPG-4 [18] .....	31
Figure 11. Sequential Figures from BARRIER VII Simulation of NPG-4.....	36
Figure 11 (continued). Sequential Figures from BARRIER VII Simulation of NPG-4 .....	37
Figure 11 (continued). Sequential Figures from BARRIER VII Simulation of NPG-4 .....	38
Figure 12. Anchor Calibration - Difference in Coordinates (X and Y) between the Simulation and Film Analysis .....	40
Figure 13. Comparison of Test and Simulation Results: (a) Longitudinal Direction and (b) Lateral Direction.....	41
Figure 14. Comparison of Test and Simulation Results of Yaw Data.....	42
Figure 15. Rail Tension Forces and Corresponding Rail Deflections .....	44
Figure 15 (continued). Rail Tension Forces and Corresponding Rail Deflections .....	45
Figure 16. Tension Forces at Selected Rail Elements versus Time .....	46
Figure 17. Maximum Tension Force in the Rail During the Simulation .....	47
Figure 18. Maximum Potential for Vehicle Pocketing .....	52
Figure 19. Sequential Figures from BARRIER VII Simulation of TTI test no. 405421-1 ...	59
Figure 19 (continued). Sequential Figures from BARRIER VII Simulation of TTI test no. 405421-1 .....	60
Figure 20. Rail Tension Forces and Corresponding Rail Deflections .....	63
Figure 20 (continued). Rail Tension Forces and Corresponding Rail Deflections .....	64
Figure 21. Tension Forces at Selected Rail Elements versus Time .....	65
Figure 22. Maximum Tension Force in the Rail during the Simulation.....	66

<b>Figure 23. Vehicle Damage After Test No. 405421-1 [14]</b> .....	<b>69</b>
<b>Figure 24. Maximum Potential for Vehicle Pocketing</b> .....	<b>70</b>
<b>Figure 25. Anchor Calibration - Difference in Coordinates (X and Y) between the Simulation and Film Analysis for the farthest visual Upstream Target</b> .....	<b>74</b>
<b>Figure 26. Post Definition Option Comparison</b> .....	<b>76</b>
<b>Figure 27. Sequential Figures from BARRIER VII Simulation of Test No. 22-14MG-1</b> .....	<b>78</b>
<b>Figure 27 (continued). Sequential Figures from BARRIER VII Simulation of Test No. 22-14MG-1</b> .....	<b>79</b>
<b>Figure 28. Anchor Calibration - Difference in Coordinates (X and Y) between the Simulation and Film Analysis Results</b> .....	<b>82</b>
<b>Figure 29. Maximum Rail Tension Force Observed During the Simulation</b> .....	<b>84</b>
<b>Figure 30. Impact Nodes for MGS CIP Analysis</b> .....	<b>88</b>
<b>Figure 31. Impact Nodes for modified G4(1S) CIP Analysis</b> .....	<b>88</b>
<b>Figure 32. Critical Position of Guardrail in Front of the Redirecting Vehicle</b> .....	<b>90</b>
<b>Figure 33. Simulation Parallel Time versus Impact Angle</b> .....	<b>104</b>
<b>Figure 34. Maximum Rail Tension Forces versus Time</b> .....	<b>105</b>
<b>Figure 35. Maximum Rail Tension Forces versus Time</b> .....	<b>110</b>
<b>Figure 36. Maximum Rail Tension Forces versus Time</b> .....	<b>115</b>
<b>Figure 37. Sequential Figures from LS-DYNA Simulation of NPG-4</b> .....	<b>121</b>
<b>Figure 37 (continued). Sequential Figures from LS-DYNA Simulation of NPG-4</b> .....	<b>122</b>
<b>Figure 37 (continued). Sequential Figures from LS-DYNA Simulation of NPG-4</b> .....	<b>123</b>
<b>Figure 37 (continued). Sequential Figures from LS-DYNA Simulation of NPG-4</b> .....	<b>124</b>
<b>Figure 38. Additional Graphical Comparison - Downstream Behind Rail</b> .....	<b>125</b>
<b>Figure 39. Additional Graphical Comparison - Upstream Behind Rail</b> .....	<b>126</b>
<b>Figure 40. Wheel Snag Observed during NPG-4 LS-DYNA Simulation</b> .....	<b>127</b>
<b>Figure 41. Sequential Figures from 13:1 Flared Impact Simulation using LS-DYNA</b> .....	<b>128</b>
<b>Figure 42. Observable Wheel Snag during 13:1 Flared Simulation using LS-DYNA</b> .....	<b>129</b>
<b>Figure 43. Rail Tension Forces Upstream of Impact</b> .....	<b>130</b>
<b>Figure 44. Rail Tension Forces Downstream of Impact</b> .....	<b>130</b>
<b>Figure 45. Midwest Guardrail System BARRIER VII Model Details</b> .....	<b>142</b>
<b>Figure 45 (continued). Midwest Guardrail System BARRIER VII Model Details</b> .....	<b>143</b>
<b>Figure 46. Modified G4(1S) Guardrail System BARRIER VII Model Details</b> .....	<b>148</b>
<b>Figure 46 (continued). Modified G4(1S) Guardrail System BARRIER VII Model Details</b>	<b>149</b>

**List of Tables**

	<b>Page</b>
<b>Table 1. AASHTO RDG Suggested Flare Rates [1].....</b>	<b>1</b>
<b>Table 2. Example Guardrail Installation Lengths Comparison.....</b>	<b>3</b>
<b>Table 3. Increased Impact Severity Calculations.....</b>	<b>4</b>
<b>Table 4. Suggested Barrier Layout [6].....</b>	<b>14</b>
<b>Table 5. Optimum Barrier Flare based upon Average Daily Traffic and Design Speed [8]15</b>	
<b>Table 6. BARRIER VII Simulation Parameters.....</b>	<b>34</b>
<b>Table 7. Working Width, Vehicle Behavior, and Barrier Displacements for NPG-4 .....</b>	<b>39</b>
<b>Table 8. Wheel Snag Analysis Results.....</b>	<b>49</b>
<b>Table 9. Energy Balance for NPG-4 Simulation (0.536 sec) .....</b>	<b>54</b>
<b>Table 10. BARRIER VII Simulation Parameters.....</b>	<b>57</b>
<b>Table 11. Vehicle Behavior and Barrier Displacements Comparison for Test No. 405421-161</b>	
<b>Table 12. Wheel Snag Analysis Results .....</b>	<b>67</b>
<b>Table 13. Energy Balance for Test No. 405421-1 Simulation (0.522 sec).....</b>	<b>71</b>
<b>Table 14. BARRIER VII Simulation Parameters.....</b>	<b>75</b>
<b>Table 15. Vehicle Behavior and Barrier Displacements for 22-14MG-1 .....</b>	<b>80</b>
<b>Table 16. Wheel Snag Analysis Results .....</b>	<b>83</b>
<b>Table 17. Flare Rate Table.....</b>	<b>87</b>
<b>Table 18. Sample CIP Evaluation Parameter Table.....</b>	<b>89</b>
<b>Table 19. MGS Baseline Post Property – 6:1 Flare Rate CIP Results .....</b>	<b>92</b>
<b>Table 20. MGS Baseline Post Property – 7:1 Flare Rate CIP Results .....</b>	<b>93</b>
<b>Table 21. MGS Baseline Post Property – 8:1 Flare Rate CIP Results .....</b>	<b>93</b>
<b>Table 22. MGS Baseline Post Property – 9:1 Flare Rate CIP Results .....</b>	<b>93</b>
<b>Table 23. MGS Baseline Post Property – 10:1 Flare Rate CIP Results .....</b>	<b>94</b>
<b>Table 24. MGS Baseline Post Property – 11:1 Flare Rate CIP Results .....</b>	<b>94</b>
<b>Table 25. MGS Baseline Post Property – 12:1 Flare Rate CIP Results .....</b>	<b>94</b>
<b>Table 26. MGS Baseline Post Property – 13:1 Flare Rate CIP Results .....</b>	<b>95</b>
<b>Table 27. MGS Baseline Post Property – 14:1 Flare Rate CIP Results .....</b>	<b>95</b>
<b>Table 28. MGS Baseline Post Property – 15:1 Flare Rate CIP Results .....</b>	<b>95</b>
<b>Table 29. MGS Early Post Release Property – 12:1 Flare Rate CIP Results.....</b>	<b>96</b>
<b>Table 30. MGS Early Post Release Property – 13:1 Flare Rate CIP Results.....</b>	<b>96</b>

<b>Table 31. MGS Early Post Release Property – 14:1 Flare Rate CIP Results.....</b>	<b>97</b>
<b>Table 32. MGS Early Post Release Property – 15:1 Flare Rate CIP Results.....</b>	<b>97</b>
<b>Table 33. Modified G4(1S) – 8:1 Flare Rate CIP Results .....</b>	<b>98</b>
<b>Table 34. Modified G4(1S) – 9:1 Flare Rate CIP Results .....</b>	<b>98</b>
<b>Table 35. Modified G4(1S) – 10:1 Flare Rate CIP Results .....</b>	<b>99</b>
<b>Table 36. Modified G4(1S) – 11:1 Flare Rate CIP Results .....</b>	<b>99</b>
<b>Table 37. Modified G4(1S) – 12:1 Flare Rate CIP Results .....</b>	<b>99</b>
<b>Table 38. Modified G4(1S) – 13:1 Flare Rate CIP Results .....</b>	<b>100</b>
<b>Table 39. Modified G4(1S) – 14:1 Flare Rate CIP Results .....</b>	<b>100</b>
<b>Table 40. Modified G4(1S) – 15:1 Flare Rate CIP Results .....</b>	<b>100</b>
<b>Table 41. Simulation Evaluation Criteria for MGS Baseline .....</b>	<b>103</b>
<b>Table 42. Energy Balances for MGS Baseline Post Property Simulations.....</b>	<b>107</b>
<b>Table 43. Simulation Evaluation Criteria for MGS Early Release Posts .....</b>	<b>109</b>
<b>Table 44. Energy Balances for MGS Early Release Post Property Simulations.....</b>	<b>112</b>
<b>Table 45. Simulation Evaluation Criteria for Modified G4(1S).....</b>	<b>113</b>
<b>Table 46. Energy Balances for Modified G4(1S) Property Simulations.....</b>	<b>117</b>
<b>Table 47. Modeling Changes for NPG-4 Simulation .....</b>	<b>120</b>

## 1. INTRODUCTION

The 2002 American Association of State Highway and Transportation Officials (AASHTO) Roadside Design Guide (RDG) recommends maximum flare rates as a function of highway design speed and barrier type [1]. Currently, the maximum flare rate suggested for a semi-rigid barrier system is 15:1 for a 110 km/h highway design speed and slightly sharper flare rates for lower design speeds, as shown in Table 1.

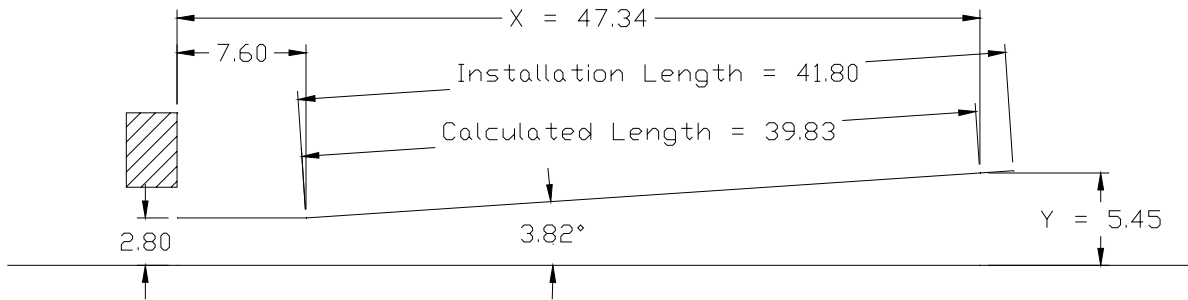
**Table 1. AASHTO RDG Suggested Flare Rates [1]**

Design Speed		Flare Rate for Barrier Beyond Shy Line
(km/h)	(mph)	
110	70	15:1
100	60	14:1
90	55	12:1
80	50	11:1
70	45	10:1
60	40	8:1
50	30	7:1

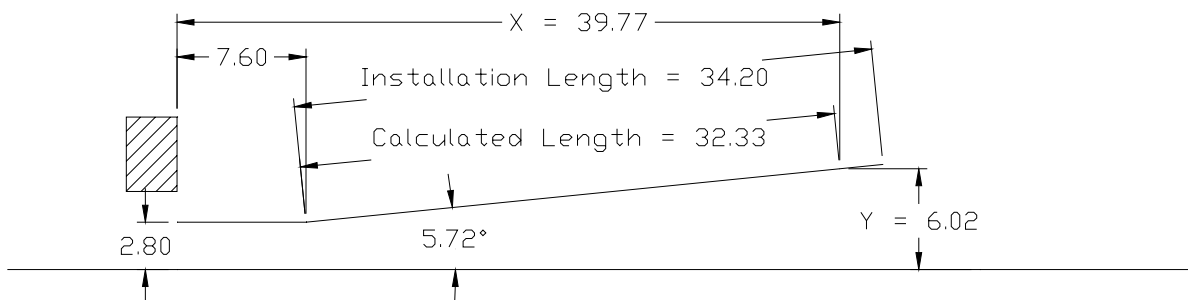
These flare rates are recommended based on the assumption that increasing impact angles greatly increases the severity of a guardrail accident. However, increasing the flare rate from 15:1 to 10:1 would increase the effective impact angle by only 2 degrees while it would reduce the length of a flared section by as much as one third, depending upon the installation.

### 1.1. Examination of Flare Rates

Increasing maximum allowable flare rates would significantly reduce guardrail lengths whenever roadside or median slopes are relatively flat. This reduction in guardrail lengths would also reduce construction costs and reduce the number of guardrail accidents. Hence, a revised flare rate design has the potential to decrease construction, maintenance, and overall accident costs. An example of the reduction in guardrail length is illustrated in Figure 1.



15:1 Flare Rate



10:1 Flare Rate

**Figure 1. Comparison of Overall Flared Guardrail Lengths (distances in meters)**

The X and Y lengths in Figure 1 were obtained using the following equations provided in the RDG:

$$X = \frac{L_A + (b/a)(L_1) - L_2}{(b/a) + (L_A/L_R)} \quad \text{and} \quad Y = L_A - \frac{L_A}{L_R}(X)$$

where: X is the minimum required length of need

Y is the lateral offset

(a:b) is the desired flare rate

The calculated length was then obtained directly from the X and Y values. Furthermore, it is only possible to construct guardrails in 3.8 m increments, leading to the installation length. Applying similar techniques, results were determined for the flared section of guardrail installations for other flare rates, as listed in Table 2.

**Table 2. Example Guardrail Installation Lengths Comparison**

Guardrail Orientation	Flare Angle	X	Y	Calculated Guardrail Length	Guardrail Installation Length
	(deg)	(m)	(m)	(m)	(m)
Baseline	0.00	82.67	0	82.67	83.6
15:1	3.81	47.34	5.45	39.83	41.8
14:1	4.09	46.05	5.55	38.55	41.8
13:1	4.40	44.66	5.65	37.17	38.0
12:1	4.76	43.16	5.76	35.68	38.0
11:1	5.19	41.53	5.88	34.07	34.2
10:1	5.71	39.77	6.02	32.33	34.2
9:1	6.34	37.85	6.16	30.44	34.2
8:1	7.13	35.75	6.32	28.37	30.4
7:1	8.13	33.44	6.49	26.11	26.6
6:1	9.46	30.90	6.68	23.62	26.6
5:1	11.31	28.07	6.89	20.89	22.8

Examination of the guardrail installation length indicates an obvious advantage to flaring the guardrail away from the road as compared to the baseline tangent installation. This reduction is one half of the entire length of the baseline installation. Further increasing the current maximum flare rate would increase this reduction in guardrail installation length even more.

The construction length information is also important when considering an increase in the maximum flare rate. It may be possible to increase the flare rate to 10:1; however virtually no benefit would be gained over specifying the 11:1 flare rate.

Impact severities will increase with increases in the impact angle, as listed in Table 3.

**Table 3. Increased Impact Severity Calculations**

Guardrail Orientation	Flare Angle	Test 3-10			Test 3-11		
		Impact Angle	Impact Severity	% Increase in IS	Impact Angle	Impact Severity	% Increase in IS
	(deg)	(deg)	(kJ)		(deg)	(kJ)	
Baseline	0.00	20	37.0	--	25	137.8	--
15:1 *	3.81	23.81	51.6	39.4	28.81	179.2	30.1
14:1	4.09	24.09	52.7	42.4	29.09	182.3	32.3
13:1	4.40	24.40	54.0	45.9	29.40	185.9	34.9
12:1	4.76	24.76	55.5	50.0	29.76	190.2	38.0
11:1	5.19	25.19	57.3	54.9	30.19	195.2	41.6
10:1	5.71	25.71	59.5	60.9	30.71	201.2	46.0
9:1	6.34	26.34	62.3	68.3	31.34	208.7	51.5
8:1	7.13	27.13	65.8	77.7	32.13	218.2	58.3
7:1	8.13	28.13	70.3	90.0	33.13	230.5	67.2
6:1	9.46	29.46	76.5	106.8	34.46	247.1	79.3
5:1	11.31	31.31	85.4	130.9	36.31	270.6	96.3

\*RDG suggested maximum flare rate for semi-rigid barrier systems on 110 km/h roadways

There is a significant increase in the impact severity from the baseline impact to a flared impact. However, the impact severities do not increase greatly with further moderate increases in the flare rate. Thus, the increase in flare rate would not greatly increase accident costs.

As a result, the overall safety performance of flared guardrails would probably be enhanced by sharper flare rates that could be expected to significantly reduce impact frequency without a similar increase in accident severity. Full-scale vehicle crash testing and computer simulation over a wide range of impact angles would help to determine the most appropriate guardrail flare rates for high-speed facilities.

## 1.2. Objective

The goal of the flare rate study is to evaluate the effect of increased flare rates on impact performance for strong-post, W-beam guardrail systems. The flare rate project has been divided into two phases, with the first phase having two parts:

Phase 1. Determine the capacity of strong post, W-beam guardrail systems.

Part 1 – Determine the critical flare rate using computer simulation. (Sponsored by NCHRP 17-20(3).)

Part 2 – Using Part 1 results as an initial guide, perform crash testing to determine the maximum flare rate that can meet NCHRP 350 requirements. (Sponsored by Midwest States.)

Phase 2. Using the information from Phase 1, determine from a cost-benefit analysis a maximum recommended flare rate for installation. (Currently unfunded.)

This report covers Part 1 of Phase 1 and includes the detailed background of flare rates. Two different strong-post, W-beam guardrail systems are investigated: the modified G4(1S) system and the Midwest Guardrail System (MGS). Justification for investigating these two systems is provided in the report.

### **1.3. Research Plan**

This project begins with a literature search and a review of current standards for flare rates of W-beam guardrail. Recent crash testing data is also reviewed in order to select which W-beam barrier systems to evaluate. Baseline models are developed for both a standard height, strong-post, W-beam guardrail system (modified G4(1S)) and the Midwest Guardrail System (MGS). These baseline models are calibrated and validated according to specific test parameters. Also, criteria are developed to analyze BARRIER VII simulation results, evaluating maximum dynamic barrier penetration, rail tension forces, wheel snag, vehicle pocketing, and vehicle vaulting. Simulation on a variety of flare rates is then completed in order to identify a critical flare rate that represents the point at which the potential for barrier penetration and severe wheel snag begins to increase rapidly. A critical impact point analysis is performed on the

various flare rates in order to suggest the optimal impact point which maximizes barrier penetration and severe wheel snag.

Finally, an initial look at detailed 3-D non-linear, finite element analysis using LS-DYNA is performed. Although this simulation work is not officially part of this NCHRP project, it does provide the reader with a more complete background of efforts related to the flare rate study. LS-DYNA modeling concentrates on the MGS, but the work done on the post in soil component model is applicable to other guardrail systems as well.

## 2. LITERATURE REVIEW

### 2.1. Background

The effect of roadside objects on driver behavior has been under study for the past fifty years. In these studies, objects were placed at or near the side of the traveled way, causing the drivers to shift the position of their vehicle away from the object as they approached closer to it. This response resulted in a measurable lateral displacement of the vehicle within the traveled way. The lateral displacement is defined as the difference between the position of the vehicle in the traveled lane in an area clear of roadside objects in advance of the test object and the position of the vehicle in the traveled lane when the driver was influenced by the test object. This section summarizes those studies that are relevant for the development of W-beam guardrail flare rates.

In 1953, Case et al. conducted a study to determine the effect that roadside structures have on the lateral positioning of motor vehicles in the traveled lanes [2]. The test object was a U-shaped screen which was covered with flat black paint and weathered for a more realistic appearance. The open side was oriented in the direction of travel, thus giving the appearance of a solid structure. The test matrix included nine scenarios, using three object widths (3½, 5, and 8 ft) at three different distances from the roadside edge (½, 3, and 7 ft) and acting on freely-moving vehicles. A freely-moving vehicle was defined as a vehicle that is not influenced by other vehicles on the roadway.

Placing the 3½ ft wide structure 7 ft perpendicularly away from the edge of the traveled way resulted in a 5 in. mean lateral displacement between the vehicle and the object. Placing the 8 ft wide structure one-half foot away from the roadside edge resulted in a 15 in. mean lateral displacement between the vehicle and the object. However, Case et al. suggested that driver

reaction, and therefore lateral displacement, may not be as pronounced when encountering a familiar structure to the roadway, like a guardrail.

In 1955, Taragin discussed driver behavior as affected by objects on highway shoulders [3]. The test matrix involved placing a passenger car, a highway maintenance truck, or a barricade either at the pavement edge, at 3 ft from the pavement edge, or at 6 ft from the pavement edge, resulting in a total of nine different scenarios. Testing was conducted on both four-lane and two-lane highways during light-to-moderate traffic volumes, which ranged from 100 to 2,000 vehicles per hour.

Vehicle speeds were reduced by 3 mph on only two-lane highways with a total lane width of 20 ft or less. Vehicle shift was only observed in the lane adjacent to the object, thus resulting in mean lateral displacements of 3.3 ft and 1.8 ft, as measured between the vehicle and the object on two-lane highways with a total lane width of 20 ft or less and on wider surfaces, respectively. These results are shown in Figure 2. If the vehicle or barrier was placed farther than 6 ft from the roadway edge, no effect was observed. Furthermore, tests involving the barricade typically resulted in half of the displacement observed during tests with either vehicle placed along the side of the traveled way.

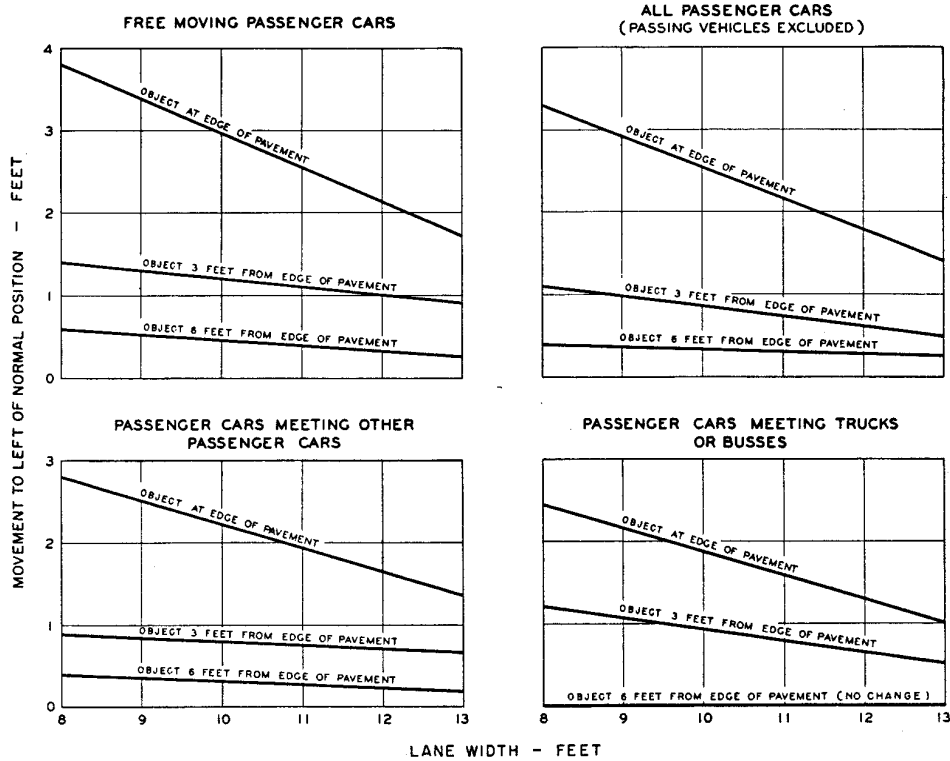


**Figure 2. Relationship between Lateral Displacement and Lane Width [3]**

In 1963, Michaels and Cozan performed a study on the perceptual and field factors which caused the lateral displacement of vehicles on their test track [4]. They proposed two models of visual perception that would cause the driver to shift their position on the roadway relative to objects located some distance perpendicular to the roadway edge. The first model was based on a trigonometric relationship which hypothesized that there exists some distance from the object at which the driver will react independent of the object location relative to their position from the roadside edge and traveled speed. The second model was based on the fact that drivers estimate the rate of change of the angle of the object in their path, or the appearance of the object moving out of their current path. Based on the second model, three hypotheses were stated: (1) the magnitude of lateral displacement will be directly related to vehicle speed; (2) the lateral displacement will begin at a distance dependent on vehicle speed; and (3) the derivative of the visual angle at the point where displacement begins will be independent of speed and object

location so long as displacement occurs. Michaels and Cozan also considered the contours of the object, based on the study by Case et al. They concluded that the dominant feature of the object would influence the magnitude of displacement.

Testing was conducted on a 25 ft wide section of concrete with an adjacent 25 ft wide asphalt shoulder located on a one mile long section of 100 ft wide jet aircraft runway. The displacing objects were two equilateral triangles 6 ft on a side. The triangles were mounted on a boom that allowed the movement of the triangle closer or farther away from the traveled way. This configuration also allowed for the triangle to be rotated about its mounting point so that the base or apex of the triangle could be oriented toward the traveled lane. The test matrix consisted of placing objects at 2,000 and 4,000 ft from the start of the course at 7.0, 7.8, 8.9, or 9.6 ft from the roadway edge. Measurements were taken for a vehicle traveling at four different test speeds of 15, 30, 45, and 60 mph. The subjects were five male, licensed drivers ranging from 25 to 40 years of age who were told the study was to determine how well they could maintain the vehicle at the constant assigned speed. The results presented below represent the average of the five drivers.

The first result was the linear relationship between the object placement and lateral displacement of the vehicle. As the object was placed farther perpendicularly away from the roadside edge, the maximum displacement of the vehicle decreased, as shown in Figure 3.

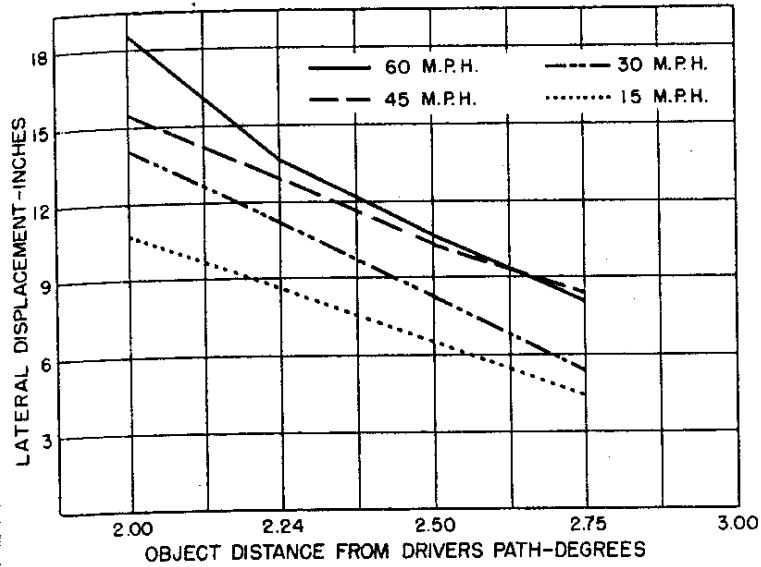


**Figure 3. Relationship between Lateral Displacement and Offset Distance [4]**

The second relationship showed that the lateral vehicle displacement away from the object increased as the speed of the vehicle increased, as shown in Figure 4.

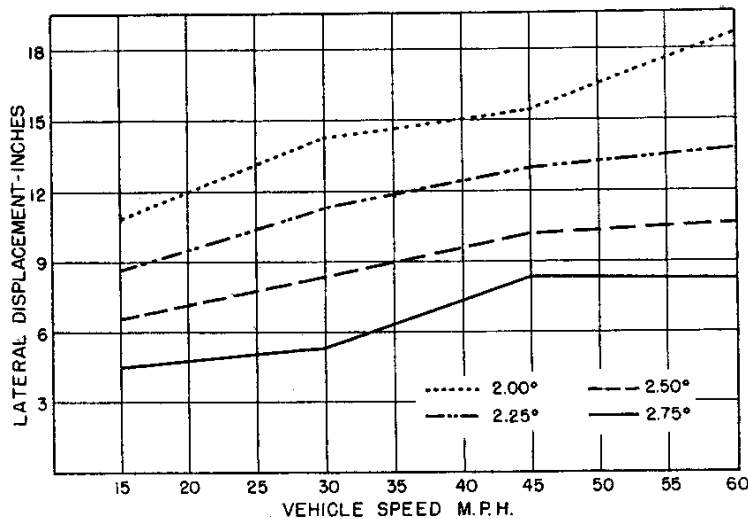


**Figure 4. Relationship between Lateral Displacement and Vehicle Speed [4]**

The first two relationships indicate that the lateral displacement of the vehicle is directly dependent upon speed and object location. The third relationship discovered was that the initiation of the lateral displacement occurred at a given distance in advance of the object, relative to the speed of the vehicle, as shown in Figure 5.

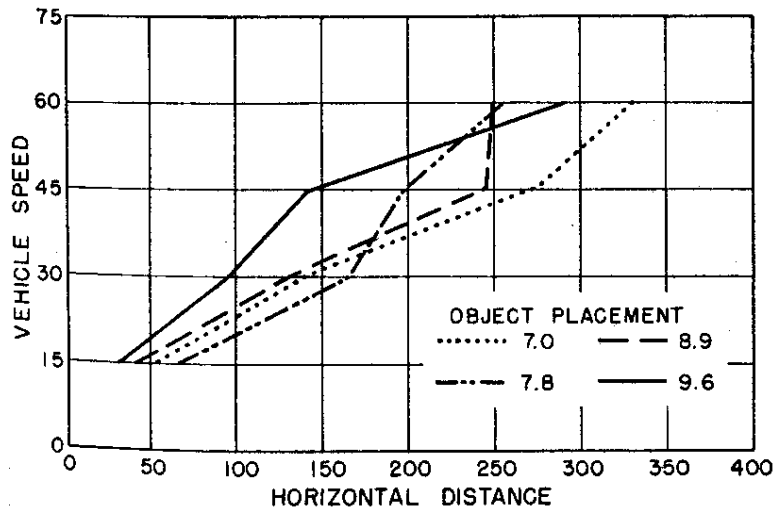


**Figure 5. Relationship of Vehicle Speed and Distance from Object at which Displacement Began [4]**

This study led to the conclusion that a model of lateral displacement should be based on the rate of change of the visual angle of the object in their path. Thus, the driver's ability to detect an object's movement out of their path of travel controls the amount of lateral displacement. The amount of displacement was found to be one-third to one-half of that found by Case et al. or by Taragin. The difference in the lateral displacement measured was attributed to three factors: (1) to a relatively wide roadway free from other distractions; (2) to the observable reflective strip down the center of the lane used for data acquisition with which the driver could orient their self; and (3) to the size of the object used along the roadside which was 15 sq ft as compared to 28 and 64 sq ft used in the other studies.

## 2.2. Previous Standards and Suggestions

The previously discussed studies have resulted in standards for the placement and flare of roadside barriers which reduce the barrier's effect on driver reaction. Barrier flare rates have also been determined using benefit-to-cost analyses and engineering judgment. Also in the past, government agencies have suggested installation standards for longitudinal guardrail, including

barrier flare rates. This section summarizes previous discussion on (1) studies which were used to develop barrier flare rates, (2) suggested barrier flare rates for guardrail installation, and (3) optimized barrier flare rates which were based on benefit-to-cost analyses in different situations.

In 1964, the Highway Research Board (HRB) suggested that the approach end of guardrail installations normally be flared [5]. The flare should be installed with the anchor approximately 8 to 10 ft away from the shoulder, and the installation should not be intrusive nor distracting to the driver. The length of the flare should not be less than 10 times the end offset (10:1 flare rate), and preferably 15 times the end offset (15:1 flare rate). Proper anchorage should be used according to current standards, and a flared and anchored arrangement was recommended, particularly on high-speed facilities.

In 1974, Hatton, wrote a draft report entitled, *A Roadside Design Procedure*, which stated that roadside design should resemble that of highway roadway geometric design [6]. Hatton addressed topics for the proper placement and flare of a guardrail. The first topic discussed was the shy distance, or the distance from the edge of the traveled way beyond which a roadside object will not be perceived as an obstacle nor result in driver reaction. These distances were based upon information provided in the study by Michaels and Cozan. The values were adjusted to account for overdriving roadways with a lower design speed and the probability the lane widths were not 12 ft wide on these lower speed roads. The resulting adjusted shy line offset distances, based upon design speed, are listed under “Shy Line Offset” in Table 4.

An additional consideration given to the results of Michaels and Cozan was the abrupt introduction of the roadside obstacle and Hatton’s personal observations of vehicles traveling near to longitudinal barriers. Thus, a transition of the barrier into the shy zone, if required by lack of the desired shy distance available, was desirable. American Association of State

Highway and Transportation Officials' (AASHTO) *Policy on Geometric Design of Rural Highways* suggests a shift of the barrier at a rate between 3 to 4 feet per second [7]. These criteria determined the rates listed under "Flare Rate to Shy Line" in Table 4.

**Table 4. Suggested Barrier Layout [6]**

Design Vehicle Speed (mph)	Traffic Volume												Shy Line Offset (ft.)	Flare Rate To Shy Line	Flare Rate Outside Shy Line		Barrier Terminal Offset (ft.)
	Design ADT Over 6,000		Design ADT 2,000-6,000		Design ADT 800-2,000 (Current ADT above 400)		Current ADT 250-400		Current ADT 100-250		Current ADT Under-100				Yielding Barrier	Rigid Barrier	
	Runout Path Length (ft.)	Clear Roadside Width (ft.)	Runout Path Length (ft.)	Clear Roadside Width (ft.)	Runout Path Length (ft.)	Clear Roadside Width (ft.)	Runout Path Length (ft.)	Clear Roadside Width (ft.)	Runout Path Length (ft.)	Clear Roadside Width (ft.)	Runout Path Length (ft.)	Clear Roadside Width (ft.)					
80	575	43	520	35	475	28.5	435	22.5	405	18	375	14	12	34:1	17:1	23:1	shld. +7
70	480	36	435	29	400	24	365	18.5	340	15	315	11.5	10	30:1	15:1	20:1	shld. +6
60	395	30	355	24	325	20.5	300	15	280	12	260	9	8	26:1	13:1	17:1	shld. +5
50	315	24	285	19.5	260	16	235	12	220	10	205	7.5	6.5	21:1	11:1	14:1	shld. +4
40	240	18	215	14.5	200	12	180	9.5	170	8	155	6	5.0	17:1	9:1	11:1	shld. +3
30	170	13	155	10.5	140	8.5	130	6.5	120	5	110	4	3.5	13:1	7:1	8:1	shld. +2

Hatton continued by introducing recommended barrier flare rates outside of the shy line distance based on four observations: (1) any contact with a barrier is hazardous; (2) the farther a barrier is located from the traffic, the less likely it is to be contacted; (3) contact with a barrier terminal usually results in a more serious accident than does contact with the longitudinal portion of a barrier, and (4) the greater the angle between a barrier and an impacting vehicle, then the greater the force on the vehicle occupants. Thus, the rates for flares outside the shy line, listed in Table 4, were based on approximately a 1G increase in impact forces calculated by Hatton, at the center of gravity of an impacting vehicle, as compared to a longitudinal impact of the same parallel system.

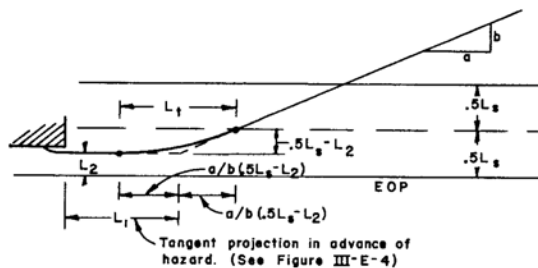
Further discussion by Hatton was directed toward barrier placement and runout length, including side slope effect, breaks in grades, and rounding of the roadside. A short discussion was also provided within this document on bridge decks and how their size considerations were directly comparable to the shy distance considerations for longitudinal barriers.

In 1977, the AASHTO *Guide for Selecting, Locating, and Designing Traffic Barriers* suggested that the ends of roadside barriers should be flared where possible [8]. Flaring the guardrail was cited to perform three functions: (1) to locate the barrier and its terminal as far away from the traveled way as was feasible; (2) to redirect an errant vehicle without serious injuries to its occupants, and (3) to minimize a driver's reaction to a hazard near the traveled way. Therefore, an optimum barrier flare was suggested based upon average daily traffic and design speed, as listed in Table 5.

**Table 5. Optimum Barrier Flare based upon Average Daily Traffic and Design Speed [8]**

Operating Speed (mph)	Design Traffic Volume (ADT)					Shy Line Offset (ft)	Flare Rate (a:b)*
	Over 6000	2000-6000	800-2000	800-250	Under 250		
70	480	440	400	360	330	10.0	15 **
60	400	360	330	300	270	8.0	13 **
50	320	290	260	240	210	6.5	11 **
40	240	220	200	180	160	5.0	9 **

\*When  $L_2 < 5L_s$ ,  $L_t$  shall have a minimum length =  $\frac{2a}{b} (.5L_s - L_2)$   
 Where  $\frac{a}{b}$  = flare rate from this table



\*\*Values are for yielding barrier ( $2'$  dynamic deflection) for rigid barriers increase numerator by  $.1 \left[ \frac{V}{10} \right]^2$   
 $V$  = operating speed (mph)

\*\*Adjustment factor for rigid barriers is  $V^2(3.86 \times 10^{-4})$ , When  $V$  is in Km/hr.

**Metric Conversions**

1 ft. = 0.305m  
 1 mph = 1.61km/h

In 1985, Sicking provided guidelines for positive barrier use in construction zones [9]. Sicking stated that barrier end treatments are a major factor in the cost-effectiveness of work-zone barriers. Thus, a 10:1 flare rate was found to be the most cost-effective over a wide range of conditions, and therefore it was suggested for implementation. However, a 17:1 flare rate was suggested if the flare began within the work zone because it does not change the overall length of the barrier.

In November 1988, Sicking et al. discussed flaring a guard fence away from the traveled way [10]. The study extensively used the BARRIER VII computer program [11] to optimize the design of metal beam guard fence, in terms of safety and cost. Sicking stated there must be an optimum flare rate that reduces the number of impacts with the barrier while not increasing the severity of impacts that still occur to an undesirable level. This optimum flare rate then could be determined using a benefit-to-cost analysis and accident severity criteria. Using a benefit-to-cost analysis based on guardrail installation and repair costs and their relationship with impact severity, it was found that a 10:1 flare rate could be used in most every case. Sicking also noted that flaring the guardrail on a slope significantly reduces the performance of the guardrail and therefore it is not recommended.

### **2.3. Current Standards**

Currently, guardrails are designed based upon information in the 2002 AASHTO Roadside Design Guide (RDG) [1]. In the 2002 RDG, flare rates are discussed for longitudinal barrier design. The RDG states that a barrier is considered flared if the system is not parallel to the traveled way. Maximum flare rates are suggested, in the form of a table, inside and outside the shy line distance as a function of design speed and traffic volume. The flare rate values were

taken from Hatton's unpublished, internal Federal Highway Administration (FHWA) report [6] and therefore are not repeated.

Two disadvantages to flaring the barrier were pointed out: (1) the impact severity is increased and (2) an increased potential for redirecting the vehicle back into the traveled way following an impact event. Discussion was also directed toward using flatter rates where excessive grading would be required to ensure a flat approach to the barrier and when locating the barrier inside the shy line.

The flare rate becomes important for the length of need calculation in the AASHTO Roadside Design Guide. Increasing the flare rate will allow the barrier to begin farther from the roadway and shorten the required length, both factors reducing the potential for contact with the barrier. However, it is pointed out that the suggested flare rates should not be exceeded in order to ensure proper impact performance.

### 3. RELEVANT CRASH TESTING

#### 3.1. Introduction

In order to study flare rates for W-beam longitudinal barriers, baseline systems and corresponding crash tests must first be determined. Once determined, these systems can be used to help create calibrated/validated BARRIER VII models, which can then be used for parametric studies to determine the effect that flare rates have on guardrail capacity and safety performance. Thus, an investigation into relevant crash testing for strong-post, W-beam guardrail systems must be performed. This section presents those tests.

Longitudinal barriers, such as W-beam guardrail systems, must satisfy Test Level 3 (TL-3) requirements provided in National Cooperative Highway Research Program (NCHRP) Report No. 350, *Recommended Procedures for the Safety Performance Evaluation of Highway Features* to be accepted for use on National Highway System (NHS) construction projects or as a replacement for existing systems not meeting current safety standards [12]. According to TL-3 of NCHRP 350, the longitudinal barriers must be subjected to two full-scale vehicle crash tests. The two crash tests are as follows:

Test Designation 3-10: An 820 kg (1,808 lb) small car impacting the guardrail system at a nominal speed and angle of 100.0 km/h (62.1 mph) and 20 degrees, respectively.

Test Designation 3-11: A 2,000 kg (4,409 lb) pickup truck impacting the guardrail system at a nominal speed and angle of 100.0 km/h (62.1 mph) and 25 degrees, respectively.

However, prior research has shown successful safety performance for small cars impacting strong-post, W-beam barriers. In several tests, the barriers remained essentially rigid with only modest deflections, with no significant potential for occupant risk problems arising from vehicle pocketing, severe wheel snagging on the guardrail posts, rail rupture, nor vehicular

instabilities due to vaulting or climbing the rail. Therefore, the small car test was not studied in this initial flare rate project.

Impact severity (IS) is one measure used by researchers to quantify the severity of a crash test. IS is calculated throughout this report using the formula:  $IS = \frac{1}{2} mV^2 \sin^2\theta$ , where  $m$  = mass,  $V$  = impact velocity, and  $\theta$  = impact angle.

### **3.2. Standard Strong-Post, W-beam Guardrail Systems**

#### **3.2.1. G4(2W) – Wood Post/Wood Blockout**

The G4(2W) guardrail system is a wood post, wood blockout, W-beam guardrail system. In 1994, Texas Transportation Institute (TTI) conducted test 471470-26 according to NCHRP 350 Test 3-11 specifications on a G4(2W) guardrail system with the following features [13]:

Rail:	Standard 2.66 mm (12-gauge) thick, 3.8-m long W-beam guardrail
Rail Mounting:	Center height at 530 mm (20.875 in.) Top height of 685.8 mm (27 in.)
Posts:	Wood – 152-mm wide x 203-mm deep x 1,625.6-mm long
Blockouts:	Wood – 152-mm wide x 203-mm deep x 356-mm long
Post spacing:	1,905 mm (75 in.) on center
Embedment Depth:	914.4 mm (36 in.)
Anchorage:	Upstream End – 11.4 m (37.5 ft) long MELT terminal Downstream End – 11.4 m (37.5 ft) long BCT terminal
System length:	68.6 m (225 ft) total (including anchorage)

Parameters and results for test 471470-26 are provided in Figure 6. For test 471470-26, a 2,074 kg (4,568 lb) pickup truck impacted at a speed of 100.8 km/h (62.6 mph) and at an angle of 24.3 degrees. The impact severity for this test was calculated to be 138 kN-m. Initial impact occurred 0.61 m (24 in.) upstream of post 14. At 0.249 sec after impact, the vehicle became

parallel to the guardrail traveling at 74.3 km/h (46.3 mph). At 0.513 sec, the vehicle exited the guardrail at a trajectory angle of 8.1 degrees and at a resultant velocity of 70.8 km/h (44.0 mph). In this test, the guardrail contained and redirected the pickup although the collision was somewhat severe. Maximum dynamic deflection of the guardrail was 0.82 m (2.7 ft) and maximum roll angle of the vehicle was 39 degrees. The front wheel, hub and spindle assembly on the impact side was separated from the vehicle. For further details, see Mak et al [13] and Buth et al [14].

Test 471470-26 passed all NCHRP 350 requirements for Test 3-11.

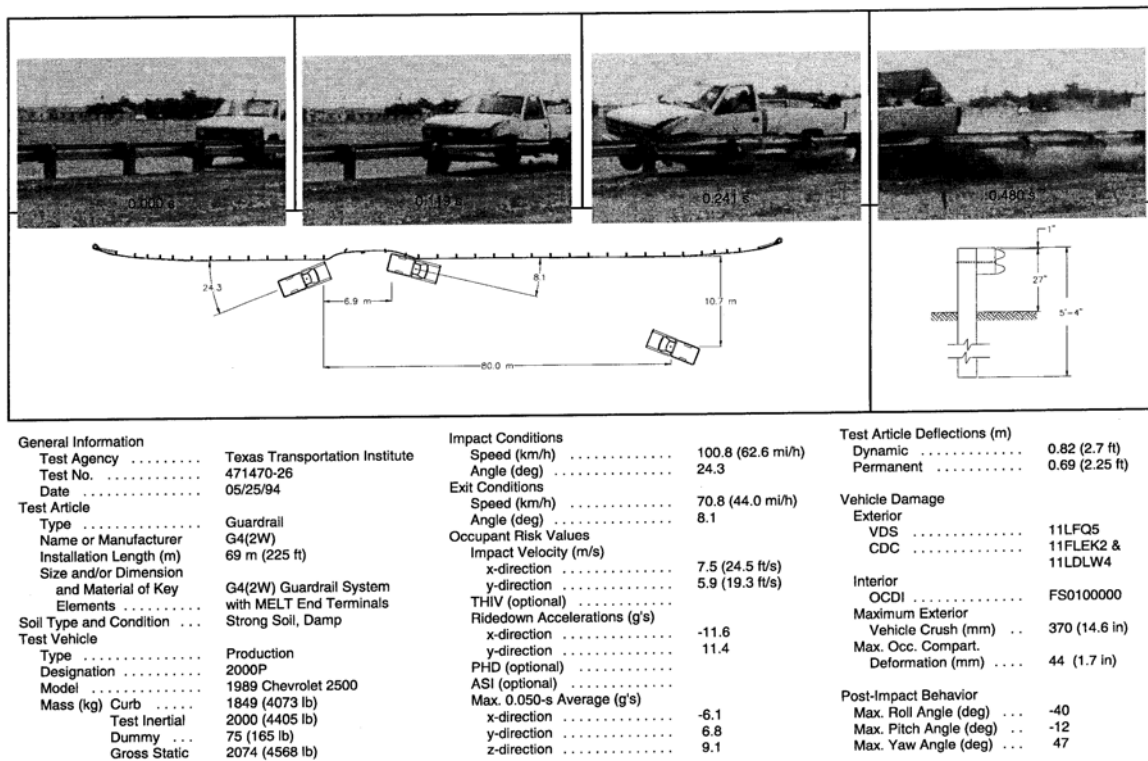


Figure 6. Parameters and Results for TTI Test 471470-26 [14]

### 3.2.2. G4(1S) – Steel Post/Steel Blockout

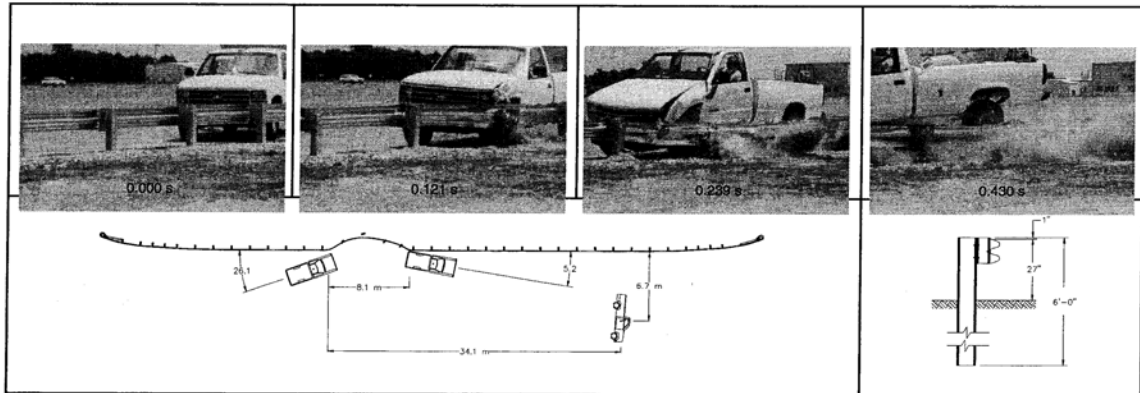
The G4(1S) guardrail system is a steel post, steel blockout, W-beam guardrail system. In 1994, TTI conducted test 471470-27 according to NCHRP 350 Test 3-11 specifications on a G4(1S) guardrail system with the following features [13]:

Rail:	Standard 2.66 mm (12-gauge) thick, 3.8-m long W-beam guardrail
Backup Plates:	W-beam rail, 305 mm (12 in.) long, at non-splice posts
Rail Mounting:	Center height at 530 mm (20.875 in.) Top height of 685.8 mm (27 in.)
Posts:	Steel – W152x13.4 (W6x9) sections, 1,828.8 mm (6 ft) long
Blockouts:	Steel – W152x13.4 (W6x9) sections, 356 mm (14 in.) long
Post spacing:	1,905 mm (75 in.) on center
Embedment Depth:	1117.6 mm (44 in.)
Anchorage:	Upstream End – 11.4 m (37.5 ft) long MELT terminal Downstream End – 11.4 m (37.5 ft) long BCT terminal
System length:	68.6 m (225 ft) total (including anchorage)

Parameters and results for test 471470-27 are provided in Figure 7. For test 471470-27, a 2,075 kg (4,570 lb) pickup truck impacted at a speed of 101.4 km/h (63.0 mph) and at an angle of 26.1 degrees. The impact severity for this test was calculated to be 159 kN-m. Initial impact occurred 0.61 m (24 in.) upstream of post 14. The left-front tire was observed to snag on post 16 at 0.213 seconds after impact, resulting in a significant bow of the truck body. At 0.274 sec after impact, the vehicle became parallel to the guardrail traveling at 66.0 km/h (41.0 mph). At 0.530 sec, the vehicle exited the guardrail at a trajectory angle of 5.2 degrees, at a resultant velocity of 58.7 km/h (36.5 mph), a roll angle of 28 degrees counter clockwise, and a clockwise yawing motion. The exit conditions resulted in the vehicle rolling onto its left side before the truck came to a stop.

Behavior of the pickup during collision was similar to that in the G4(2W) test, except interaction was slightly more severe, and the pickup rolled onto its left side after being contained and redirected.

Test 471470-27 failed NCHRP 350 requirements for Test 3-11.



<b>General Information</b>		<b>Impact Conditions</b>		<b>Test Article Deflections (m)</b>	
Test Agency	Texas Transportation Institute	Speed (km/h)	101.4 (63.0 mi/h)	Dynamic	0.91 (3.0 ft)
Test No.	471470-27	Angle (deg)	26.1	Permanent	0.64 (2.1 ft)
Date	06/09/94	<b>Exit Conditions</b>		<b>Vehicle Damage</b>	
<b>Test Article</b>		Speed (km/h)	58.7 (36.5 mi/h)	<b>Exterior</b>	
Type	Guardrail	Angle (deg)	5.2	VDS	11LFQ6 9L&T3
Name or Manufacturer	G4(1S)	<b>Occupant Risk Values</b>		CDC	11FLEK3 & 00LDAO3
Installation Length (m)	69 m (225 ft)	Impact Velocity (m/s)		<b>Interior</b>	
Size and/or Dimension and Material of Key Elements	G4(1S) Guardrail System with MELT End Terminals	x-direction	7.5 (24.8 ft/s)	OCDI	LF0100000
Soil Type and Condition	Strong Soil, Damp	y-direction	4.9 (16.0 ft/s)	<b>Maximum Exterior</b>	
<b>Test Vehicle</b>		THIV (optional)		Vehicle Crush (mm)	570 (22.4 in)
Type	Production	Ridedown Accelerations (g's)		Max. Occ. Compartment Deformation (mm)	53 (2.1 in)
Designation	2000P	x-direction	-7.8	<b>Post-Impact Behavior</b>	
Model	1988 Chevrolet 2500	y-direction	6.2	Max. Roll Angle (deg)	-119
Mass (kg)	1944 (4282 lb)	PHD (optional)		Max. Pitch Angle (deg)	-19
Test Inertial	2000 (4405 lb)	ASI (optional)		Max. Yaw Angle (deg)	79
Dummy	75 (165 lb)	Max. 0.050-s Average (g's)			
Gross Static	2075 (4570 lb)	x-direction	-6.0		
		y-direction	4.7		
		z-direction	3.9		

**Figure 7. Parameters and Results for TTI Test 471470-27 [14]**

### 3.2.3. Discussion – G4(2W) versus G4(1S)

Major differences between the G4(2W) and G4(1S) crash tests described above were three-fold: (1) the impact severity was 16% greater on the G4(1S) system (159 kN-m versus 138 kN-m), mainly due to the increased impact angle (26.1 degrees versus 24.3 degrees); (2) the blockout depth for the G4(1S) was 152 mm versus 203 mm for the G4(2W) system, and (3) there was significant deformation and collapse of the W150x13.4 steel blockouts on the G4(1S) system, while the wood blockouts in the G4(2W) did not collapse. Because of these differences and failure of the G4(1S) test, a modified G4(1S) was designed and tested (discussed in the next section).

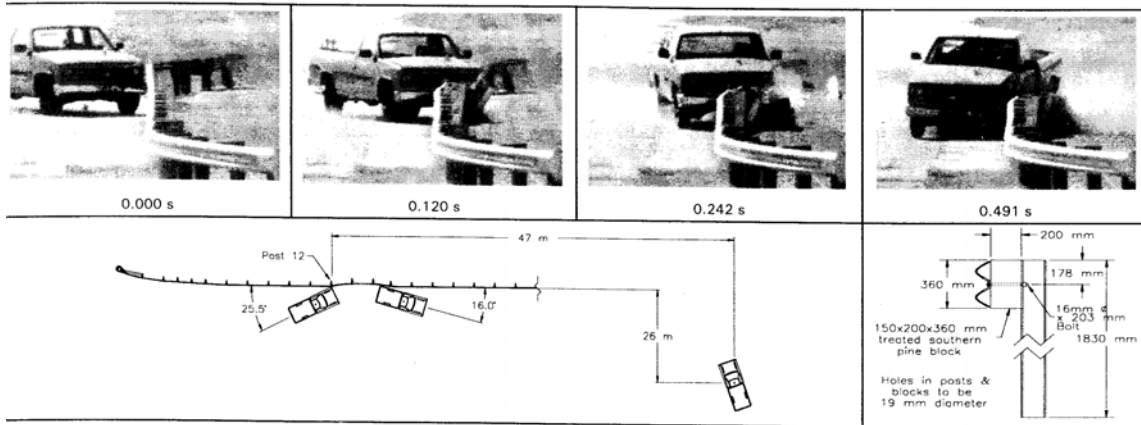
### 3.2.4. Modified G4(1S) – Steel Post/Routed Wood Blockout

The modified G4(1S) guardrail system is a steel post, routed wood blockout, W-beam guardrail system. In 1995, TTI conducted test 405421-1 according to NCHRP 350 Test 3-11 specifications on a modified G4(1S) guardrail system with the following features [15]:

Rail:	Standard 2.66 mm (12-gauge) thick, 3.8-m long W-beam guardrail
Rail Mounting:	Center height at 550 mm (21.65 in.) Top height of 706 mm (27.8 in.)
Posts:	Steel – W150x12.6 (W6x8.5) sections, 1,828.8 mm (6 ft) long
Blockouts:	Wood – routed, 150-mm wide x 200-mm deep x 360-mm long
Post spacing:	1,905 mm (75 in.) on center
Embedment Depth:	1,100 mm (43.3 in.)
Anchorage:	11.4 m long MELT terminal, both ends
System length:	53.3 m (175 ft) total (including anchorage)

Parameters and results for test 405421-1 are provided in Figure 8. For test no. 405421-1, a 2,076 kg (4,577 lb) pickup truck impacted at a speed of 101.5 km/h (63.1 mph) and at an angle of 25.5 degrees. The impact severity for this test was calculated to be 153 kN-m. Initial impact occurred 0.61 m (24 in.) upstream of post 12. At 0.278 sec after impact, the vehicle became parallel to the guardrail with a velocity of 68.9 km/h (42.8 mph). The vehicle was safely redirected in a very stable manner with very little roll or pitch. At 0.691 sec, the vehicle exited the guardrail at a trajectory angle of 16.0 degrees and at a resultant velocity of 55.0 km/h (34.2 mph). The vehicle exited the test installation in a very stable manner.

Test 405421-1 passed all NCHRP 350 requirements for Test 3-11.



General Information		Impact Conditions		Test Article Deflections (m)	
Test Agency	Texas Transportation Institute	Speed (km/h)	101.5	Dynamic	1.0
Test No.	405421-1	Angle (deg)	25.5	Permanent	0.7
Date	11/16/95	Exit Conditions		Vehicle Damage	
Test Article		Speed (km/h)	55.0	Exterior	
Type	Guardrail	Angle (deg)	16.0	VDS	11LFQ4
Name	Modified G4(1S)	Occupant Risk Values		CDC	11FYEW3
Installation Length (m)	53.3	Impact Velocity (m/s)		Interior	
Size and/or dimension		x-direction	7.1	OCDI	
and material of key	W-beam guardrail on steel posts	y-direction	4.4	Maximum Exterior	
elements	with timber blockouts	THIV (optional)		Vehicle Crush (mm)	
Soil Type and Condition	Standard soil, dry	Ridedown Accelerations (g's)		Max. Occ. Compart.	
Test Vehicle		x-direction	-7.9	Deformation (mm)	
Type	Production	y-direction	8.4	Post-Impact Behavior	
Designation	2000P	PHD (optional)		Max. Roll Angle (deg)	
Model	1989 Chevrolet 2500 pickup	ASI (optional)		Max. Pitch Angle (deg)	
Mass (kg) Curb	2005	Max. 0.050-sec Average (g's)		Max. Yaw Angle (deg)	
Test Inertial	2000	x-direction	-5.3		
Dummy	76	y-direction	4.3		
Gross Static	2076	z-direction	-4.8		

**Figure 8. Parameters and Results for TTI Test 405421-1 [15]**

### 3.2.5. System Differences – G4(1S) versus Modified G4(1S)

The differences between the G4(1S) and the modified G4(1S) are that the modified G4(1S):

1. Uses routed wood blockouts instead of steel blockouts, resulting in an effective W-Beam blockout distance of 190 mm, as opposed to 152 mm for the G4(1S).
2. Uses W150x12.6 (W6x8.5) steel posts instead of W150x13.4 (W6x9).
3. Raises the guardrail mounting height 20 mm, and thus decreases the soil embedment depth by 20 mm.
4. Was tested with a system length of 53.3 m instead of 68.5 m.

### 3.3. Additional Strong-Post W-Beam (G4) Testing

Two additional strong-post, W-beam tests warrant mention in this report: (1) a wood post, wood blockout system and (2) a steel post, wood blockout system known as the Michigan Type B system. Both of these tests were conducted at the Midwest Roadside Safety Facility (MwRSF) and are described below.

#### 3.3.1. Wood Post, Wood Blockout, W-Beam Guardrail System - MwRSF

In 1996, the MwRSF conducted test BSP-5 according to NCHRP 350 Test 3-11 specifications on a wood post, wood blockout, W-beam guardrail system with the following features [16]:

Rail:	Standard 2.66 mm (12-gauge) thick, 3.8-m long W-beam guardrail
Rail Mounting:	Center height at 550 mm (21.65 in.) Top height of 706 mm (27.8 in.)
Posts:	Wood - 150-mm wide x 200-mm deep x 1,830-mm long
Blockouts:	Wood - 150-mm wide x 200-mm deep x 360-mm long
Post spacing:	1,905 mm (75 in.) on center
Embedment Depth:	1,100 mm (43.3 in.)
Anchorage:	Two 140-mm wide x 190-mm deep x 1,080-mm long wood posts in 1,830 mm (6-ft) long steel foundation tubes, with ground line strut
System length:	45.7 m (150 ft) total (including anchorage)

For test BSP-5, a 2,002 kg (4,414 lb) pickup truck impacted at a speed of 102.0 km/h (63.4 mph) and at an angle of 26.0 degrees. Initial impact occurred at mid-span between two posts. Five posts were snapped off, not allowing for post rotation in soil. Because of the post failures, the system behaved similar to a weak post system, reflected in the large permanent set,

equal to 848 mm (33.4 in.). The vehicle was safely redirected in a very stable manner with very little roll or pitch.

Test BSP-5 passed NCHRP 350 requirements for Test 3-11. However, analysis of BSP-5 results indicated that this test did not meet testing standards. Specifically, a few of the broken posts were determined to be below the standard specified grade, the soil grading did not meet NCHRP 350 specifications, and the soil was found to be frozen in several locations. Thus, BSP-5 was not used for the flare rate study.

### **3.3.2. Michigan Type B - Steel Post/Wood Blockout**

The Michigan Type B guardrail system is a steel post, wood blockout, W-beam guardrail system. In 2000, the MwRSF conducted test MIW-2 according to NCHRP 350 Test 3-11 specifications on the Michigan Type B guardrail system with the following features [17]:

Rail:	Standard 2.66 mm (12-gauge) thick, 3.8-m long W-beam guardrail
Rail Mounting:	Center height at 550 mm (21.65 in.) Top height of 706 mm (27.8 in.)
Posts:	Steel – W152x13.4 (W6x9) sections, 1,829 mm (6 ft) long
Blockouts:	Wood – 152-mm wide x 203-mm deep x 356-mm long with a nail used to prevent rotation
Post spacing:	1,905 mm (75 in.) on center
Embedment Depth:	1,100 mm (43.3 in.)
Anchorage:	Two modified BCT posts in foundation tubes with soil plates, separated by a ground line strut, and BCT cable anchor (both ends)
System length:	53.3 m (175 ft) total (including anchorage)

Parameters and results for test MIW-2 are provided in Figure 9. For test MIW-2, a 2,034 kg (4,484 lb) pickup truck impacted at a speed of 99.8 km/h (62.0 mph) and at an angle of 27.7

degrees. The impact severity for this test was calculated to be 169 kN-m. Initial impact occurred at the center of post 13. At 0.129 sec after impact, the vehicle began to redirect. At 0.158 sec, the front bumper rose above the top of the rail. At 0.432 sec, the right-rear tire, which had been riding along the traffic-side face of the rail, lost contact with the rail and was located on the back side of the rail. At 0.541 sec, the vehicle, which was partially airborne, began to roll away from the rail that was positioned along the longitudinal midpoint of the vehicle. At 0.640 sec, the vehicle was completely airborne and free from the rail. At 0.810 sec, the vehicle returned to an unpitched state. Subsequently, the vehicle came to rest 28.58 m (93.8 ft) downstream from impact and on top of the guardrail between post nos. 26 and 29, with the left-front tire located 0.61 m (24.0 in) laterally away from the traffic-side of the rail.

Test MIW-2 failed NCHRP 350 requirements for Test 3-11. Evaluation of the crash test film and photographic documentation indicated that the test failure was caused when the post bolt did not pull through the W-beam rail element at post no. 15 causing the vehicle to vault and land on top of the guardrail with its right-side wheels contacting the ground behind the barrier system and coming to rest on top of the downstream end of the guardrail system.

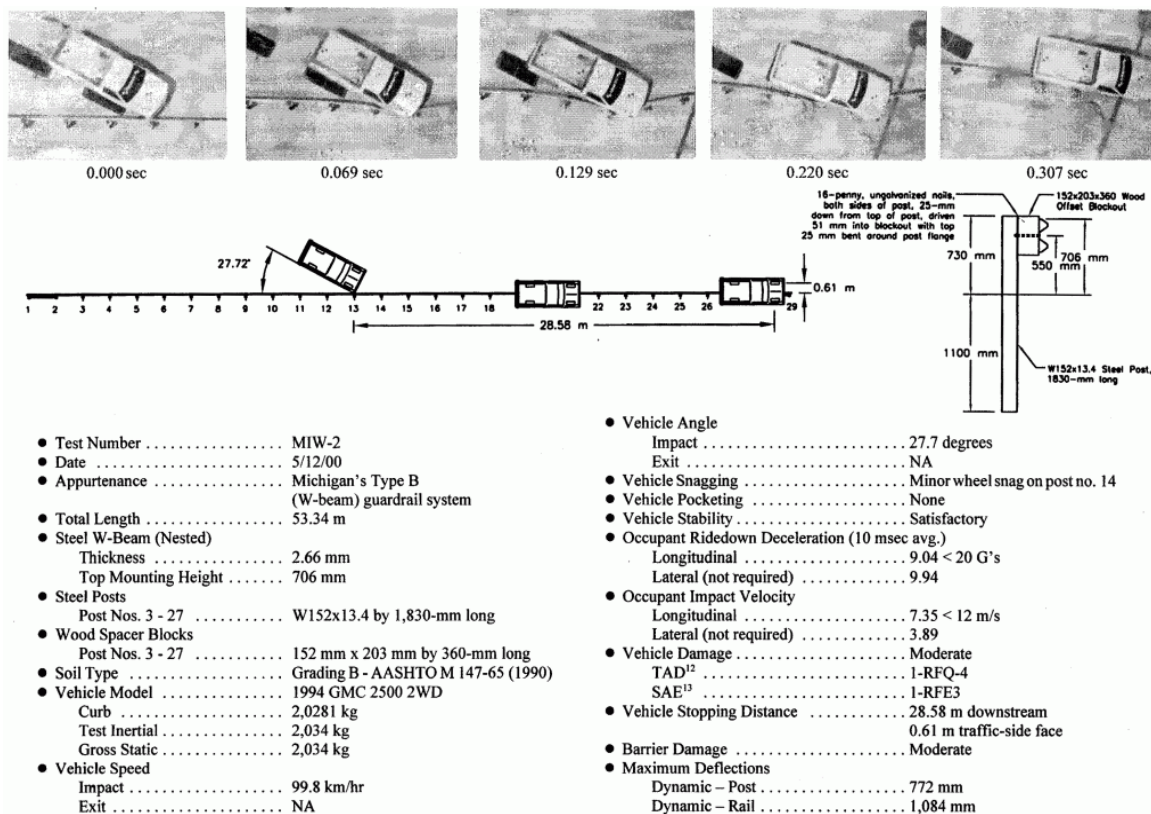


**Figure 9. Parameters and Results for MwRSF Test MIW-2 [17]**

### 3.4. Conclusion for Standard, Strong-Post, W-Beam Guardrail System

A comparison between the modified G4(1S) system and the G4(2W) system is as follows. The impact point for both systems was 4.5 m (14.76 ft) upstream of a splice location, but the modified G4(1S) system had an 11% increase in impact severity over that observed for the G4(2W) system, 153 kN-m versus 138 kN-mm, respectively. The modified G4(1S) system had a larger maximum dynamic deflection than the G4(2W) system, 1.0 m versus 0.82 m, but a comparable maximum permanent set deflection of 0.7 m versus 0.69 m. The vehicle took longer to exit the modified G4(1S) than the G4(2W), taking 0.691 sec versus 0.513 sec, and was also slower upon exit, 55.0 km/h versus 70.8 km/h. Another difference between the two exit conditions was the exit trajectory, 16.0 degrees for the modified G4(1S) system versus 8.1

degrees for the G4(2W). The total length of contact for the modified G4(1S) system was shorter than the G4(2W) system, 5.8 m versus 6.9 m.

From the comparisons, the modified G4(1S) system was selected for the flare rate study due to the larger dynamic deflection associated with the successful test. Larger dynamic deflections indicate a greater potential for the vehicle to penetrate the barrier. Penetrating into the barrier further will produce more load on the rail as it detaches from the posts, producing a potential to tear the W-beam rail. Also resulting from the larger dynamic deflection was the potential for a greater degree of pocketing and wheel snag.

Comparisons were also made between the Michigan Type B guardrail system and the modified G4(1S) system. The truck impacted 1.6 km/h faster, but 2.2 degrees shallower into the modified G4(1S) system. It should also be pointed out that the post in the modified G4(1S) system was a W152x12.6 versus a W152x13.4 (W6x8.5 versus a W6x9) for the Michigan Type B system. However, it was believed that this difference would not affect the comparison nor the results of the tests. The modified G4(1S) system and the Michigan Type B system had a comparable maximum dynamic deflection of 1.0 m versus 1.1 m and a comparable maximum permanent set deflection of 0.7 m versus 0.77 m. The truck impacting the modified G4(1S) was redirected in a safe manner, while the truck impacting the Michigan Type B system was observed to begin redirection, but then became airborne, subsequently landing on the downstream end of the guardrail.

These very similar systems with very different crash test results are an indication of the sensitivity of the standard, strong-post, W-beam guardrail system. In regards to the flare rate study, it was believed that extensive parameter studies using BARRIER VII would be needed to determine the robustness of any proposed flare rate changes.

Additionally, due to recognized sensitivity in the standard guardrail system, the Midwest States' Regional Pooled Fund Program funded the MwRSF to perform an extensive multi-year project to develop a more robust W-beam guardrail system. Resulting, and still on-going, from that project, was a relatively new system known as the Midwest Guardrail System (MGS), which will be discussed in the following section.

The modified G4(1S) system will be studied during the flare rate study. TTI test 405421-1 will be used as the baseline test for calibration/validation of the BARRIER VII model used in the project.

### **3.5. Midwest Guardrail System**

The Midwest Guardrail System (MGS) is a steel post, wood blockout, W-beam guardrail system [18-20]. In 2002, the MwRSF conducted test NPG-4 according to NCHRP 350 Test 3-11 specifications on a MGS with the following features:

Rail:	Standard 2.66 mm (12-gauge) thick, 3.8-m long W-beam guardrail with additional post bolt slots at half post spacing
Rail Mounting:	Center height at 632 mm (24.875 in.) Top height of 787 mm (31 in.) Splices are at mid-span between posts
Posts:	Steel – W152x13.4 (W6x9) sections, 1,829 mm (6 ft) long
Blockouts:	Wood – 152-mm wide x 305-mm deep x 356-mm long
Post spacing:	1,905 mm (75 in.) on center
Embedment Depth:	1,016 mm (40 in.)
Anchorage:	Two modified BCT posts in foundation tubes with soil plates, separated by a ground line strut, and BCT cable anchor (both ends)
System length:	53.3 m (175 ft) total (including anchorage)

Parameters and results for test NPG-4 are provided in Figure 10. For test NPG-4, a 1,986 kg (4,378 lb) pickup truck impacted the MGS at a speed of 98.1 km/h (61.0 mph) and at an angle of 25.6 degrees. The impact severity for this test was calculated to be 138 kN-m. Initial impact occurred 4,839 mm (190.5 in.) upstream from the centerline of the splice between post nos. 14 and 15. At 0.396 sec after impact, the vehicle became parallel to the guardrail with a resultant velocity of 61.2 km/h (38.0 mph). At 0.597 sec, the vehicle exited the guardrail at a trajectory angle of 19.3 degrees and at a resultant velocity of 55.1 km/h (34.2 mph). The vehicle was safely redirected in a very stable manner with very little roll or pitch.

Test NPG-4 passed all NCHRP 350 requirements for Test 3-11.

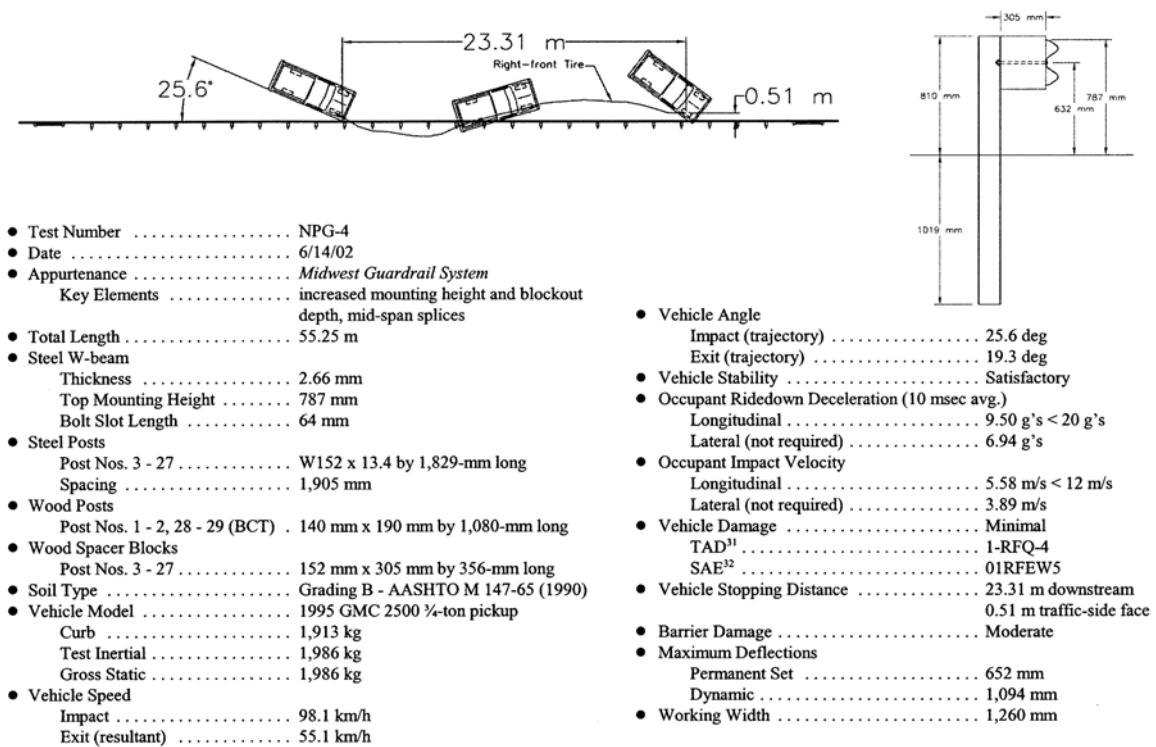


Figure 10. Parameters and Results for MwRSF Test NPG-4 [18]

### **3.6. Comparison and Conclusion for Midwest Guardrail System**

Differences between the MGS and the standard W-Beam guardrail system (i.e., the modified G4(1S) system) are that the MGS system: (1) increases the rail height; (2) uses a non-routed deeper wood blockout; (3) places the rail splice at the mid-span between posts, and (4) has a shallower post embedment depth.

The MGS will be studied in detail during the flare rate study. MwRSF test NPG-4 will be used as the baseline test for calibration/validation of the BARRIER VII model used in the project.

## **4. BARRIER VII BASELINE MODEL DEVELOPMENT**

### **4.1. Midwest Guardrail System**

#### **4.1.1. Introduction**

Non-linear, 2-dimensional (2-D) computer simulation with BARRIER VII was used to create a baseline model of the Midwest Guardrail System (MGS) for use in the flare rate study. Although other computer programs exist to study vehicular impacts with longitudinal barriers, BARRIER VII is probably the most validated program for the prediction of barrier deflections. As stated previously, the NCHRP Report No. 350 requires that roadside barriers be subjected to test no. 3-11, a 1,986 kg pickup truck impacting at 100 km/h and 25 degrees, before their implementation on the nation's highways. As such, the Midwest Roadside Safety Facility (MwRSF) completed test no. NPG-4 for the MGS. For test no. NPG-4, a 2000-kg pickup truck impacted the system at 98.17 km/h and 25.6 degrees. These impact conditions fall within the allowable range for the successful evaluation of the barrier's performance. The data acquired during test no. NPG-4 from the overhead high-speed film, onboard vehicle accelerometers, and speed traps were used to calibrate the model to the physical test.

#### **4.1.2. Development of the MGS Model**

A finite element model of the MGS was developed for use in BARRIER VII. The model had a total of 173 nodes, 201 members (172 beam members and 29 post members), 4 different beam types, and 3 different post types. The model has a total length of 175 ft. The BARRIER VII input deck is listed in Appendix A.

The four different types of beam members correlated to the four different discretization lengths used, dependent upon their location along the rail, while all the other properties remain

the same. The beam member length was reduced from 37.5 in. at the ends, to 4.6875 in. near posts in the impact region. Typical beam member length in the impact region was 9.375 in, resulting in 8 or 9 members between posts. The impact region consisted of 3 posts upstream and 9 posts downstream of the impact location. The rail was attached to posts through a common node every 75 in.

Two of the post types used represent the two BCT posts (anchor posts), on both the upstream and downstream ends, used during test no. NPG-4. The ground-line strut and cable were not modeled for simplicity. Thus, the anchor post strength was given particular attention and is discussed further in another section. The other post type used represents the W152x13.5 (W6x9) system posts for the MGS.

#### 4.1.3. Calibration of the MGS Model

For the calibration effort, several simulations were performed at the impact conditions of test no. NPG-4 in order to attune selected BARRIER VII input parameters. For the posts, initial parameters were obtained from the dynamic post testing [21]. Other parameters that were calibrated include post failure displacement based on guardrail release, vehicle-to-barrier dynamic coefficient of friction, and the yaw-mass-moment-of-inertia for the pickup truck, as provided in Table 6.

**Table 6. BARRIER VII Simulation Parameters**

BARRIER VII Parameters		Initial Input Values	NPG-4 Final Validation Run Values
$K_B$ - Post Stiffness Along B (strong axis)	kN/mm (kip/in.)	1.021 (5.830)	1.056 (6.030)
$K_A$ - Post Stiffness Along A (weak axis)	kN/mm (kip/in.)	0.701 (4.002)	0.701 (4.002)
$M_A$ - Moment About A (strong axis)	kN*mm (kip*in.)	18549 (164.17)	16230 (143.65)
$M_B$ - Moment About B (weak axis)	kN*mm (kip*in.)	10494 (92.88)	10494 (92.88)
$\delta_F$ - Failure Displacement Along B	mm (in.)	381 (15)	381 (15)
$\mu_k$ - Kinetic Friction Coefficient	Vehicle to Barrier	0.350	0.400
$I_{m_z}$ - 2000P Mass Moment of Inertia - Yaw	N*m*s <sup>2</sup> (lb*ft*s <sup>2</sup> )	4971 (44000)	5356 (47400)

Using a parametric technique, initial simulations showed a need to tune input parameters for posts located both in the impact region as well as at the ends. Considerable effort was directed towards the accurate simulation of the upstream anchor. This effort was accomplished by tracking the farthest visible upstream target in the overhead film analysis and plotting those longitudinal displacements with the corresponding nodal displacements from the simulations. Further discussion is also included in another section of this chapter.

It was also necessary to adjust the vehicle to rail friction coefficient and the vehicle's yaw-mass-moment-of-inertia in order to more accurately predict vehicle behavior at the parallel and exit conditions. As with the anchor performance, the vehicle to rail friction coefficient was of particular interest to this calibration. It was discovered that the friction coefficient not only deals with the friction between the truck and the barrier, but also incorporates wheel contact and snag on additional posts, effectively causing additional vehicle drag and energy loss in the actual system that BARRIER VII cannot predict. Therefore, adjustment of the effective coefficient of friction was deemed appropriate.

#### **4.1.4. Validation of the MGS Model**

One important validation method was the graphical comparison of the simulation and physical crash test barrier profiles. The input parameters were said to be calibrated if BARRIER VII was able to accurately predict the barrier profile. The barrier profile during the physical crash test was obtained from the overhead film analysis. A graphical comparison of the simulated and actual barrier displacements for test no. NPG-4 are provided in Figure 11. The final validated BARRIER VII input parameters are provided in Table 6.

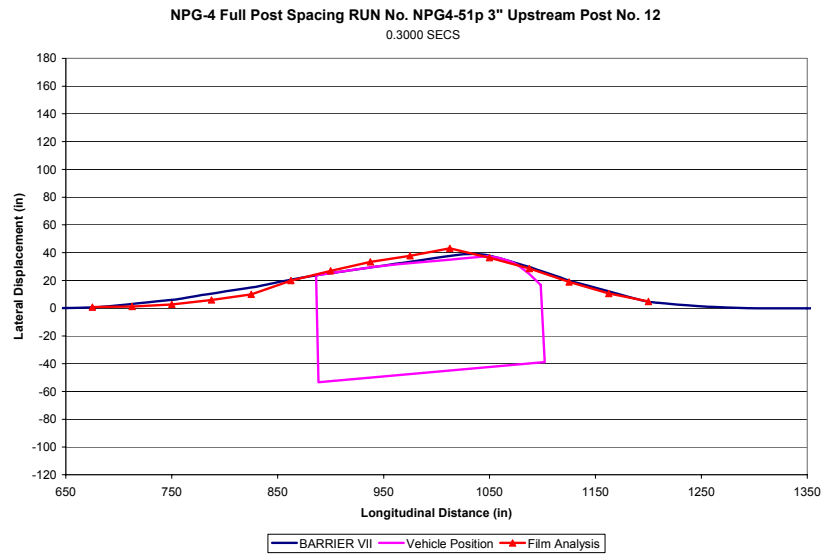
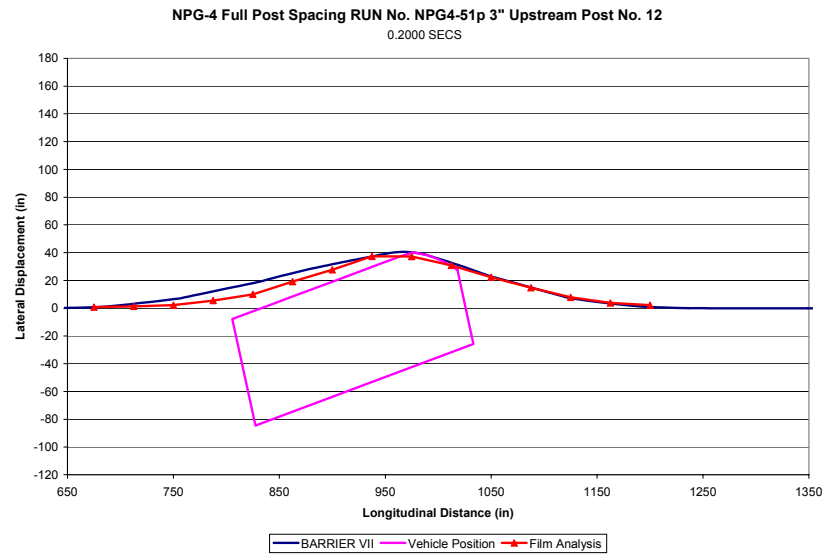
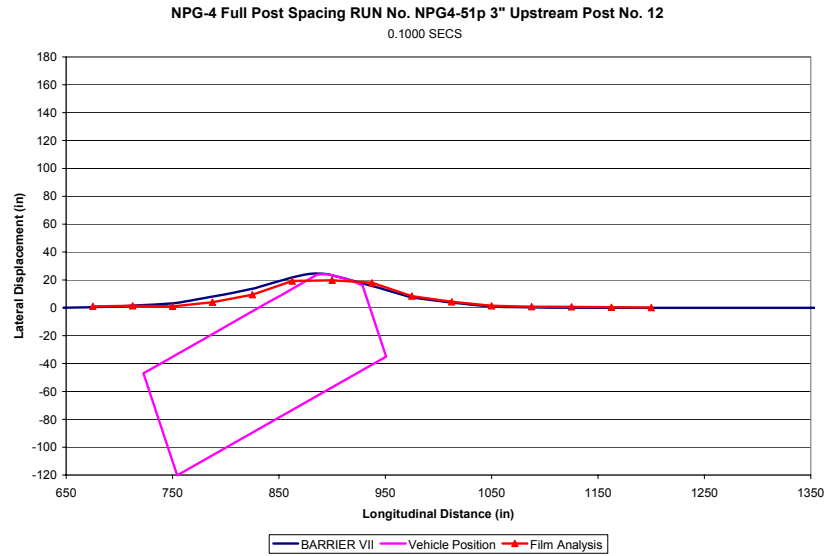
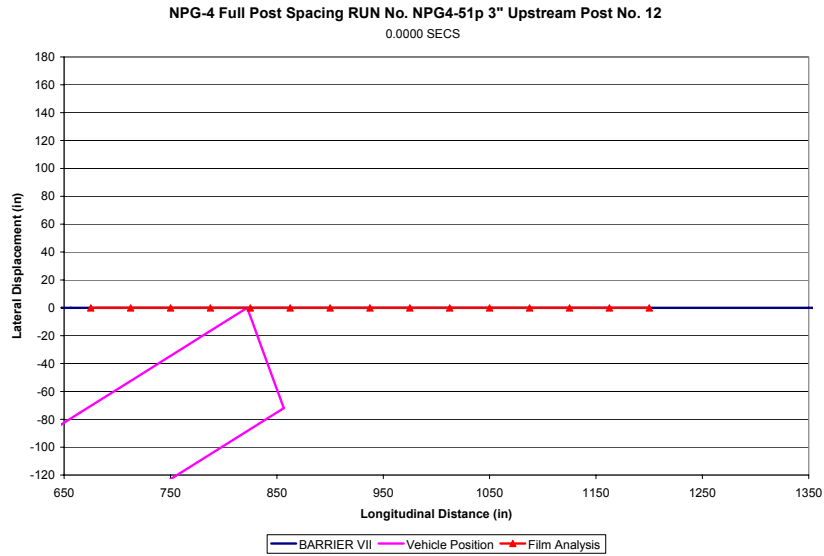


**Figure 11. Sequential Figures from BARRIER VII Simulation of NPG-4**

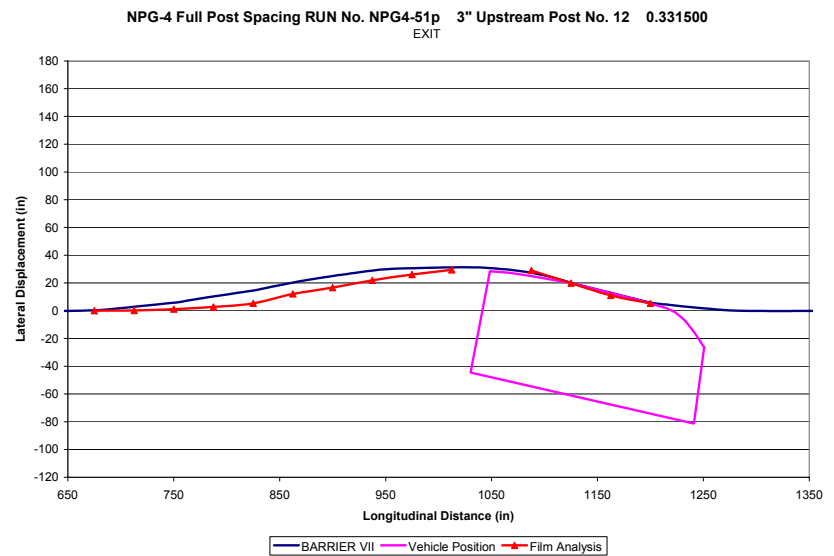
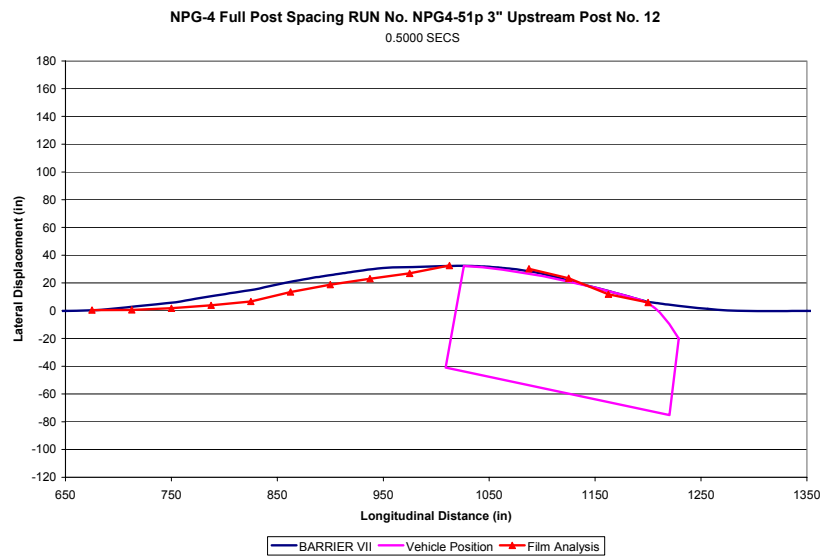
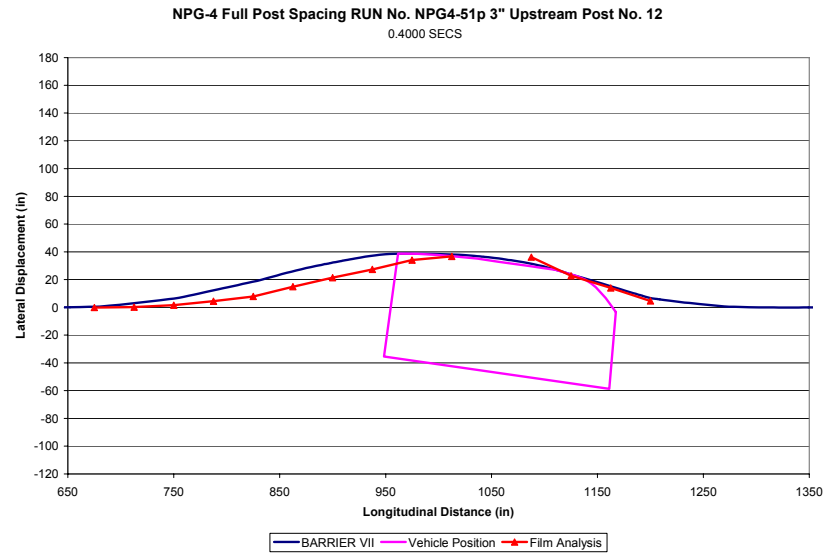
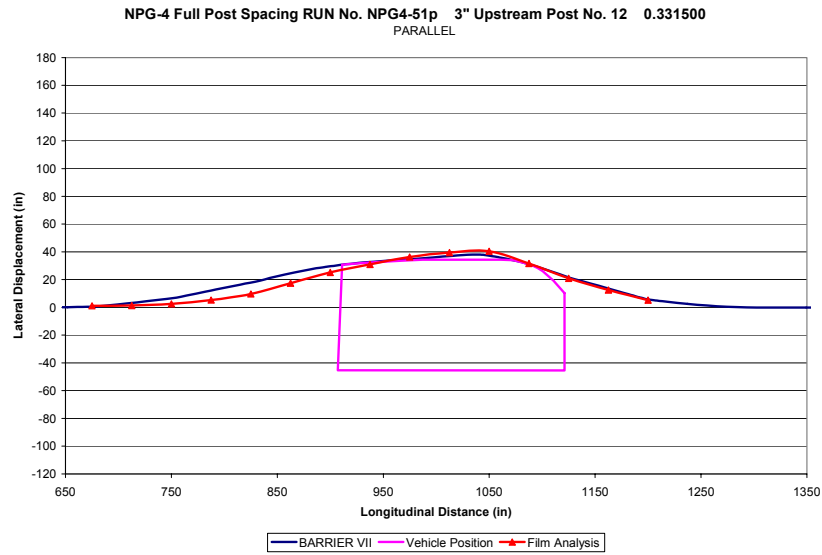
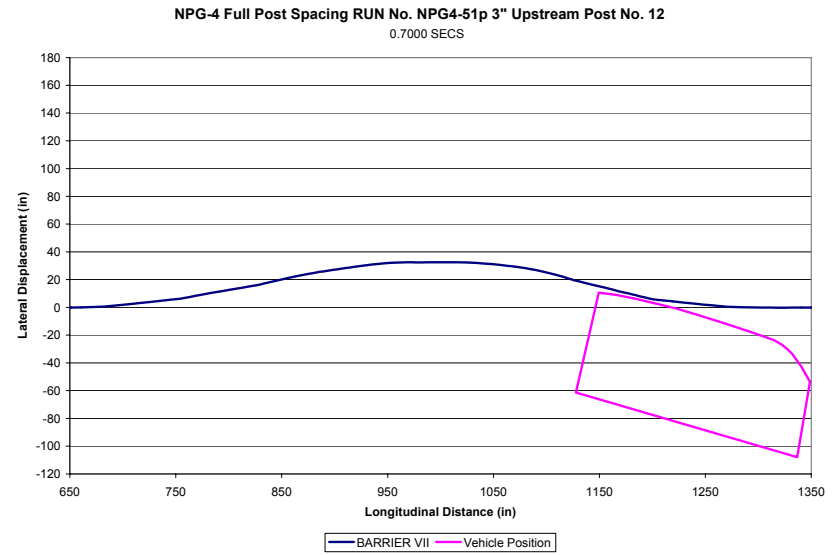
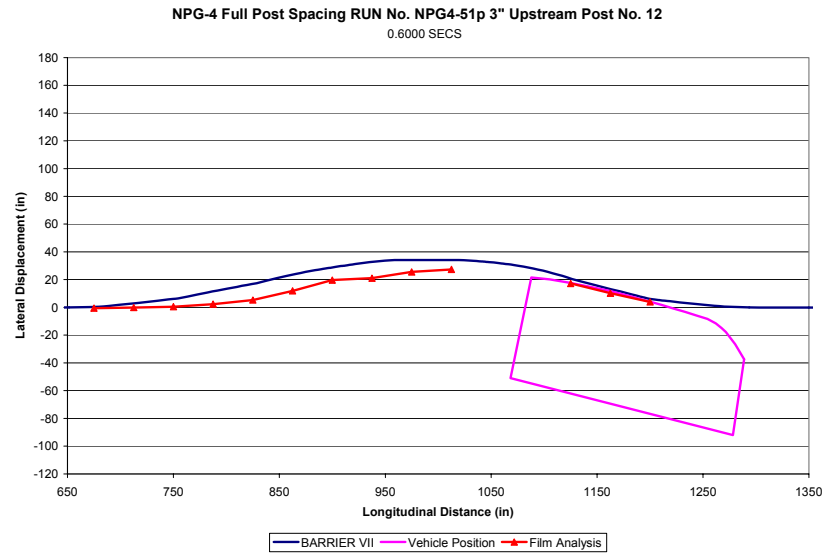


Figure 11 (continued). Sequential Figures from BARRIER VII Simulation of NPG-4



**Figure 11 (continued). Sequential Figures from BARRIER VII Simulation of NPG-4**

BARRIER VII had some difficulty fully reproducing the guardrail shape near the upstream end of the deformed region, as shown in Figure 11. However, it should be noted that during the actual test, the vehicle's rear end pitched up and protruded over the rail during redirection. Since BARRIER VII is limited to planar motion, it is unable to reproduce roll and pitch angular motions. Therefore, it would calculate greater vehicle tail slap into the barrier, thus potentially increasing the predicted barrier displacements in this region.

A second validation method incorporates different evaluation parameters. Tabulated validation results for vehicle behavior, barrier displacements, and working width for the calibration are listed in Table 7.

**Table 7. Working Width, Vehicle Behavior, and Barrier Displacements for NPG-4**

Evaluation Parameters	Results Comparison	
	1905-mm Post Spacing	
	Test No. NPG-4	Simulation
Parallel Time (ms)	396	332
Dynamic Rail Deflection (mm)	1094	1054
Working Width (mm)	1260	1391*
Working Width Indicator	Hood Corner	Post*
Exit Time (ms)	597	536
Exit Angle (degrees)	8.8	9.9
Exit Velocity Vector (degrees)	19.4	13.2
Resultant Velocity at Exit (km/hr)	55	56

\*Although the post was the working width indicator, it is unlikely that the post would remain attached to the rail for that displacement. Thus, the working width is governed by the engine/hood corner intrusion, the estimated working width would be 1235 mm.

The most observable difference between the simulation and physical test are the parallel (396 ms versus 332 ms, respectively) and exit times (597 ms versus 536 ms, respectively). This 10% difference in exit time can be attributed to differences in film analysis and computer simulation. BARRIER VII is able to exactly detect any loss of contact from the barrier, while this may not be observable during film analysis. Closer examination of the graph at 600 ms indicates this may be the case, as the truck still appears to be in contact, although it is known not to be. The 16% parallel time difference is likely due to the inability to predict pitch and roll,

leading to a quicker redirection (this will be discussed later). The other observable difference is in the exit velocity vector (19.4 degrees for the physical test versus 13.2 degrees for the simulation). This 32% difference can be attributed to the 2-D limitation previously discussed, leading to the under prediction of the exit vector.

As stated previously, the anchor behavior was of particular importance. The calibration of the anchor was achieved by calculating the difference between the simulation and the film analysis coordinates of post no. 10, in both the x and y directions, at each time step, as shown in Figure 12.

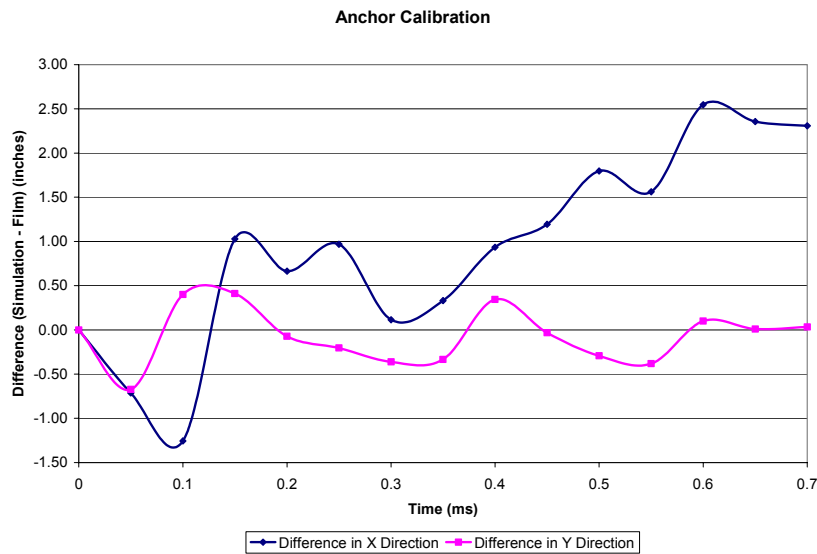


**Figure 12. Anchor Calibration - Difference in Coordinates (X and Y) between the Simulation and Film Analysis**

The behavior of the farthest visible upstream target compared to the simulation is very good in the y direction (within  $\pm 0.5$  in.). This minimal difference can be attributed to the exactness of the simulation coordinates and the objective film analysis coordinates. The behavior in the x direction is not as good. However, the difference is within an acceptable  $\pm 1.0$  in. for the first 300 ms. The difference after the parallel time can be attributed to the method by

which the vehicle was redirected by BARRIER VII, as compared to that of the physical test discussed previously.

In addition to the graphical comparisons shown previously, further validation was obtained with comparisons of the longitudinal and lateral accelerations, as well as with changes in the vehicle's velocity between the final validated NPG-4 simulation and the physical test. Therefore, the same SAE filtering procedures outlined in NCHRP Report No. 350 were applied to the simulation data in order to obtain CFC 60 (100 Hz) vehicle accelerations and CFC 180 (300 Hz) changes in velocity and on data acquired with the same sample rate. The results of this comparison are shown in Figure 13.

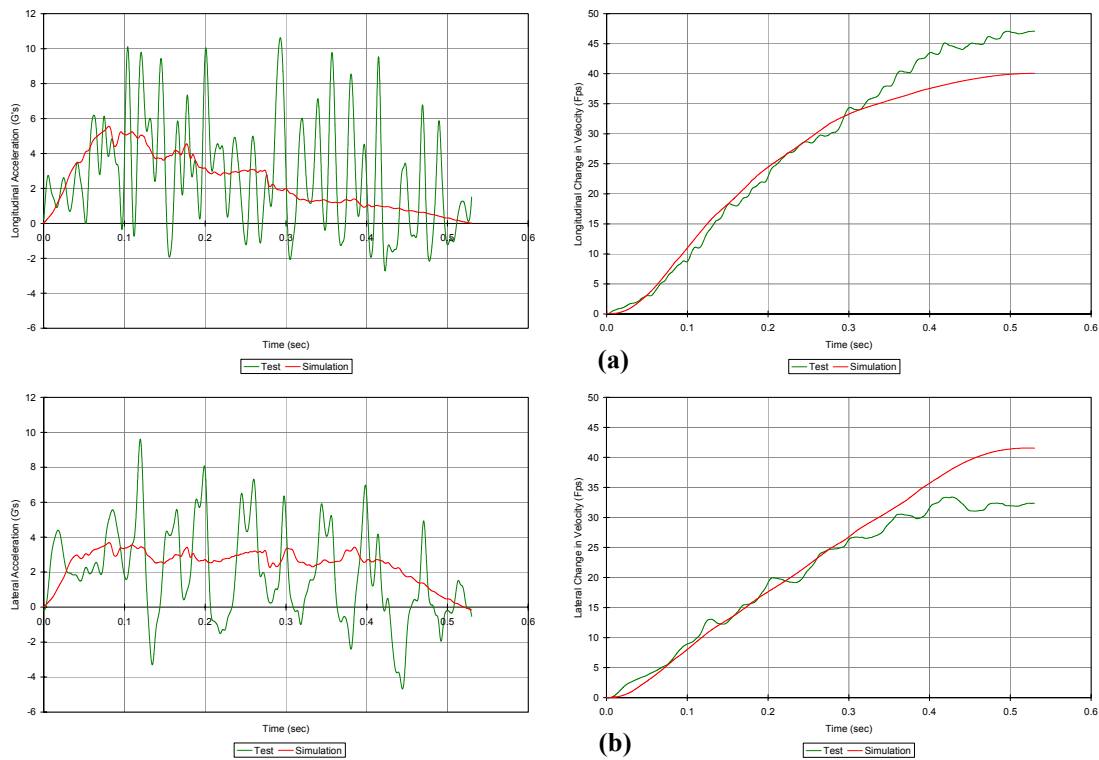


**Figure 13. Comparison of Test and Simulation Results: (a) Longitudinal Direction and (b) Lateral Direction**

BARRIER VII generally predicted the acceleration trends but could not predict peaks in either the longitudinal and lateral directions. While peak accelerations could not be reproduced,

changes in vehicle velocity were shown to be reasonably accurate through approximately 300 ms or close to a vehicle parallel condition, again in both directions.

Another validation for the baseline model can be made through the examination of the vehicle yaw in the simulation and the physical test. The yaw is measured as the change in angle of the vehicle's trajectory. The results of this comparison are shown in Figure 14.

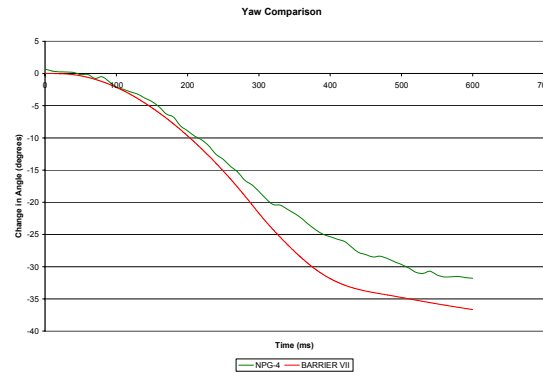


**Figure 14. Comparison of Test and Simulation Results of Yaw Data**

As with the velocity and acceleration comparisons, the simulation was able to predict the vehicle yaw observed during the full-scale vehicle crash test for the first 300 ms. This difference after parallel time can be attributed to the redirection of the vehicle in BARRIER VII as compared to the crash test. After parallel time in the simulation, the rail profile matches well with that of the film analysis. However, due to the 2-D limitations, the vehicle was redirected along that path, where during testing the vehicle was able to roll and pitch and did not fully follow the path of the rail.

From these validation efforts, researchers determined that the final simulation accurately predicted barrier performance and vehicle behavior for the standard-post spacing configuration and could be used in the flare rate study. Although the validation effort was complete with the available data, there remained other output data from BARRIER VII that were deemed important and useful. These simulation results are discussed in the following section.

#### **4.1.5. Further Analysis of the MGS Model**

Further analysis of the BARRIER VII output was also believed capable of revealing potential problems to be later observed during physical crash testing. These potential problems were not obvious and therefore required further post-processing of the results as well as some engineering judgement.

##### **4.1.5.1. Rail Tension Forces**

Another method used to quantify the impact was to investigate the rail tension forces determined by BARRIER VII. Examination of the tension forces provided an understanding of the rail behavior during the impact and its influence on vehicle redirection. The rail tension forces also provided information for the potential rupture of the guardrail, which would result in the failure of the test.

The tension force in the guardrail, along with the corresponding deflections, at 50 ms intervals, is shown in Figure 15. For each plot, the darkened line represents the tension force throughout the rail. The scale for the tensile force is on the left vertical axis. The lighter curve represents the barrier deflection. The scale for the deflection is on the right vertical axis. Both curves are plotted according to the barrier member number and are related to the length along the rail, but they are not drawn to scale since member lengths vary.

The most noticeable feature of the tension forces is the stepwise appearance of the tensile forces. Each “step” represents a section of rail between two posts. This indicates that the posts are carrying a portion of the load, thus reducing the force on the next section of guardrail. The run of the “steps” from member nos. 1 to 35 and 139 to 172 was shorter than that of member nos. 36 to 138 due to the number of grid points between the posts, but the rise is comparable.

The sharp decrease of the peak force in the downstream direction was due to the interaction of the guardrail and the truck. The deflection of the barrier system puts the entire rail in tension. Then, due to the friction between the vehicle and the guardrail, the vehicle pulls on the upstream anchor, while it pushes on the downstream end. Thus, this vehicle-to-barrier interaction results in the difference in the tensile forces upstream and downstream of the impact region.

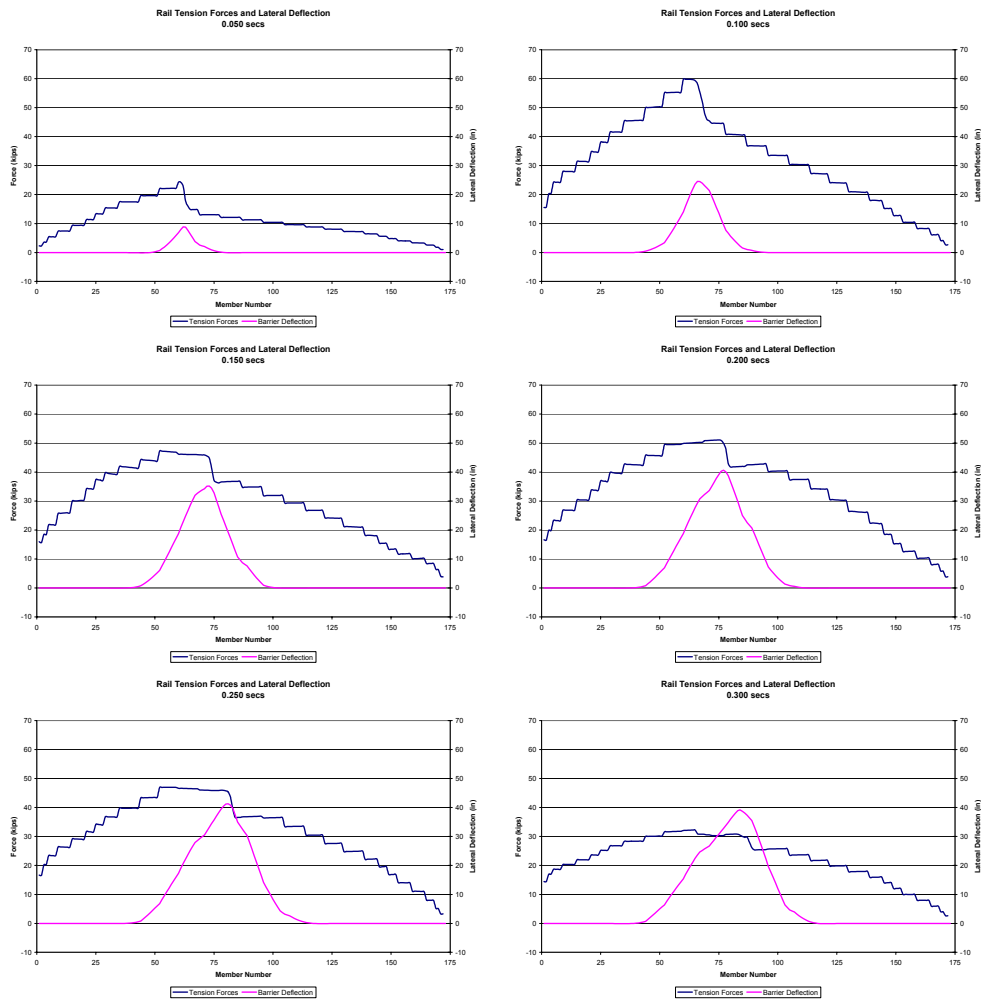


**Figure 15. Rail Tension Forces and Corresponding Rail Deflections**

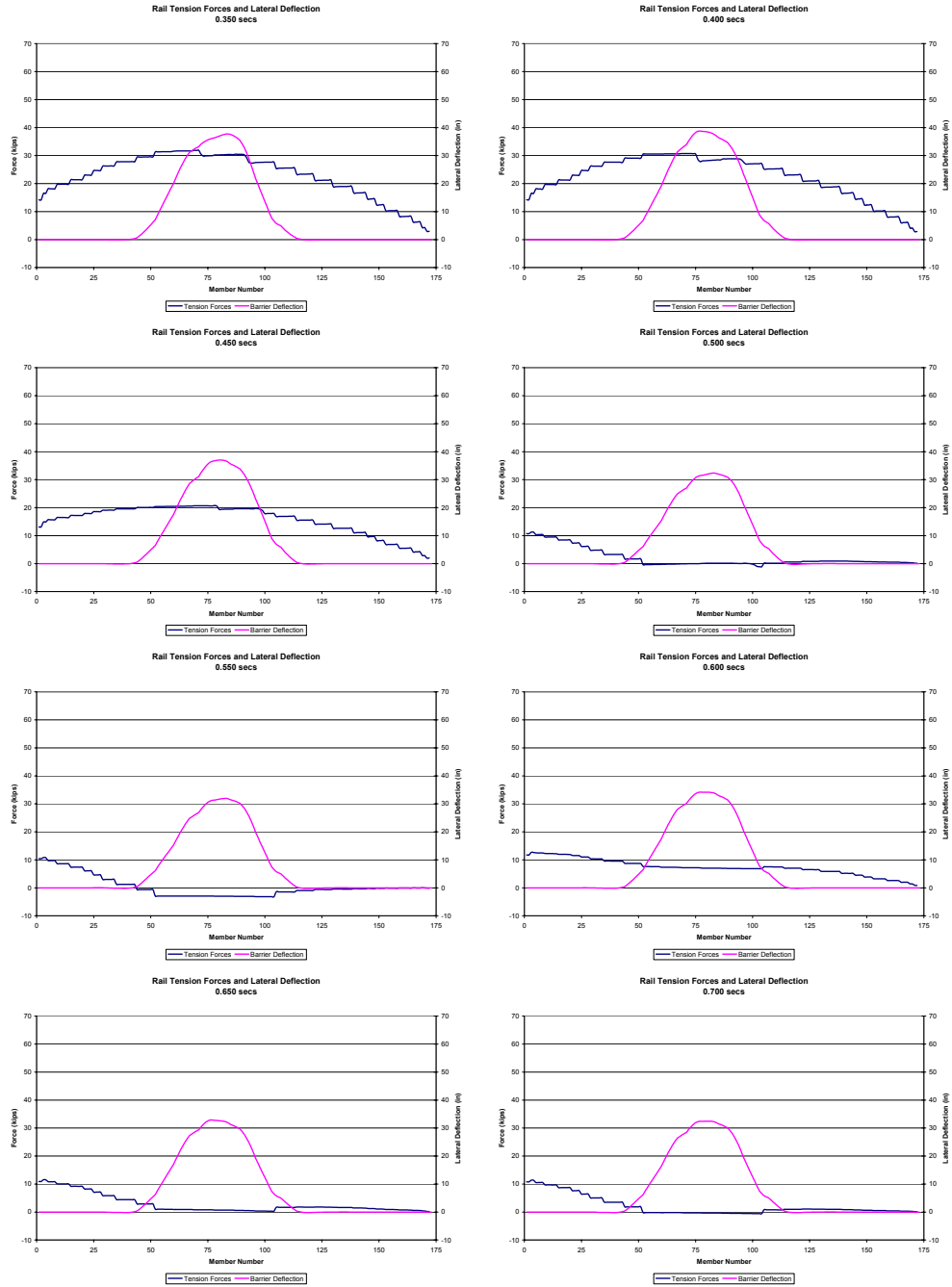


**Figure 15 (continued). Rail Tension Forces and Corresponding Rail Deflections**

The tension forces were observed to decrease as the vehicle was captured and redirected. At 500 ms, the tension forces in the rail were negligible due to the truck exiting the guardrail along the deformed section of rail and having minimal interaction with the rail. However, there existed some tension at the upstream end. The tension force is a result of the posts in this region

yielding plastically (observed in the BARRIER VII output file, indicated by the code number), thus resulting in the permanent tension in the rail.

Tension forces through cross sections of the rail revealed how and when loads were transmitted through the rail during the simulation. For the NPG-4 simulation, the forces through rail element nos. 1, 25, 50, 75, 100, 125, 150, and 172 are shown in Figure 16. Element nos. 1, 25, and 50 are upstream of the impact region, element nos. 75 and 100 are in the impact region, and element nos. 125, 150, and 172 are downstream of the impact region. In reality, the forces might not directly correspond to the simulated behavior, due to the presence of slots in the guardrail at post locations as well as differences between a real and simulated vehicle.

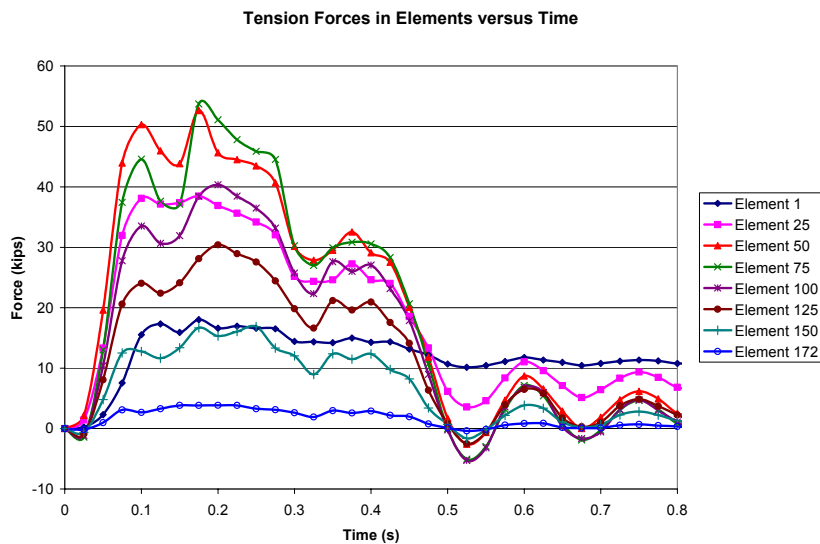


**Figure 16. Tension Forces at Selected Rail Elements versus Time**

An interesting feature of the tension forces was the oscillating behavior of the forces after the truck had exited the system at 0.536 s. This behavior is an indication that BARRIER VII is still calculating the tension forces in the rail after loss of contact with the truck and is trying to reach a steady-state value, resulting in the permanent set deflections of the rail. This behavior, as provided in Figure 11, has shown that the shape of the rail changes even after the pickup was no

longer in contact with the barrier. The rail has damped out the majority of the oscillations after 1.2 seconds. As before and shown in Figure 15 and Figure 16, there was an indication of the permanent tension in the rail due to the deformation that had occurred, even in regions where the posts were not observed to yield or fail.

In order to quantify the tension force in the rail, it was important to examine the maximum tension force in the rail throughout the simulation, as shown in Figure 17. The maximum force was obtained by measuring the rail tension force in all the members and recording the maximum value at each time step.

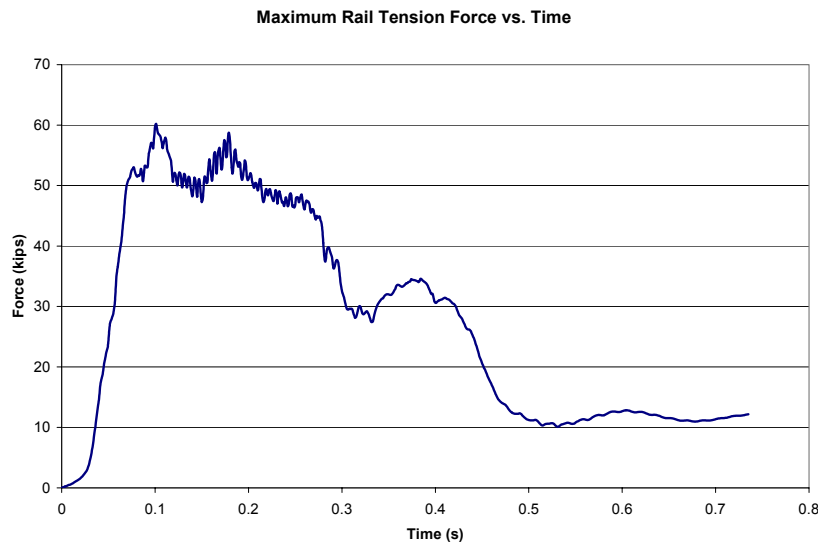


**Figure 17. Maximum Tension Force in the Rail During the Simulation**

Furthermore, an examination of the maximum rail the tension force provided an indication of insignificant risk for guardrail rupture. The maximum tensile force during the simulation was found to be 60.21 kips. Guardrail rupture during the simulation can be detected when the tension forces exceed the tensile capacity of the guardrail. Calculation of the tensile capacity for the typical W-beam cross-section (no slots) revealed a tensile capacity of 99.5 kips. Calculation of the tensile capacity at post bolt slot locations along the W-beam section revealed a

tensile capacity of 95.4 kips. Testing of the guardrail splice by Worcester Polytechnic Institute (WPI) revealed a tensile capacity of 90.0 kips at splice locations [22]. Thus, the tension force is well under the allowable force levels. However, guardrail rupture has been observed during full-scale vehicle crash testing where the axial loads remained relatively small [23]. Thus, W-beam failure during a full-scale crash test is likely the result of a complex loading condition, in combination with stress concentrations, and would require a more complex program to completely evaluate the stress in the guardrail.

#### **4.1.5.2. Wheel Snag**

Another potential problem associated with vehicle-to-post interaction is wheel snag. Wheel snag was defined as the amount of overlap between a tire and a post. The degree of wheel snag on the guardrail posts was determined by the overlap of a vehicle's front wheel and a barrier post and at a specified height above ground. MwRSF researchers believe that a wheel snag condition can result in the failure of the barrier system due to vehicle roll over or due to rail rupture. A wheel snag criterion has also been shown to control the critical impact point (CIP) for continuous longitudinal barriers [24] and approach guardrail transitions [25-33]. It was therefore beneficial to calculate the wheel snag for the flare rate study. This analysis was completed by running a secondary program using a combination of the rotation point of the post below ground, post deflection, and tire position at the time of contact with the post in order to check for potential wheel snag problems. The resulting comparison between film analysis results and those obtained from the BARRIER VII simulation are listed in Table 8.

**Table 8. Wheel Snag Analysis Results**

	Calculations from BARRIER VII Output						
	Film	Simulation	Snag	Post X	Post Y	Post dx	Post dy
	(sec)	(sec)	(in.)	(in.)	(in.)	(in.)	(in.)
Post 13 (Node 69)	0.0960	0.0930	1.76	897.34	25.74	0.34	10.34
Post 14 (Node 78)	0.1900	0.1750	9.57	973.23	33.03	1.23	17.63
Post 15 (Node 87)	0.2820*	0.2620	9.47	1048.36	33.03	1.36	17.63
Post 16 (Node 96)	0.3790*	0.3570	0.97	1122.62	26.73	0.62	11.33

\* Film time was obtained from Mini DV and is therefore a close approximation.

The information output from the wheel snag analysis consisted of the location of the front, upstream edge of the post at ground level in the x- and y-directions, Post X and Post Y, respectively. Also provided was the displacement of the front, upstream edge of the post at ground level, again in the x- and y-directions, Post dx and Post dy, respectively. The locations and displacements are given at the time of wheel snag detection, which is also provided during the wheel snag analysis. The most important result from this analysis was the snag value, or the amount of overlap between the wheel and the front, upstream edge of the post in inches.

The simulation was able to accurately predict the occurrence of wheel snag observed in the physical test. In order to examine the potential for problems associated with wheel snag, it was important to examine the snag value and the post dy value. From the simulation results, there existed a potential for the vehicle to snag on post nos. 13, 14, 15, and 16. However, the degree of overlap is small for post nos. 13 and 16. Therefore, the potential for problems associated with wheel snag are minimal for these two posts. For post nos. 14 and 15, the snag was much more pronounced; however, the Post dy value was greater than 15 in. Previous research with the crash testing of guardrails has indicated that the post becomes disengaged from the W-beam at around 15 inches or more of displacement [34]. As such, this failure deflection was specified in the BARRIER VII input deck. Therefore, the potential for significant problems

associated with wheel snag are slightly reduced if the top of the post are no longer attached to the rail by the post bolt.

This analysis provided further validation of the model as well as provided an indication of the potential for wheel snag.

#### **4.1.5.3. Vehicle Vaulting**

The potential for the vehicle to ride up a post and vault over the rail is another potential problem identifiable with this post processing. It is likely during the flare rate study that this behavior may occur due to the large vehicle penetrations expected into the barrier system. This analysis was completed by tracking the location of the posts, the position of the vehicle, and using some engineering judgement to determine the potential for vaulting.

As before, the amount of wheel overlap was important, since the overlap distance serves as an indicator for the potential for the vehicle to ride up the post. It is unlikely during situations with significant overlap that the post will not yield or rotate in the soil, considering the mass of the 2000P test vehicle and the strength of the W152x13.5 (W6x9) posts. However, at times near the initiation of redirection, the potential for vaulting exists in situations with small overlap. This situation arose in the simulation at post no. 13 (node 69) at 0.096 sec, although vaulting did not occur in the physical test. The difference between the simulation and the physical test results were attributed to differences in the guardrail mounting height. The MGS has a top mounting height of 787 mm (31 in.), while the NCHRP 350 W-beam and standard height, strong post, W-beam systems have a top mounting heights of 706 mm and 686 mm (27.78 in. and 27 in.), respectively. Thus, due to the additional 76.2 mm (3 in.) plus in top mounting height over the

other guardrail configurations, it was better able to capture and redirect the vehicle, thus preventing vaulting from occurring.

#### **4.1.5.4. Vehicle Pitch and Roll – Auto-Barrier Contact Forces**

The BARRIER VII calibration effort has validated the simulation results to the available physical test results. However, it has been previously stated that BARRIER VII has limitations. With only a 2-D analysis, it was difficult, if not impossible, to predict the amount of vehicle pitch or roll in a computer-generated impact simulation. These two behaviors are coupled and are only available from a three dimensional simulation program. Although it would be beneficial to have the pitch and roll data available in BARRIER VII, it is not necessary for the calibration of the model nor for the validity of the results stated thus far. A suggestion for the calculation of vehicle roll is suggested below, but is not performed due to the impracticality of the analysis at this time.

It is believed that vehicle roll may possibly be calculated using the auto-barrier contact force. The force magnitudes in the longitudinal and lateral directions are provided in the output file for the nodes that are in contact. These forces could then be used, in combination with the known rail height (or calculated rail height after the impact has begun) and the center-of-gravity height of the vehicle, in order to predict the amount of vehicle roll.

The auto-barrier contact forces may possibly serve as a basis for further determination of vehicle vaulting. The analysis resulting from the auto-barrier contact forces could also provide the basis for comparing the Midwest Guardrail System to the 706 mm (27.78 in.) high, W-beam guardrail system as well as evaluating different flare rates for each configuration.

#### 4.1.5.5. Pocketing

The potential for vehicle pocketing was another problem that could be evaluated with post processing. During the flare rate study, it was likely that this behavior would occur due to the large vehicle penetrations expected into the barrier system. This analysis was completed by tracking the slope of the guardrail in advance of the automobile. The maximum slope for the simulation was 0.270, as shown in Figure 18. Slopes of 0.425 and higher have generally lead to problems during previous research [35]. Typically, high guardrail slopes lead to a roll over condition with the standard height guardrail and W-to-thrie beam transitions. However, the guardrail slope indicator was used in a similar manner for the determination of guardrail pocketing until a better criterion exists. Therefore, pocketing was not determined to be a potential problem associated with this simulation.

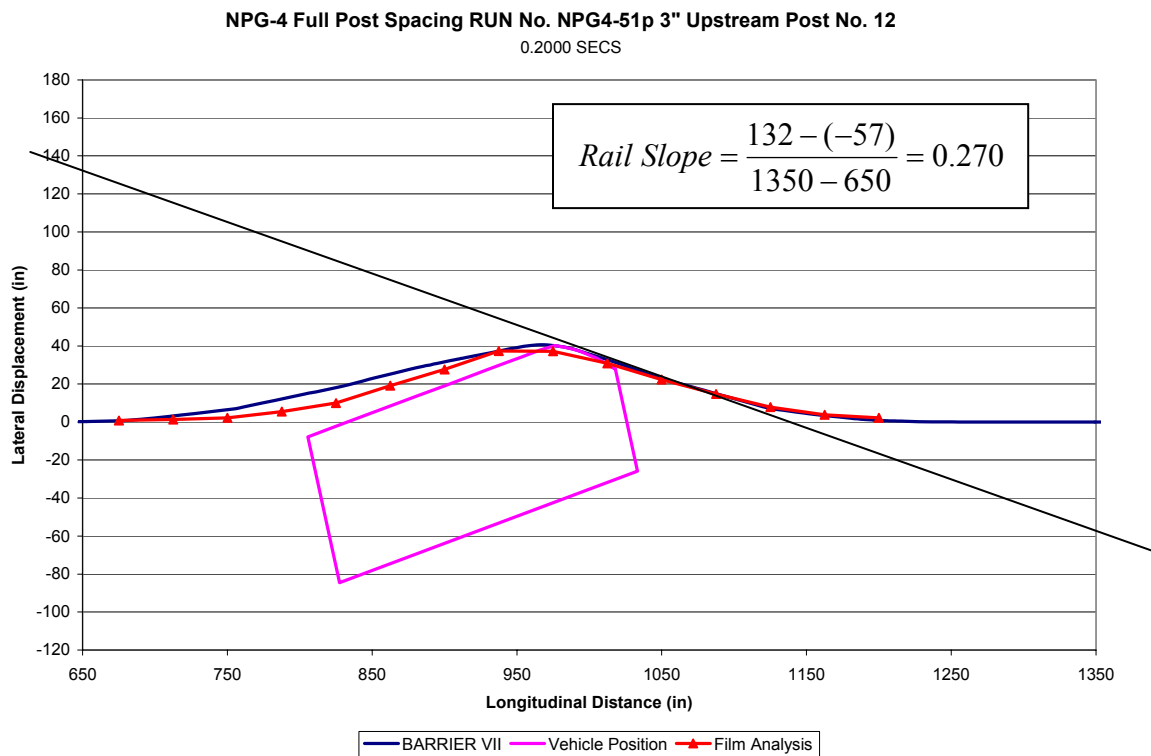


**Figure 18. Maximum Potential for Vehicle Pocketing**

Furthermore, the criterion for evaluating potential pocketing was believed to also be capable of revealing a potential for the vehicle to climb the rail. As the rail slope increases in advance of the vehicle, the potential for the vehicle to climb the rail also increases. Therefore, the potential for vehicle climbing will be evaluated using the same slope criterion.

#### **4.1.5.6. Energy Balance**

The energy balance analysis also serves as an important source of information as it provides an indication of the energy distribution in the system. This energy balance will vary depending upon the barrier configuration, member properties, and time within a given impact simulation. Thus, the information can serve as a useful comparison tool when analyzing various impact scenarios and between different flare rate systems. The energy balance for test no. NPG-4 simulation is listed in Table 9 at 0.536 sec after impact (exit).

**Table 9. Energy Balance for NPG-4 Simulation (0.536 sec)**

TYPE OF ENERGY		PERCENT OF ORIG AUTO K.E.
TRANSLATIONAL K.E. OF AUTO =		42.4
ROTATIONAL K.E. OF AUTO =		2.1
BARRIER K.E. =		0.1
ELASTIC ENERGY IN MEMBERS		
BEAMS =		0.3
POSTS =		0.5
INELASTIC WORK ON MEMBERS		
BEAMS =		4.5
POSTS =		10.3
ELASTIC ENERGY IN AUTO =		0
INELASTIC WORK ON AUTO =		3
DAMPING LOSSES =		6.9
AUTO-BARRIER FRICTION LOSS =		29.6
AUTO-PAVEMENT FRICTION LOSS =		1.9
SUM OF ALL CONTRIBUTIONS =		101.7

#### 4.1.6. Conclusions for the MGS Model

Calibration and validation of the MGS baseline model was achieved by tuning specific BARRIER VII member properties to match the barrier profiles from the simulation and the physical test. Further validation was achieved through comparisons made between the accelerometer and high-speed film results. As such, the MGS model was calibrated and validated.

It has also been shown that further analysis may be beneficial. Potential problems that cannot be readily observed in the BARRIER VII output are apparent after additional post processing. The potential for the tearing of the guardrail was examined by plotting the rail tension forces. Examination of the tension forces in the rail was also made as the vehicle was

redirected. Wheel snag was also accurately predicted from the BARRIER VII simulation. It was found that wheel snag and other vehicle to post interaction occurred, although it did not pose a significant risk to the successful capture and redirection of the impacting vehicle. It was stated that pitch and roll may be beneficial to the analysis of the simulation and prediction of undesirable behaviors, but it was determined to be impractical at this time. Finally, because vehicular impacts into guardrail systems are essentially energy management problems, it is important to track the energy balance of the system, which can provide a useful comparison tool when analyzing various impact scenarios.

#### **4.1.7. The MGS Baseline Model**

The calibrated and validated element properties were then used to create the MGS baseline model for use in the flare rate study. The baseline model differed from the calibration/validation model due to the impact conditions. For the calibration/validation model, the impact conditions were the same as those of test no. NPG-4. The baseline model for the flare rate study incorporated an impact condition consisting of a 2,000-kg pickup truck with an impact angle of 25.0 degrees and an impact velocity of 100 km/h (62.14 mph).

## **4.2. The Standard NCHRP 350 Strong-Post, W-Beam BARRIER VII Model**

### **4.2.1. Introduction**

The development of the standard NCHRP Report 350 strong-post, W-beam guardrail system BARRIER VII baseline model was completed by applying similar techniques used during the creation of the baseline model of the Midwest Guardrail System (MGS). Previously, it was determined to model the modified G4(1S) W-beam guardrail system for the flare rate study. The

full-scale vehicle crash test used for calibration was test no. 405421-1, as performed by the Texas Transportation Institute (TTI). For test no. 405421-1, a 2,076-kg pickup truck impacted the modified G4(1S) guardrail system at 101.5 km/h and 25.5 degrees. These impact conditions fall within the allowable range for the successful evaluation of the barrier's performance. The data acquired from the overhead high-speed film was used to calibrate the model to the physical test.

#### **4.2.2. Development of the Modified G4(1S) Model**

A finite element model of the modified G4(1S) guardrail system was developed for use in BARRIER VII. The model has a total of 191 nodes, 220 members (190 beam members and 30 post members), 7 different beam types, and 7 different post types. The model has a total length of 175 ft. The BARRIER VII input deck is listed in Appendix B.

The seven different types of beam members correlated to the seven different discretization lengths used, while all the other properties remain the same. The beam member length was reduced from 37.5 in. at the ends to 4.6875 in. near posts in the impact region. A typical beam member length in the impact region was 9.375 in, resulting in 8 or 9 members between posts. The impact region consisted of 3 posts upstream and 9 posts downstream of the impact location. The rail was attached to posts through a common node every 75 in.

Five different post types were used in the modeling of the MELT anchorage used to anchor the upstream end of the system. Two of the post types were used to represent the first two anchor posts. The third post type represented the three CRT posts and the fourth post type represented the single 6"x8" wood post. The fifth post type represented the W152x12.6 (W6x8.5) system posts implemented into the guardrail system and evaluated by test no. 405421-

1. The final two post types consisted of the two BCT posts (anchor posts) on the downstream end of the system. The ground-line strut and cable were not modeled for simplicity. Thus, the anchor post strength was given particular attention.

#### 4.2.3. Calibration of the Modified G4(1S) Model

For the calibration effort, several simulations were performed at the impact conditions of test no. 405421-1 in order to tune selected BARRIER VII input parameters. For the posts, initial parameters were obtained from previous BARRIER VII simulations and dynamic post testing [21]. The other calibrated parameter was the post failure displacement. The values are provided in Table 10.

**Table 10. BARRIER VII Simulation Parameters**

BARRIER VII Parameters		Initial Input Values	405421-1 Final Validation Run Values
<b>K<sub>B</sub> – Post Stiffness Along B (strong axis)</b>	<b>kN/mm (kip/in.)</b>	1.056 (6.030)	1.056 (6.030)
<b>K<sub>A</sub> - Post Stiffness Along A (weak axis)</b>	<b>kN/mm (kip/in.)</b>	0.701 (4.002)	0.701 (4.002)
<b>M<sub>A</sub> - Moment About A (strong axis)</b>	<b>kN*mm (kip*in.)</b>	19299 (170.81)	17645 (156.17)
<b>M<sub>B</sub> - Moment About B (weak axis)</b>	<b>kN*mm (kip*in.)</b>	12297 (108.84)	12297 (108.84)
<b>δ<sub>F</sub> - Failure Displacement Along B</b>	<b>mm (in.)</b>	381 (15)	356 (14)

Using the parametric technique based on experience gained from the MGS calibration, input parameters were adjusted to replicate the full-scale vehicle crash test.

#### 4.2.4. Validation of the Modified G4(1S) Model

One important validation method is the graphical comparison of the simulation and physical crash test barrier profiles. The input parameters are determined to be calibrated if BARRIER VII is capable of accurately predicting the actual dynamic barrier profiles. The dynamic barrier profiles were obtained from the overhead film analysis. A graphical comparison

of the simulated and actual barrier displacements for test no. 405421-1 are provided in Figure 19. The final validated BARRIER VII input parameters are provided in Table 10.

BARRIER VII had some difficulty fully reproducing the guardrail shape near the downstream end of the deformed region, as shown in Figure 19. However, it should be noted that during the actual test, post no. 16 (at 1,050 inches) was observed to be displaced significantly but did not fail. As such, the post was observed to rotate laterally to near its original position. This behavior was not believed to be repeatable in the BARRIER VII simulation effort unless an individual post type was specified at each post location to replicate such behaviors. The objective of this validation as well as subsequent baseline model development was to simulate general guardrail system behavior.

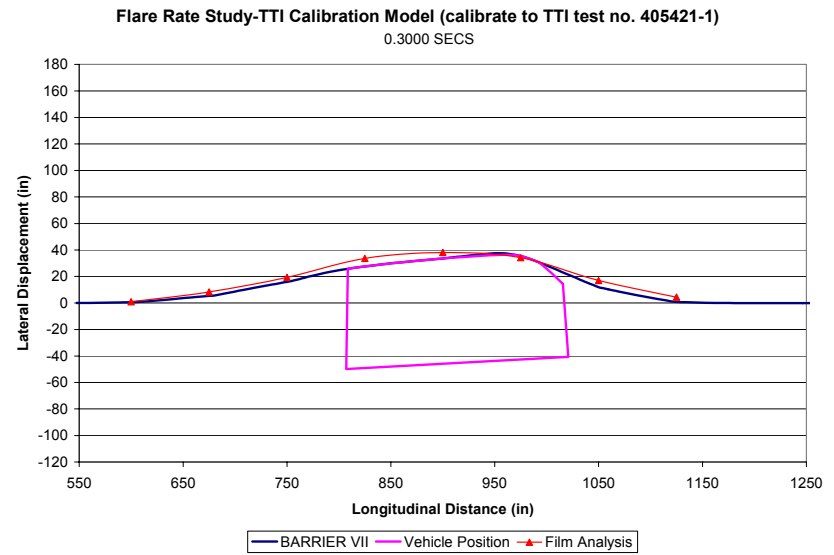
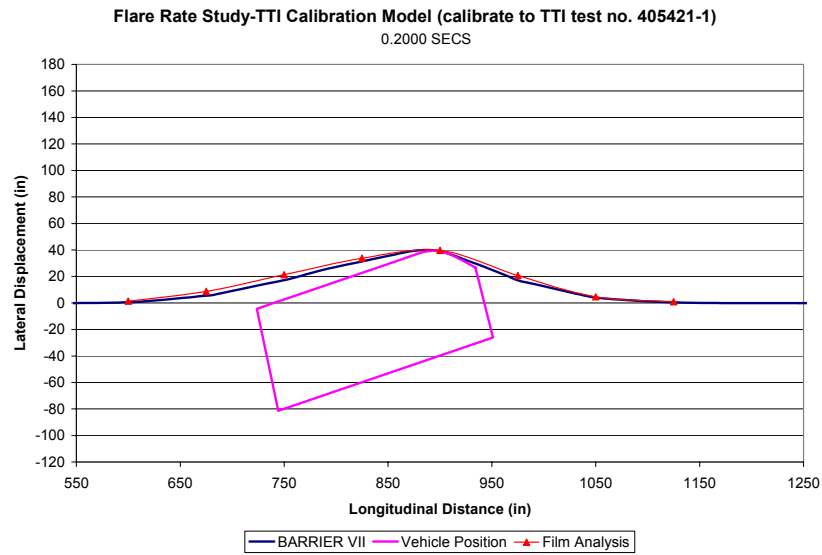
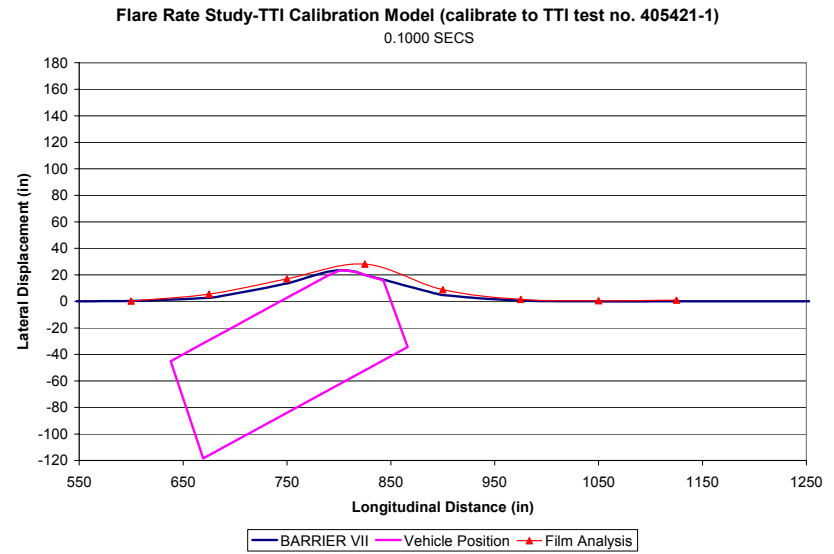
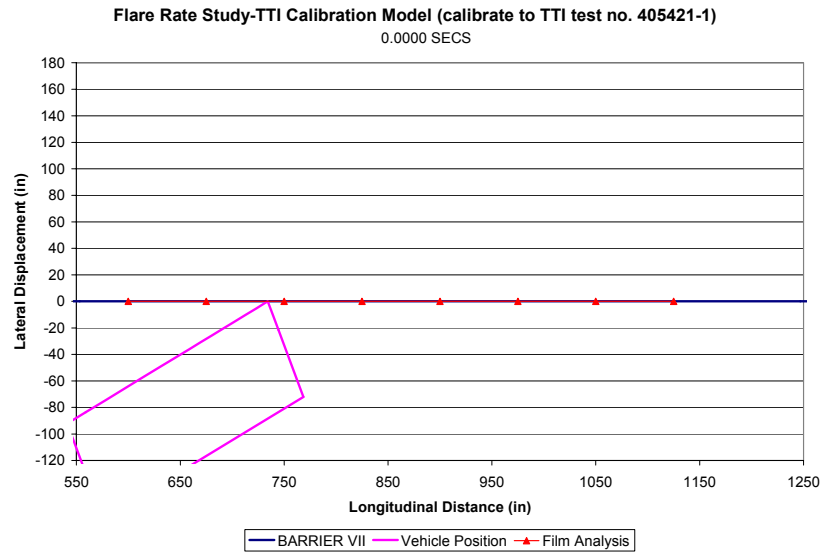


**Figure 19. Sequential Figures from BARRIER VII Simulation of TTI test no. 405421-1**

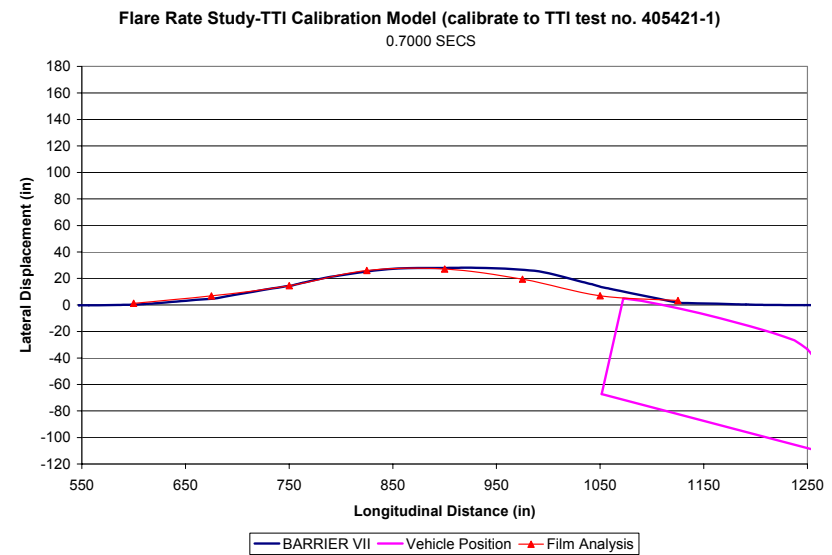
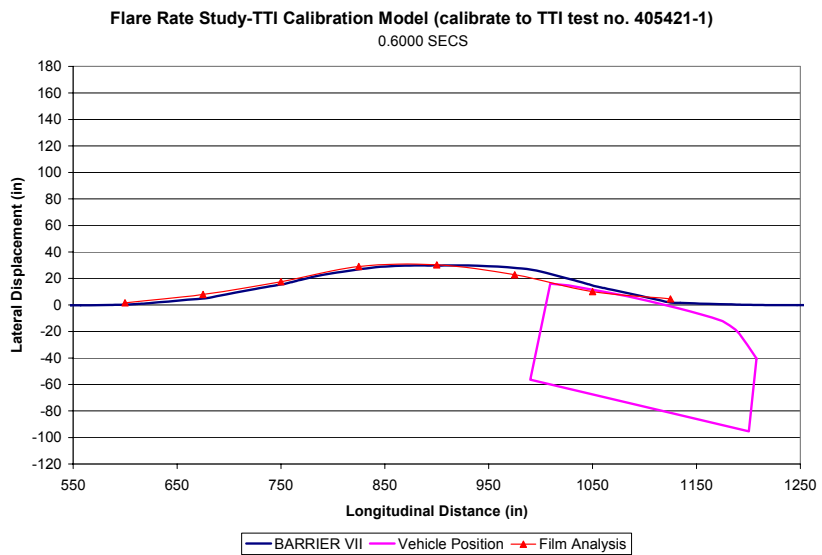
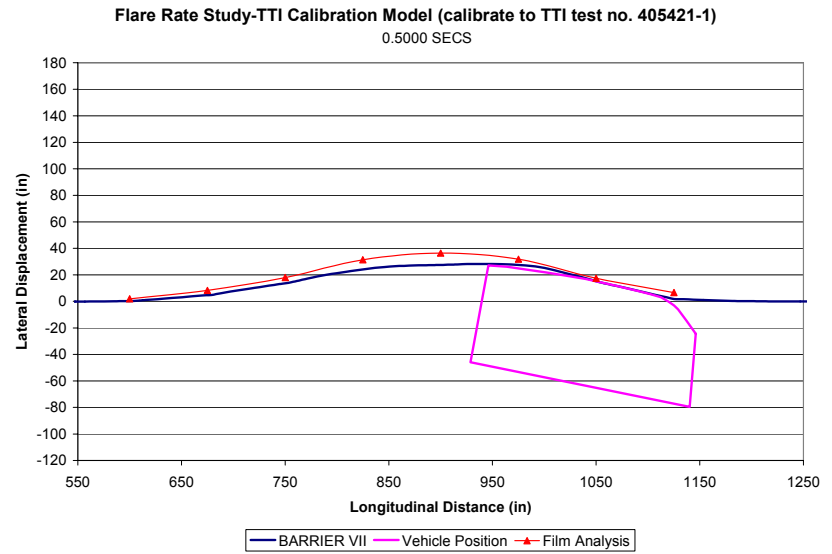
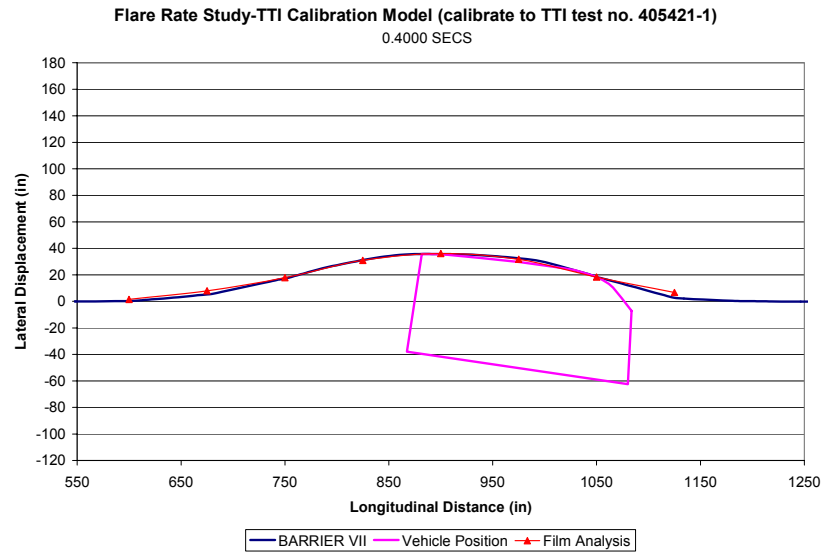


Figure 19 (continued). Sequential Figures from BARRIER VII Simulation of TTI test no. 405421-1

A second validation method incorporates different evaluation parameters. Tabulated validation results for vehicle behavior, barrier displacements, and working width for the calibration are listed in Table 11.

**Table 11. Vehicle Behavior and Barrier Displacements Comparison for Test No. 405421-1**

Evaluation Parameters	Results Comparison	
	Test No. 405421-1	Simulation
Parallel Time (ms)	278	320
Dynamic Rail Deflection (mm)	1000	1051
Exit Time (ms)	557*	522
Exit Velocity Vector (degrees)	16.0	12.5
Resultant Velocity at Exit (km/hr)	55	58

\*Exit time is based on film analysis done at MwRSF; the reported exit time was 691 ms.

The most observable difference between the simulation and physical test results were the parallel (278 ms versus 320 ms, respectively) and exit times (557 ms versus 522 ms, respectively). The 6% difference in exit time was attributed to differences in the film analysis and computer simulation results. BARRIER VII was capable of exactly detecting any loss of vehicle contact from the barrier, while loss of contact may not be immediately discernable during film analysis. Closer examination of the simulation results at 600 ms indicated this may be the case, as the truck still appears to have just lost contact with the barrier, although contact was not detected by BARRIER VII. The 15% parallel time difference was likely due to the increased maximum rail deflection, allowing for a later parallel time. The other observable difference was the exit velocity vector (16.0 degrees for the physical test versus 12.5 degrees for the simulation). This 22% difference was attributed to the 2-D limitation previously discussed in the MGS baseline model development, leading to the under prediction of the exit vector.

Previously, in addition to the graphical comparisons shown, further validation was obtained with comparisons of the longitudinal and lateral accelerations as well as changes in the vehicle's velocity between the final validated simulation and that of the physical test. However,

this information was not available due to the physical test being run at another crash test facility. Thus, these results were not presented.

From the validation efforts, researchers determined that the final simulation accurately predicted barrier performance and vehicle behavior for the modified G4(1S) guardrail system and could be used in the flare rate study. Although the validation effort was completed with the available data, there remained other output data from BARRIER VII that were deemed important and useful. These are discussed in the following section.

#### **4.2.5. Further Analysis of the Modified G4(1S) Model**

Further analysis of the BARRIER VII simulation results were also believed capable of revealing potential problems to be later observed during physical crash testing. These potential problems were not obvious and therefore required further post-processing of the results as well as some engineering judgement. This analysis was identical to that completed for the MGS and as such, much of the discussion is similar.

##### **4.2.5.1. Rail Tension Forces**

Another method used to quantify the impact was to investigate the rail tension forces determined by BARRIER VII. Examination of the tension forces provided an understanding of the rail behavior during the impact and its influence on vehicle redirection. The rail tension forces also provided information for the potential rupture of the guardrail, which would result in the failure of the test.

The tension force in the guardrail, along with the corresponding deflections, at 50 ms intervals, is shown in Figure 20. For each plot, the darkened line represents the tension force

throughout the rail. The scale for the tensile force is on the left vertical axis. The lighter curve represents the barrier deflection. The scale for the deflection is on the right vertical axis. Both curves are plotted according to the barrier member number and are related to the length along the rail, but they are not drawn to scale since member lengths vary.

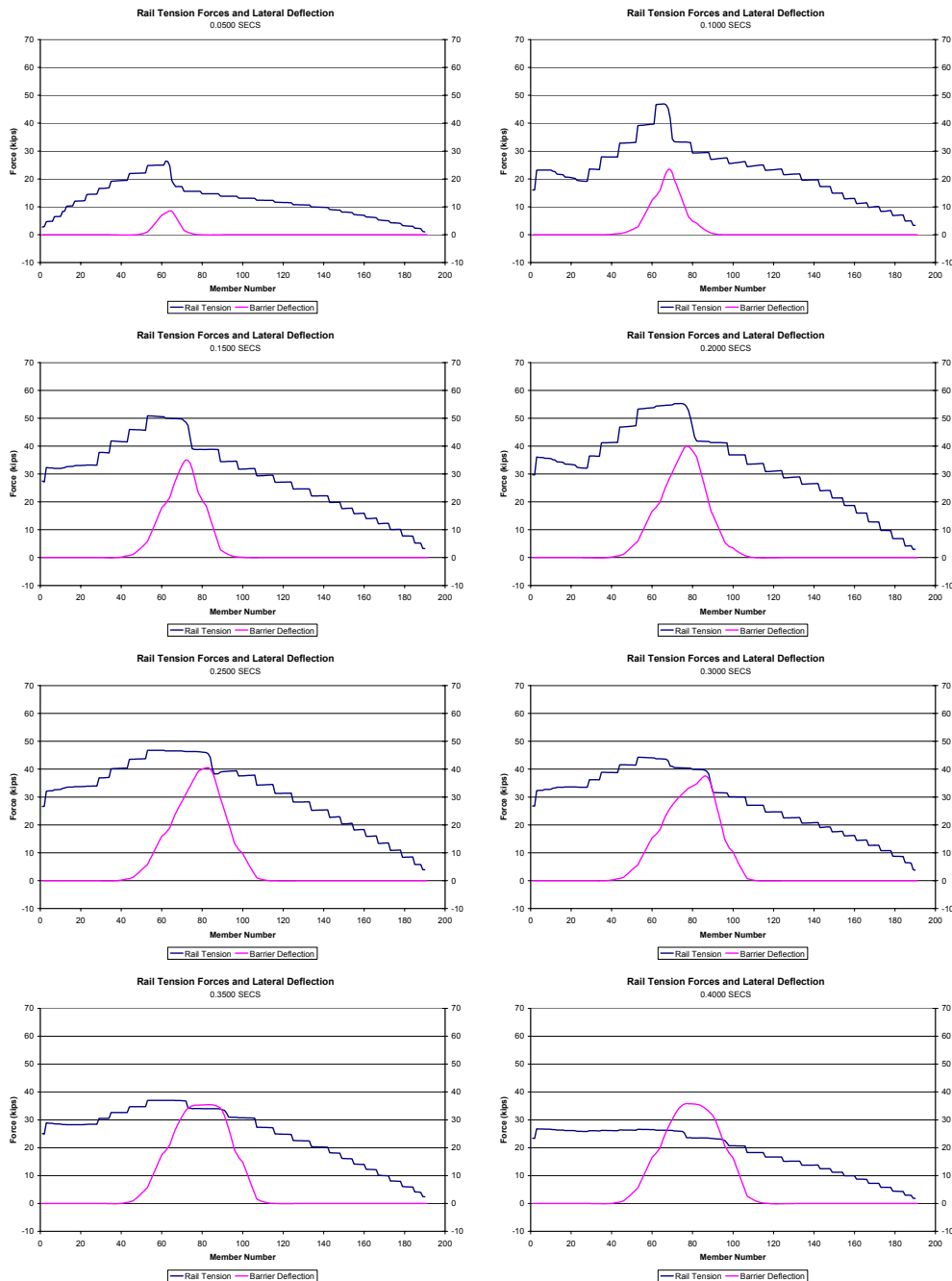


**Figure 20. Rail Tension Forces and Corresponding Rail Deflections**

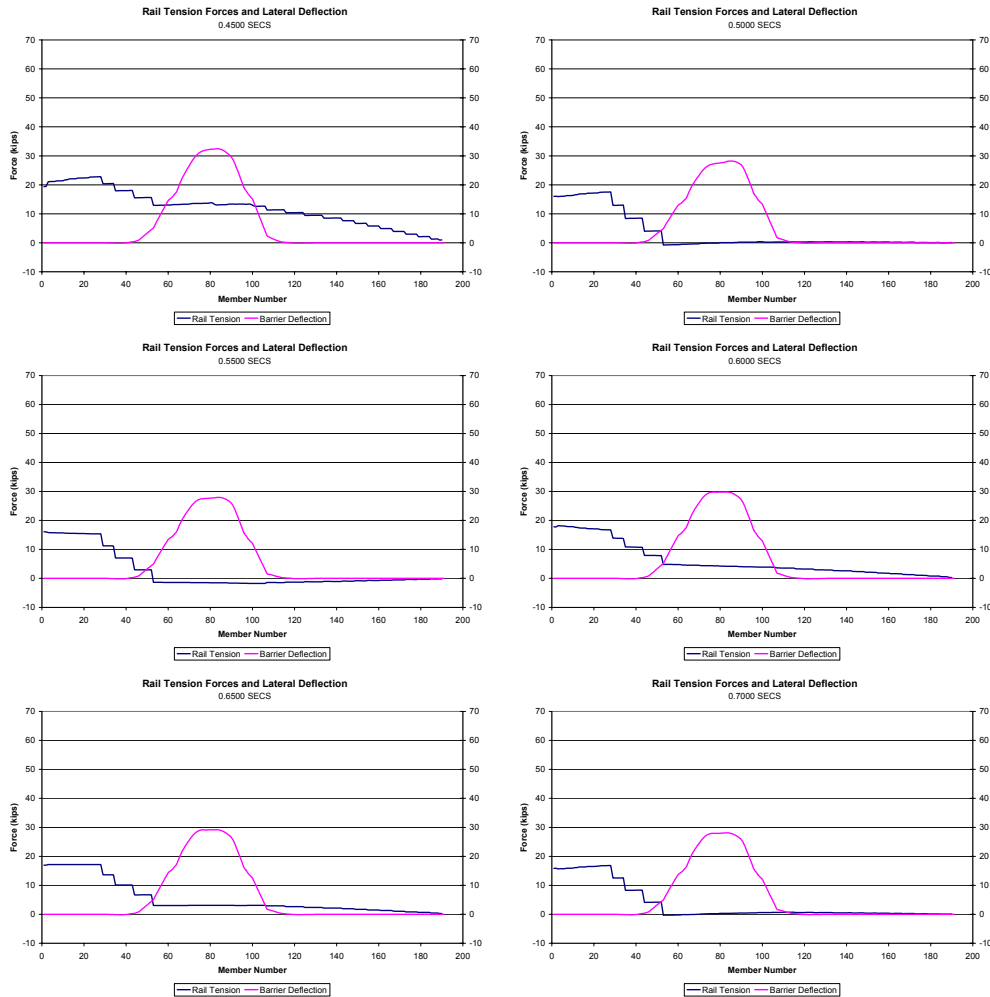


**Figure 20 (continued). Rail Tension Forces and Corresponding Rail Deflections**

The tension forces were observed to decrease as the vehicle was captured and redirected. At 500 ms, the tension forces in the rail were negligible due to the pickup truck exiting the guardrail along the deformed section of rail and having minimal interaction with the rail. However, there existed some tension at the upstream end. The tension force is a result of the posts in this region yielding plastically (observed in the BARRIER VII output file, indicated by the code number), thus resulting in the permanent tension in the rail.

Tension forces through cross sections of the rail revealed how and when loads were transmitted through the rail during the simulation. For the simulation, the forces through rail

element nos. 1, 25, 50, 75, 100, 125, 150, 175, and 190 are shown in Figure 21. Element nos. 1, 25, and 50 are upstream of the impact region, element nos. 75 and 100 are in the impact region, and element nos. 125, 150, 172, and 190 are downstream of the impact region. In reality, the forces might not directly correspond to the simulated behavior, due to the presence of slots in the guardrail at post locations as well as differences between a real and simulated vehicle.

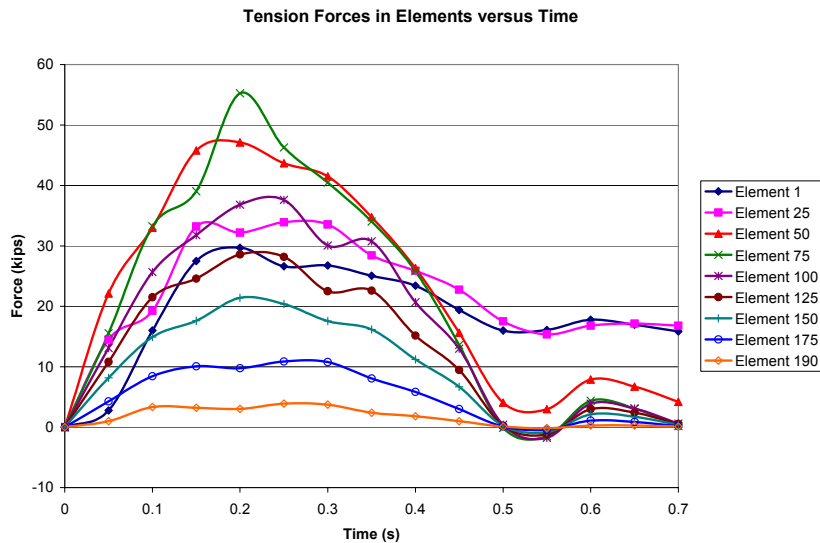


**Figure 21. Tension Forces at Selected Rail Elements versus Time**

As before and shown in Figure 20 and Figure 21, there was an indication of the permanent tension in the rail due to the deformation that had occurred, even in regions where the posts were not observed to yield or fail. In order to quantify the tension force in the rail, it was important to examine the maximum tension force in the rail throughout the simulation, as shown in Figure 22. The maximum force is obtained by measuring the rail tension force in all the members and recording the maximum value at each time step.

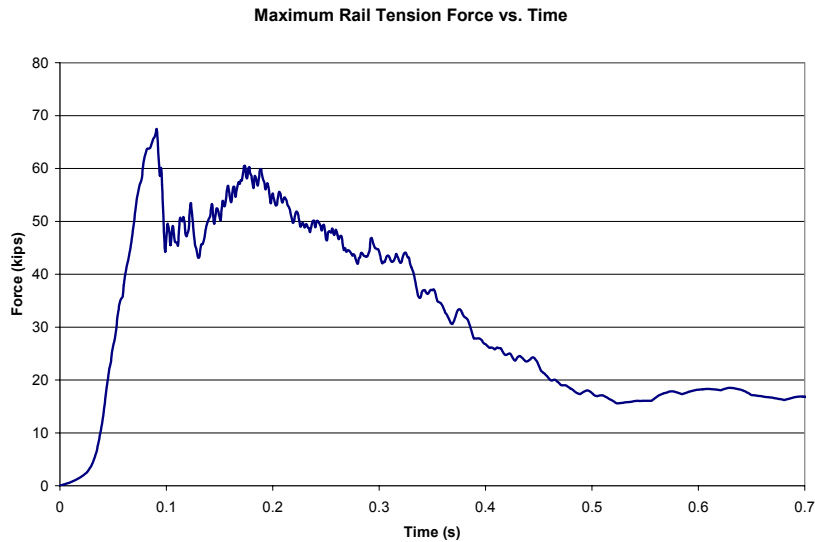


**Figure 22. Maximum Tension Force in the Rail during the Simulation**

Furthermore, an examination of the maximum rail the tension force provided an indication of insignificant risk for guardrail rupture. The maximum tensile force during the simulation was found to be 67.41 kips. Guardrail rupture during the simulation can be detected when the tension forces exceed the tensile capacity of the guardrail. Previous research and discussion revealed a tensile capacity of 90.0 kips at splice locations and 95.4 kips at non-splice locations. Thus, the tension force is well under the allowable force levels. However, guardrail rupture has been observed during full scale crash testing where the axial loads remained relatively small. Thus, W-beam failure during a full scale crash test is likely the result of a complex loading condition, in combination with stress concentrations, would require a more complex program to completely evaluate the stress in the guardrail, since the splice is located at post locations.

#### 4.2.5.2. Wheel Snag

Another potential problem associated with vehicle to post interaction is wheel snag. Wheel snag is defined as the amount of overlap between a tire and a post. The degree of wheel snag on the guardrail posts was determined by the overlap of a vehicle's front wheel and a barrier post and at a specified height above ground. MwRSF researchers believe that a wheel snag condition can result in the failure of the barrier system due to vehicle roll-over or due to rail rupture. A wheel snag criterion has also been shown to control the critical impact point (CIP) for continuous longitudinal barriers and approach guardrail transitions. It was therefore beneficial to calculate the wheel snag for the flare rate study. This analysis was completed by running a secondary program using a combination of the rotation point of the post below ground, post deflection, and tire position at the time of contact with the post in order to check for potential wheel snag problems. The resulting comparison between film analysis results and those obtained from the BARRIER VII simulation are listed in Table 12.

**Table 12. Wheel Snag Analysis Results**

	Calculations from BARRIER VII Output						
	Film	Simulation	Snag	Post X	Post Y	Post dx	Post dy
	(sec)	(sec)	(in.)	(in.)	(in.)	(in.)	(in.)
<b>Post 13 (Node 71)</b>	0.107	0.103	7.63	822.55	23.47	0.55	12.07
<b>Post 14 (Node 80)</b>	0.178	0.183	13.32	898.52	30.48	1.52	19.08
<b>Post 15 (Node 89)</b>	0.278	0.268	11.81	973.53	29.39	1.53	17.99
<b>Post 16 (Node 98)</b>	0.364	0.364	1.98	1047.53	21.42	0.53	10.02

\* Film time was obtained from Mini DV and is therefore a close approximation.

The simulation was able to accurately predict the occurrence of wheel snag observed in the physical test. In order to examine the potential for problems associated with wheel snag, it was important to examine the snag value and the post dy value. From the simulation results, there existed a potential for the vehicle to snag on post nos. 13, 14, 15, and 16.

The degree of overlap was small for post no. 16 and therefore, the potential for problems associated with wheel snag were minimal for this post. For post nos. 14 and 15, the snag was much more pronounced; however, the Post dy value was greater than 15 in. Previous research with the crash testing of guardrails has indicated that the post becomes disengaged from the W-beam at around 15 inches of displacement. As such, this failure deflection was specified in the BARRIER VII input deck. Therefore, the potential for significant problems associated with wheel snag are slightly reduced if the top of the post is no longer attached to the rail by the post bolt.

As for post no. 13, the risk of wheel snag and problems associated with it were significant. There existed a large amount of overlap, 7.63 in., and the Post dy value of 12 in., which was not greater than the specified failure value of 15 in. Thus, the wheel snag that occurred apparently did not have a large influence on the redirection of the vehicle, although it may in other cases. An examination of the vehicle's post-crash results showed that the left-front (impact) tie rod, stabilizer bar, and upper and lower A-arms were bent, and the floorpan was buckled. The left-front (impact) tire and rim were also damaged. The vehicle damage is shown in Figure 23. The fact that the tire remained attached throughout the impact event most likely aided in the prevention of significant roll and appreciably reduced the problems associated with the wheel snag.



**Figure 23. Vehicle Damage After Test No. 405421-1 [14]**

This analysis provided further validation of the model as well as provided an indication of the potential for wheel snag. However, in this instance, the wheel snag did not cause any problems. In future simulations, comparable amounts of wheel snag will likely be considered to cause substantial problems with vehicle capture and redirection.

#### **4.2.5.3. Vehicle Vaulting**

The potential for the vehicle to ride up a post and vault over the rail is another potential problem identifiable with post processing. At times near the initiation of redirection, the potential for vaulting exists in situations with small wheel overlap or a small snag value. Instances with a snag value between 2 and 6 in. are a good indication of such an event. This situation never occurred in the simulation.

#### 4.2.5.4. Pocketing

The potential for vehicle pocketing was another problem that could be evaluated with post processing. As stated previously, slopes of 0.425 and higher have generally lead to vehicular instabilities during previous research studies with standard height guardrail and W-to-thrie beam transition, specifically roll over. However, once again here it was used to evaluate guardrail pocketing until better criteria can be developed. The maximum slope for the simulation was 0.284, as shown in Figure 24. Therefore, pocketing was not determined to be a potential problem associated with this simulation.

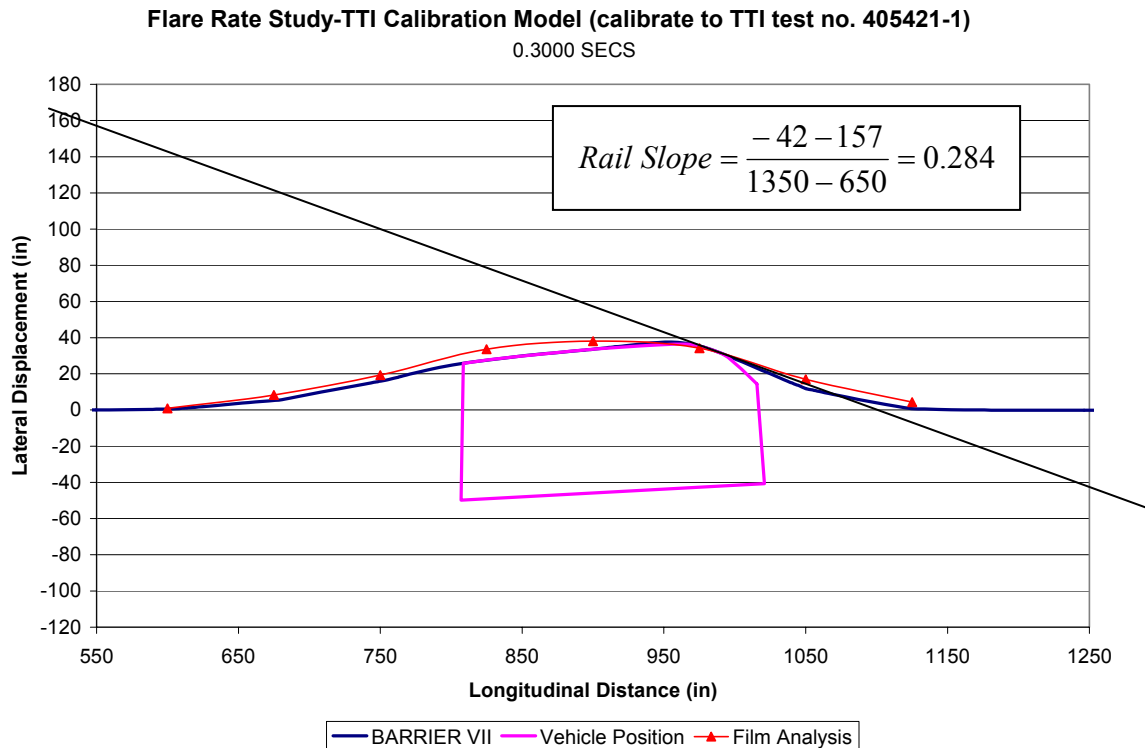


**Figure 24. Maximum Potential for Vehicle Pocketing**

Furthermore, the criterion for evaluating potential pocketing was also believed to be capable of revealing a potential for the vehicle to climb the rail. As the rail slope increases in

advance of the vehicle, the potential for the vehicle to climb the rail also increases. Therefore, the potential for vehicle climbing will be evaluated using the same slope criterion.

#### 4.2.5.5. Energy Balance

The energy balance analysis also serves as an important source of information as it provides an indication of the energy distribution in the system. This energy balance will vary depending upon the barrier configuration, member properties, and time within a given impact simulation. Thus, the information can serve as a useful comparison tool when analyzing various impact scenarios and between different flare rate systems. The energy balance for test no. 405421-1 simulation is listed in Table 13 at 0.522 sec after impact (exit).

**Table 13. Energy Balance for Test No. 405421-1 Simulation (0.522 sec)**

TYPE OF ENERGY		PERCENT OF ORIG AUTO K.E.
TRANSLATIONAL K.E. OF AUTO	=	32.5
ROTATIONAL K.E. OF AUTO	=	0.0
BARRIER K.E.	=	0.0
ELASTIC ENERGY IN MEMBERS		
BEAMS	=	0.1
POSTS	=	0.4
INELASTIC WORK ON MEMBERS		
BEAMS	=	5.4
POSTS	=	9.7
ELASTIC ENERGY IN AUTO		
INELASTIC WORK ON AUTO	=	3.8
DAMPING LOSSES		
	=	8.2
AUTO-BARRIER FRICTION LOSS		
	=	39.4
AUTO-PAVEMENT FRICTION LOSS		
	=	2.6
SUM OF ALL CONTRIBUTIONS		
	=	102.1

#### **4.2.6. Conclusions for the Modified G4(1S) Model**

Calibration and validation of the standard NCHRP 350 strong-post, W-beam guardrail system, the modified G4(1S), baseline model was achieved by tuning specific BARRIER VII member properties to match the barrier profiles from the simulation and the physical test. Validation was achieved through comparisons made between the film analysis and simulation displacements, the parallel and exit times, and the maximum deflections. As such, the standard NCHRP 350 height guardrail system model was calibrated and validated.

It has also been shown that further analysis may be beneficial. Potential problems that cannot be readily observed in the BARRIER VII output are apparent after additional post processing. The potential for the tearing of the guardrail was examined by plotting the rail tension forces. Examination of the tension forces in the rail was also made as the vehicle was redirected. Wheel snag was also accurately predicted from the BARRIER VII simulation. It was found that wheel snag and other vehicle to post interaction occurred, although it did not pose a significant risk to the successful capture and redirection of the impacting vehicle. Vehicle pocketing was also examined and found not to pose any potential problems. Finally, because vehicular impacts into guardrail systems are essentially energy management problems, it is important to track the energy balance of the system, which can provide a useful comparison tool when analyzing various impact scenarios.

#### **4.2.7. The Standard NCHRP 350 Strong-Post, W-Beam BARRIER VII Baseline Model**

The calibrated and validated element properties were then used to create the standard NCHRP 350 strong post, W-beam baseline model for use in the flare rate study. The baseline model differs from the calibration/validation model due to the impact conditions. For the

calibration/validation model, the impact conditions were the same as those of test no. 405421-1. The baseline model for the flare rate study incorporated an impact condition consisting of, a 2,000-kg pickup truck with an impact angle of 25.0 degrees and an impact velocity of 100 km/h (62.14 mph).

### **4.3. Additional BARRIER VII Modeling – Anchor Calibration**

#### **4.3.1. Introduction**

BARRIER VII model calibration is generally completed by comparing the predicted barrier displacements to those observed during a full-scale vehicle crash test. However, the barrier displacements documented from the overhead film were generally limited to the area of contact. Therefore, it was difficult to accurately calibrate anchorage performance without an expanded viewing area or additional cameras specifically assigned to track anchor movement. As such, an additional camera was placed perpendicular to the upstream anchor for MwRSF test no. 22-14MG-1. The anchor displacement information was beneficial in the calibration of the simplified anchorage used in the baseline models for the flare rate study.

#### **4.3.2. Test Description**

MwRSF test no. 22-14MG-1 was completed on the Midwest Guardrail System (MGS) for NCHRP Project 22-14 [36]. The test was conducted to evaluate possible future impact conditions for test no. 3-11 in NCHRP Report 350. Currently, test no. 3-11 consists of a 2,000 kg pickup truck impacting at 100 km/h and 25 degrees. The proposed future impact conditions for test no. 3-11 use a 2,268 kg pickup truck impacting at 100 km/h and 25 degrees. For test no.

22-14MG-1, a 2,286 kg pickup truck impacted the system at 100.7 km/h and 26.97 degrees. The barrier successfully captured and redirected the vehicle in a safe manner.

#### 4.3.3. MGS Baseline Model

A calibrated/validated BARRIER VII model of the MGS was created for the flare rate study. Previously, the anchor behavior was calibrated based upon the predicted versus actual displacements of the farthest visible upstream target in the overhead film, as shown in Figure 25.

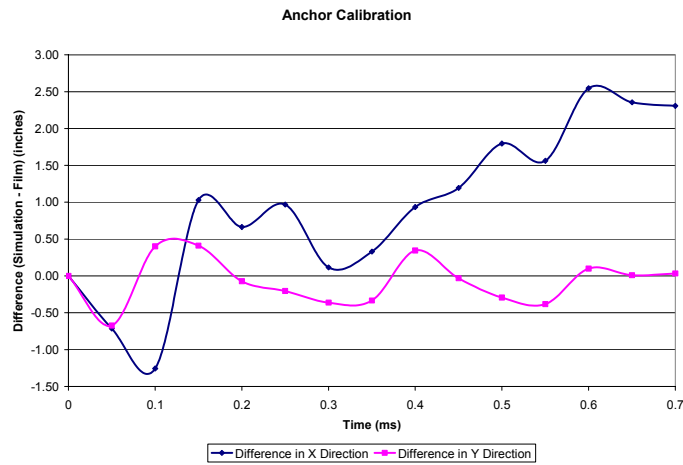


**Figure 25. Anchor Calibration - Difference in Coordinates (X and Y) between the Simulation and Film Analysis for the farthest visual Upstream Target**

This analysis, although as complete as possible with the currently available overhead film data, is not through. However, this baseline model was modified to the impact conditions of test no. 22-14MG-1, and an anchor calibration can be completed. The resulting properties were then implemented into the MGS baseline model for use in the flare rate study.

#### 4.3.4. Calibration of the MGS Model to Test No. 22-14MG-1

For the calibration effort, several simulations were performed at the impact conditions of test no. 22-14MG-1 in order to tune selected BARRIER VII input parameters. The input

parameters of particular interest were the anchor post's yielding moment and failure deflection. Close examination of the high-speed film revealed that the guardrail released from post nos. 3 through 9 between 190 and 220 ms. At this point, it was unclear why this occurred, but it was believed to be the result of the increased impact severity which caused a larger tensile load in the guardrail. As a result, significant twisting occurred in post nos. 3 through 9, in combination with poorly formed post bolt slots, caused the guardrail to release away from the posts. Therefore, a new post type definition was needed to replicate this behavior for post nos. 3 through 9. This early release also resulted in an increased loading condition on the upstream anchor. Using a parametric technique, the input parameters were adjusted to replicate the behaviors observed in test no. 22-14MG-1. The initial and final values are provided in Table 14. The BARRIER VII input deck is listed in Appendix C.

**Table 14. BARRIER VII Simulation Parameters**

BARRIER VII Parameters		Initial Input Values	22-14MG-1 Final Validation Run Values
<b>Anchor Post 1</b>			
<b>M<sub>A</sub> - Moment About A (strong axis)</b>	<b>kN*mm (kip*in.)</b>	50843 (450)	76265 (675)
<b>M<sub>B</sub> - Moment About B (weak axis)</b>	<b>kN*mm (kip*in.)</b>	50843 (450)	76265 (675)
<b>δ<sub>F</sub> - Failure Displacement Along B</b>	<b>mm (in.)</b>	254 (10)	381 (15)
<b>δ<sub>F</sub> - Failure Displacement Along A</b>	<b>mm (in.)</b>	254 (10)	381 (15)
<b>Anchor Post 2</b>			
<b>M<sub>A</sub> - Moment About A (strong axis)</b>	<b>kN*mm (kip*in.)</b>	16948 (150)	25422 (225)
<b>M<sub>B</sub> - Moment About B (weak axis)</b>	<b>kN*mm (kip*in.)</b>	11299 (100)	16948 (150)
<b>δ<sub>F</sub> - Failure Displacement Along B</b>	<b>mm (in.)</b>	177.8 (7)	381 (15)
<b>δ<sub>F</sub> - Failure Displacement Along A</b>	<b>mm (in.)</b>	177.8 (7)	381 (15)
<b>System Post Nos. 3 through 9</b>			
<b>δ<sub>F</sub> - Failure Displacement Along B</b>	<b>mm (in.)</b>	381 (15)	152 (6)
<b>δ<sub>F</sub> - Failure Displacement Along A</b>	<b>mm (in.)</b>	381 (15)	152 (6)

#### 4.3.4.1. Early Release Modeling

During calibration, two different cases were considered in order to model the early guardrail release away from the end posts: (1) a single post definition with decreased failure

deflection criteria (Option A) and (2) a two post definition at each post location, one providing the lateral support and the other providing the longitudinal support (Option B). For Option B, the failure deflection was lowered for the post providing the longitudinal support to induce the early post release. Option B was believed to be more realistic since lateral support was provided in this region even though the guardrail was released from the posts.

Although two possibilities were evaluated, it was found that both post definitions produced similar results, as shown in Figure 26. Since both options produced similar results, it was determined to use the single post definition (Option A) for simplicity.

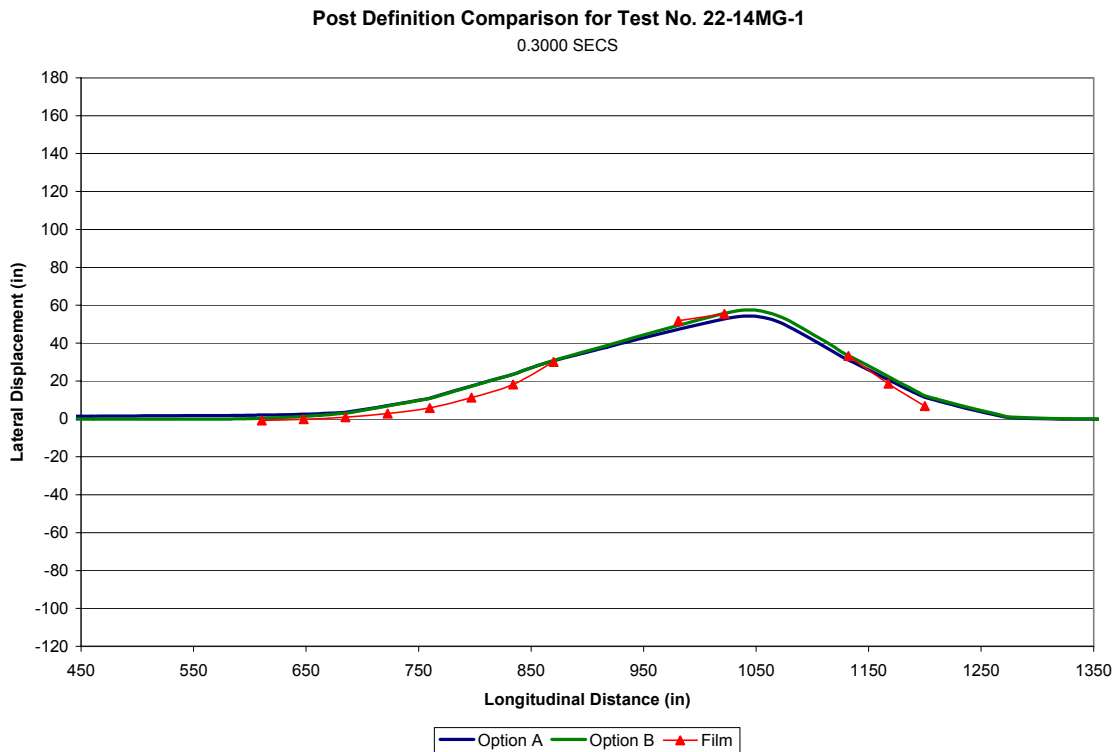


**Figure 26. Post Definition Option Comparison**

#### **4.3.5. Validation of the MGS Model to Test No. 22-14MG-1**

The validation of the BARRIER VII model was completed through a number of different measurements. For this simulation, the important parameters used in the calibration were general barrier profile, barrier and vehicle behavior, early post release, upstream anchor displacement, and wheel snag analysis. These topics are discussed in the following sections.

##### **4.3.5.1. General Barrier Profile**

As stated previously, the input parameters were believed to be calibrated if BARRIER VII was capable of accurately predicting the dynamic barrier profiles. A graphical comparison of the simulated and actual barrier displacements for test no. 22-14MG-1 is provided in Figure 27.

As with the previous MGS calibration, BARRIER VII had some difficulty fully reproducing the guardrail shape near the upstream end of the deformed region. This over prediction is similar to that observed during the calibration of test no. NPG-4 and a similar explanation is offered. The general profile of the barrier was predicted, and further discussion of the model validation is provided in the following sections.

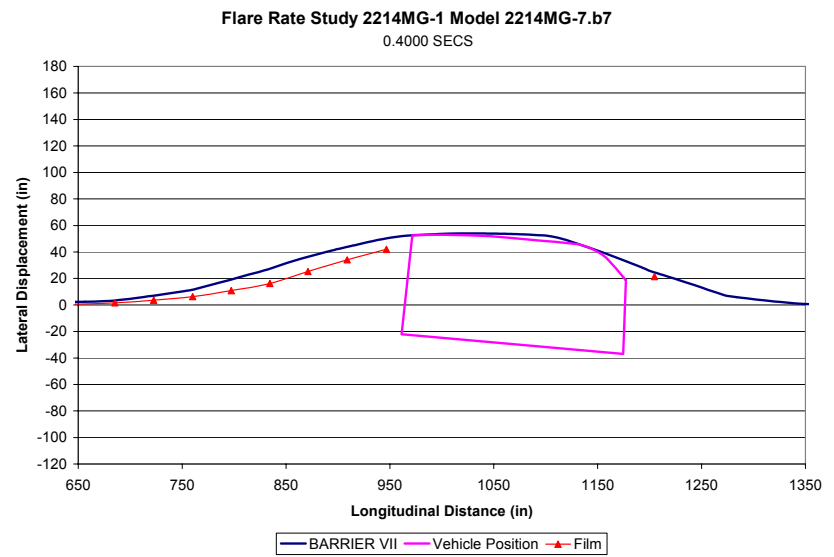
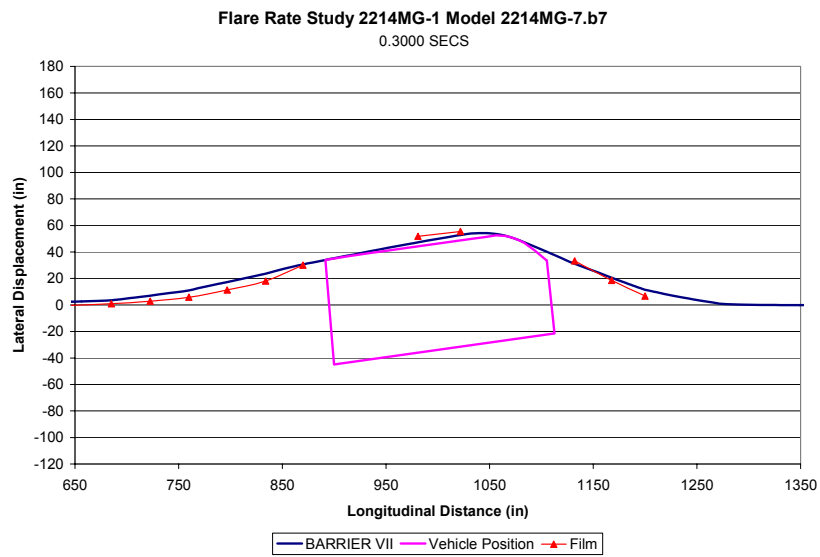
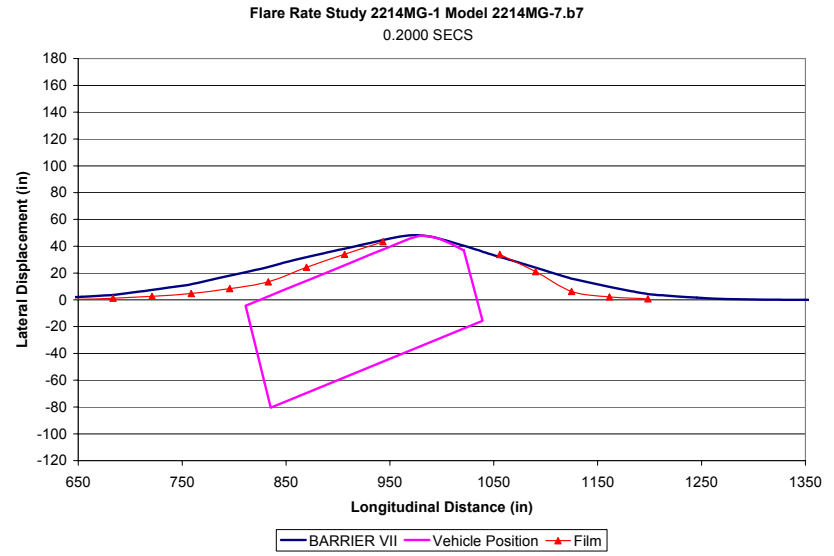
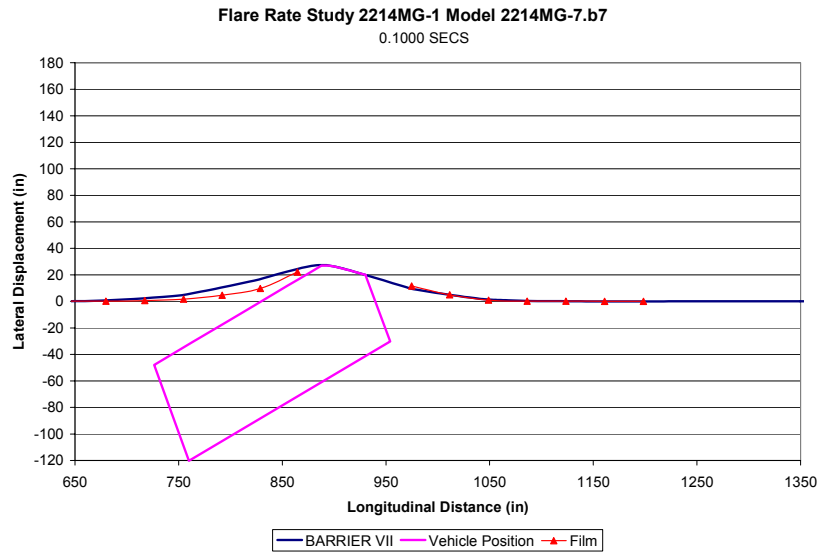


**Figure 27. Sequential Figures from BARRIER VII Simulation of Test No. 22-14MG-1**

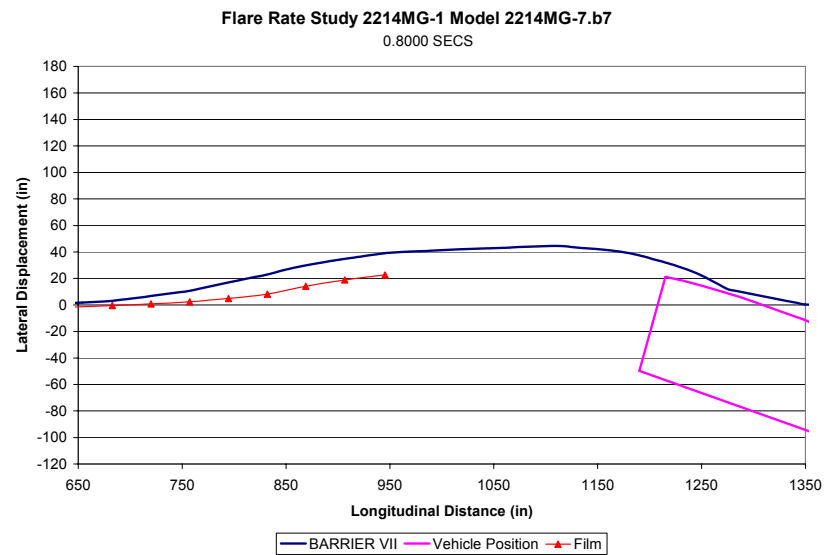
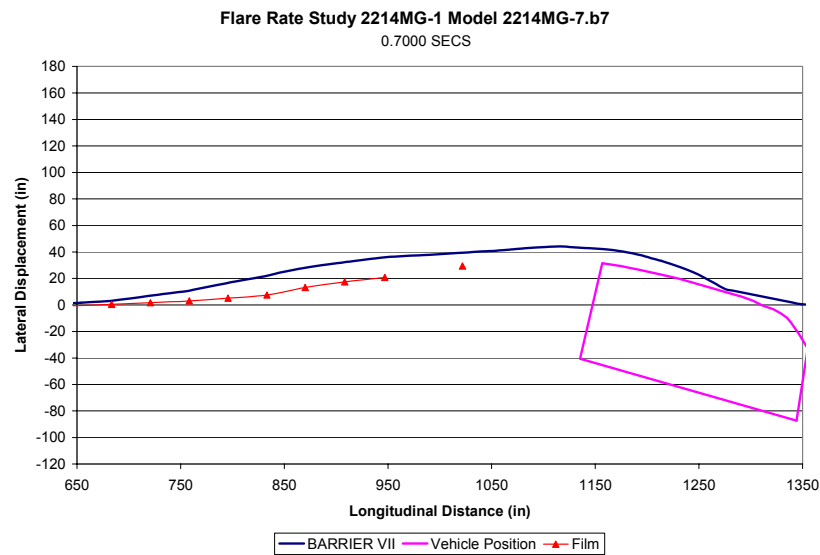
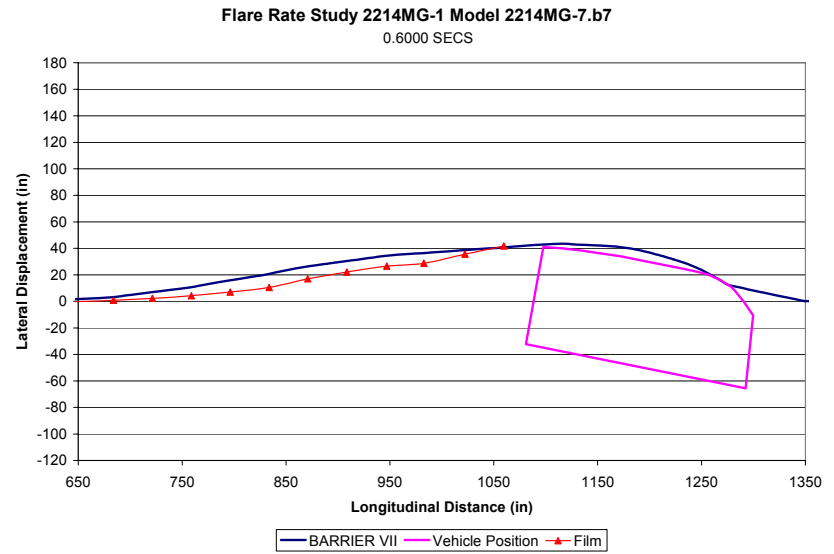
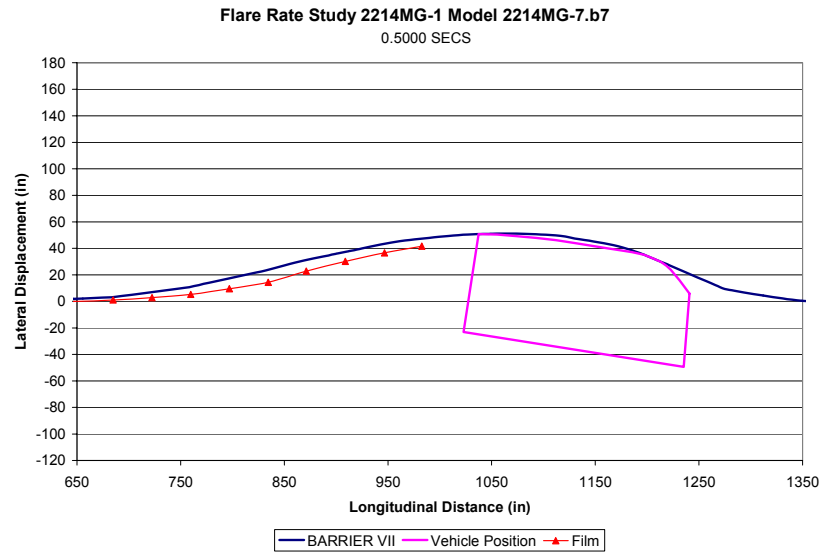


Figure 27 (continued). Sequential Figures from BARRIER VII Simulation of Test No. 22-14MG-1

#### 4.3.5.2. Barrier and Vehicle Behavior

Tabulated validation results for vehicle behavior and barrier displacements for the validation are listed in Table 15.

**Table 15. Vehicle Behavior and Barrier Displacements for 22-14MG-1**

Evaluation Parameters	Results Comparison	
	Test No. 22-14MG-1	Simulation
Parallel Time (ms)	364	353
Maximum Dynamic Rail Deflection (mm)	1447	1389
Exit Time (ms)	874	620
Exit Angle (degrees)	5 to 7*	9.7
Exit Velocity Vector (degrees)	NA**	16.1
Resultant Velocity at Exit (km/hr)	50.2	52.8

\*Angle assumed from gyro data due to truck out of view for film analysis

\*\*Truck out of view

The most observable differences between the simulation and test no. 22-14MG-1 were the exit time (620 ms versus 874 ms, respectively) and exit angle (9.7 degrees versus 5 to 7 degrees, respectively). The 29% difference in exit time was attributed to two factors. First, is the difference in the detection of loss of contact between BARRIER VII simulation and film analysis, previously discussed. As such, examination of the impact sequential figure at 800 ms of Figure 27 provided an indication that the truck was still be in contact with the barrier, although this was not the case. Second, there was significant wheel snag during redirection. This wheel snag resulted in the front end of the truck yawing toward the barrier, thus holding the vehicle in contact with the barrier for a longer period. The 28-48% over prediction in exit angle was also attributed to this observation. Later, determination of wheel snag will be calculated during post processing of the BARRIER VII results. However, it should be noted that wheel snag does not influence the redirection of the vehicle in BARRIER VII since it is only calculated after the simulation is complete.

It should also be noted that the BARRIER VII simulations were able to replicate the vehicle's parallel time and have only a 4% difference in dynamic rail deflection and a 5% difference in exit velocity.

#### **4.3.5.3. Early Post Release**

Using BARRIER VII computer simulation, early post release behavior due to twisting was replicated by lowering the failure deflection of the post in the longitudinal direction. However, it was necessary to ensure that the timing and post displacement of this release in BARRIER VII correlated with that observed during the physical crash test.

For post nos. 3 through 9, it was determined that a longitudinal failure displacement of 6 in. corresponded well with the displacement observed in test no. 22-14MG-1. From the digital video footage, the time of guardrail release occurred between 180 and 200 ms. Post failure in BARRIER VII is indicated by a code state indicator. Examination of the BARRIER VII output file indicated that post nos. 3 through 9 failed between 187 and 205 ms, corresponding well with test no. 22-14MG-1.

#### **4.3.5.4. Upstream Anchor Displacement**

During test no. 22-14MG-1, the upstream end anchorage was loaded more severely than observed in test no. NPG-4, which was used to calibrate the original MGS baseline model. This increase in loading was deemed beneficial for the flare rate study since an increase in flare rate resulted in an increase in impact severity, thus increasing the anchor loading. Furthermore, the loading that occurred during test no. 22-14MG-1 was even more critical because the guardrail tensile load was carried completely by the upstream anchor due to the early release of the

guardrail. Therefore, test no. 22-14MG-1 was used to evaluate the simplified, strong-post end anchorage used in the MGS BARRIER VII baseline and future models. The simplified, strong-post end anchorage consisted of two strong posts, but without modeling the anchor cable or groundline strut.

Calibration of this anchor was satisfied by using two measurements: (1) film analysis results from the camera placed perpendicular to the upstream end anchorage versus the simulation displacements and (2) the farthest visible upstream target in the overhead film. A maximum upstream anchor displacement of 9.51 in. was observed during the film analysis of test no. 22-14MG-1. BARRIER VII predicted a maximum displacement of 9.77 in, resulting in only a 3% difference. The difference between simulation and film for the farthest visible upstream target is shown in Figure 28.

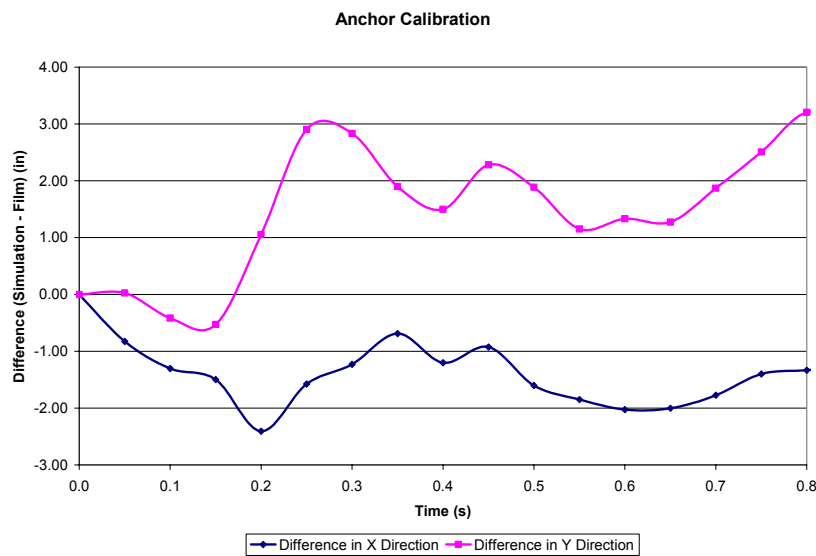


**Figure 28. Anchor Calibration - Difference in Coordinates (X and Y) between the Simulation and Film Analysis Results**

BARRIER VII had some difficulty replicating the displacements of the farthest visible upstream target. For the difference in the Y direction, even though the guardrail had released from the posts, they were able to provide lateral resistance. Conversely, after the posts failed in

BARRIER VII around 200 ms, the simulation had over-predicted the lateral displacements. The simulation under-predicted the barrier displacements in the X direction. However, near the parallel time of 364 ms, the pickup truck was in full contact with the barrier, the lateral displacement was within acceptable limits. At that time, the difference increased by an inch, due to wheel snag that occurred during the physical test, thus causing increased vehicular contact with the barrier and thus increased the guardrail displacement in the downstream direction.

#### 4.3.5.5. Wheel Snag

Tabulated validation results for vehicle behavior and barrier displacements are listed in Table 16.

**Table 16. Wheel Snag Analysis Results**

Wheel Snag Results		Calculations from BARRIER VII Output					
	Film*	Simulation	Snag	Post X	Post Y	Post dx	Post dy
	(sec)	(sec)	(in.)	(in.)	(in.)	(in.)	(in.)
<b>Post 13 (Node 69)</b>	0.1030	0.0920	3.67	897.47	26.83	0.47	11.43
<b>Post 14 (Node 78)</b>	0.1720	0.1720	13.39	973.33	36.51	1.33	21.11
<b>Post 15 (Node 87)</b>	0.2760	0.2560	15.91	1049.06	39.59	2.06	24.19
<b>Post 16 (Node 96)</b>	0.3440	0.3470	13.19	1124.20	35.71	2.20	20.31
<b>Post 17 (Node 105)</b>	0.4830	0.4530	4.92	1198.36	30.48	1.36	15.08

\* Film time was obtained from Mini DV and is therefore a close approximation.

The BARRIER VII simulation was able to accurately predict the occurrence of wheel snag observed in the physical crash test. As stated previously, this wheel snag resulted in a longer contact time and a lower exit angle. This wheel snag analysis provided further validation of the model as well as provided an indication of the potential for wheel snag.

#### 4.3.5.5. Maximum Rail Force versus Time

It was also deemed important to examine the maximum rail force versus time for the simulation, as shown in Figure 29.

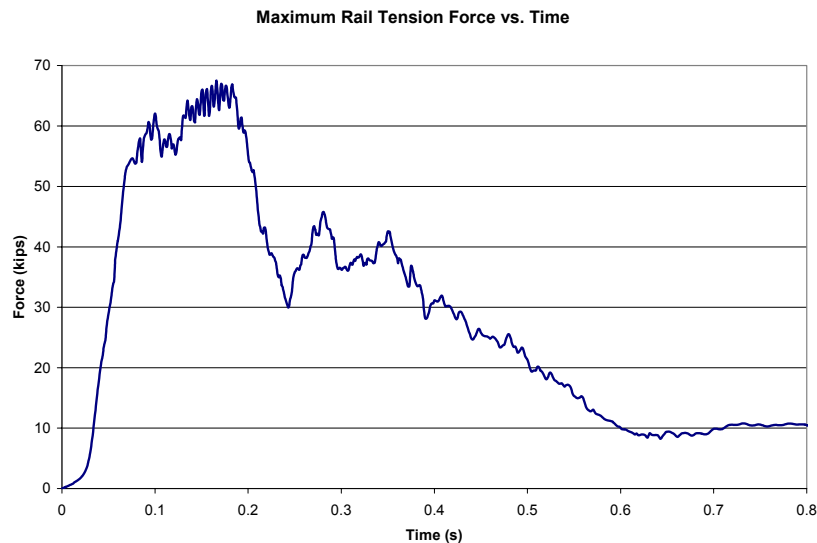


**Figure 29. Maximum Rail Tension Force Observed During the Simulation**

Examination of the maximum rail tension force revealed that the force magnitude did not exceed the force required to rupture the guardrail at a splice nor a non-splice location. The force was also observed to drop as the upstream posts failed around 200 ms in the simulation. Then, the force increased as the vehicle became parallel to the barrier, and then decreased as the vehicle exited the system.

#### 4.3.6. Conclusions for Test No. 22-14MG-1

Calibration and validation of test no. 22-14MG-1 was completed by tuning specific BARRIER VII member properties to match barrier profiles and vehicle behaviors. Resulting from this study, a calibrated and validated strong-post end anchor was developed. This anchor was capable of producing more realistic displacements than previous anchor models, and thus,

was used in the baseline MGS model for the flare rate study. This study also revealed that implementation of the anchor cable and groundline strut were not necessary and believed to cause complications in future simulation efforts.

## 5. CRITICAL IMPACT POINT SIMULATIONS

### 5.1. Introduction

Guidelines for evaluating the safety performance of roadside safety hardware have always recommended that a worst case impact scenario or CIP be selected for crash testing purposes. However, these reports gave only general suggestions regarding where a CIP on a longitudinal barrier may be located. NCHRP Report No. 350 states that the CIP is the point with the greatest potential for causing failure of the test, whether this be by excessive wheel snag, excessive pocketing, or structural failure of the device. NCHRP Report No. 350 suggests that BARRIER VII computer simulation be used to select the CIP for longitudinal barriers. As such, BARRIER VII was used in the flare rate study to determine the CIP on all of the flare rates in order to evaluate the differences in performance of the barrier under these worst case impact conditions.

The flared impact simulations were completed by increasing the impact angle of the vehicle in the baseline model, effectively resulting in a flared guardrail system. Impact angles for the different flare rates were determined by adding the angle of the flare rate to the 25 degree impact angle provided by the worst case impact scenario from NCHRP Report No. 350 Test Designation No. 3-11. The flare angle and corresponding impact angle for Test Nos. 3-10 and 3-11 are listed in Table 17. Values for impact severity (IS) and the increase in IS between the baseline and flared impacts are also provided.

**Table 17. Flare Rate Table**

Guardrail Orientation	Flare Angle	Test 3-10			Test 3-11		
		Impact Angle	Impact Severity	% Increase in IS	Impact Angle	Impact Severity	% Increase in IS
	(deg)	(deg)	(kJ)		(deg)	(kJ)	
Baseline	0.00	20	37.0	--	25	137.8	--
15:1*	3.81	23.81	51.6	39.4	28.81	179.2	30.1
14:1	4.09	24.09	52.7	42.4	29.09	182.3	32.3
13:1	4.40	24.40	54.0	45.9	29.40	185.9	34.9
12:1	4.76	24.76	55.5	50.0	29.76	190.2	38.0
11:1	5.19	25.19	57.3	54.9	30.19	195.2	41.6
10:1	5.71	25.71	59.5	60.9	30.71	201.2	46.0
9:1	6.34	26.34	62.3	68.3	31.34	208.7	51.5
8:1	7.13	27.13	65.8	77.7	32.13	218.2	58.3
7:1	8.13	28.13	70.3	90.0	33.13	230.5	67.2
6:1	9.46	29.46	76.5	106.8	34.46	247.1	79.3
5:1	11.31	31.31	85.4	130.9	36.31	270.6	96.3

\*RDG suggested maximum flare rate for semi-rigid barrier systems on 110 km/h roadways.

## 5.2. CIP Analysis

Identifying the CIP for a longitudinal barrier using the BARRIER VII program involved conducting impact simulations for a large number of closely spaced impact points. The simulation that predicted the worst case combination of maximum barrier deflection, wheel snag, maximum rail slope, and maximum rail tensile forces was used to determine the CIP. As such, the impact locations chosen were at the nodes from the midspan location between post nos. 11 and 12 to the midspan location between post nos. 12 and 13 for the Midwest Guardrail System and the modified G4(1S) guardrail system, as shown highlighted in Figure 30 and Figure 31, respectively.

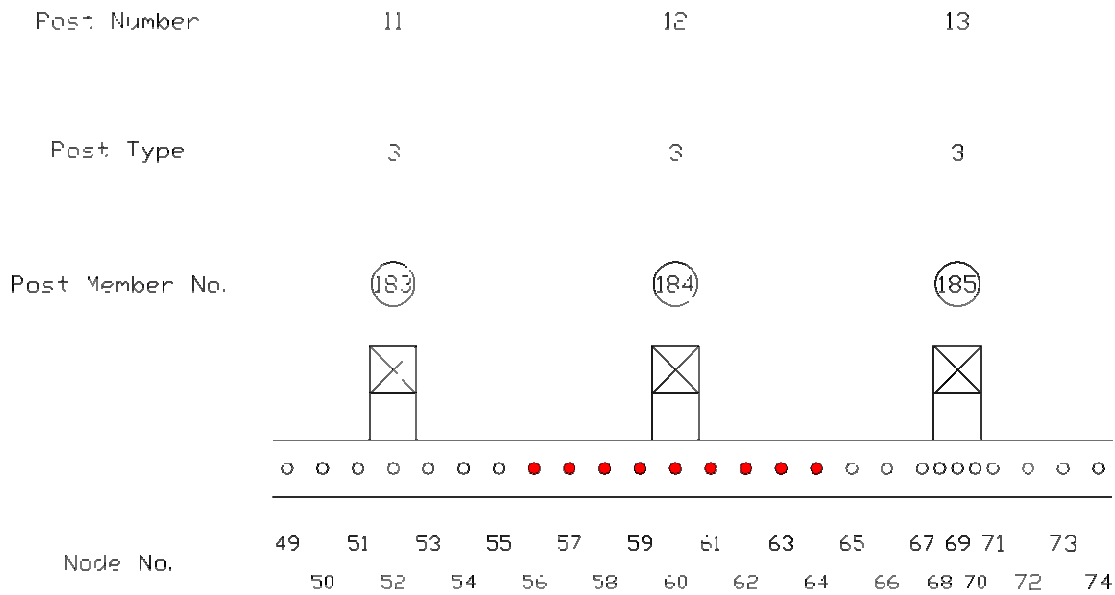


**Figure 30. Impact Nodes for MGS CIP Analysis**

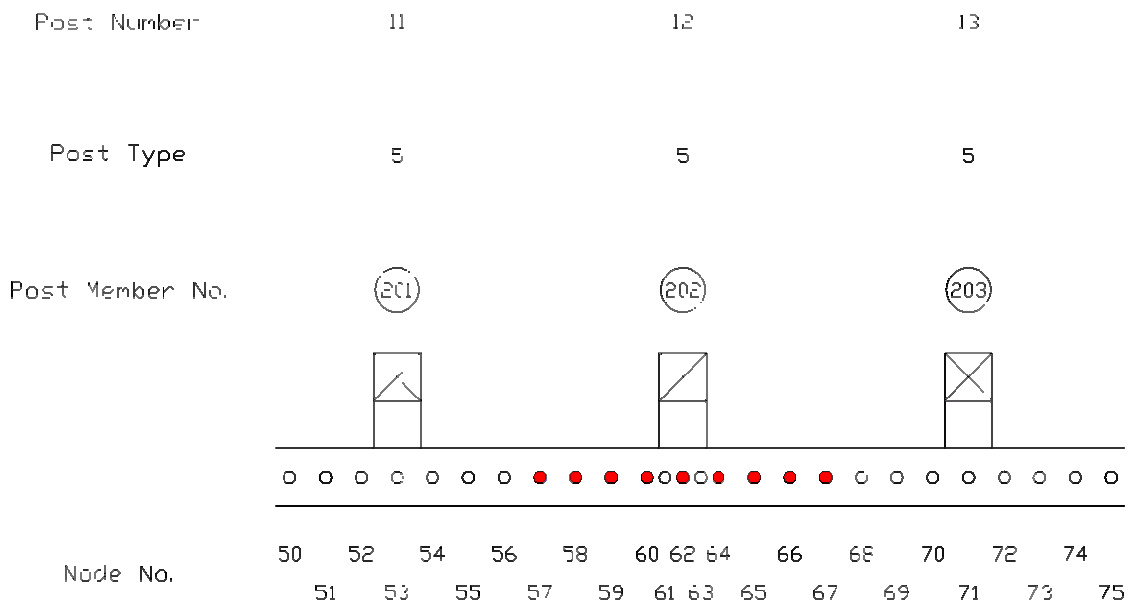


**Figure 31. Impact Nodes for modified G4(1S) CIP Analysis**

As stated previously, the impact location that results in the severest combination of results determines the CIP for the longitudinal barrier. An example of the table used to evaluate the different CIP simulations is Table 18.

**Table 18. Sample CIP Evaluation Parameter Table**

Impact Node	Impact Location	Parallel Time	Max. Deflection	Max. Tension	Pocketing Analysis		Snag Analysis		
					3 Node	5 Node	node	snag	dy
(no.)	(from post 12)	(s)	(in.)	(kips)	(rail slope)		(no.)	(in.)	(in.)
56	37.5" u.s.								
57	28.125" u.s.								
58	18.75" u.s.								
59	9.375" u.s.								
60	at post 12								
61	9.375" d.s.								
62	18.75" d.s.								
63	28.125" d.s.								
64	37.5" d.s.								

It should be noted that the impact node may change based upon the guardrail system being examined (MGS versus modified G4(1S)). However, the impact location is the same. The following sub-sections address the columns of the CIP evaluation table. For each set of impact simulations, the CIP will be highlighted.

**5.2.1. Parallel Time**

Baseline simulations have been shown to be very accurate up to the vehicle parallel condition. Although an introduction of parallel time as an evaluation criterion may be unnecessary, it can provide some idea of the total interaction time. Long vehicle-barrier interaction times may be an indicator of significant problems due to vehicle-post interaction. Thus, examination of this behavior was deemed important.

**5.2.2. Maximum Dynamic Rail Deflection**

Until now, there had been no suggested maximum rail deflection limit that was believed to result in the failure of a strong-post, W-beam guardrail system. A maximum rail deflection resulting in failure was difficult to access because failure typically occurs for other reasons, such

as rail rupture or vehicle pocketing. However, it was believed that a large rail displacement would result in conditions that would cause a failure to occur and therefore examination of the maximum dynamic deflection was deemed important.

A maximum deflection of 1626 mm (64 in.) was suggested for failure of the system. This distance corresponded to 80% of the pickup truck's width, potentially resulting in critical position of the guardrail in front of the vehicle during redirection, as shown in Figure 32.

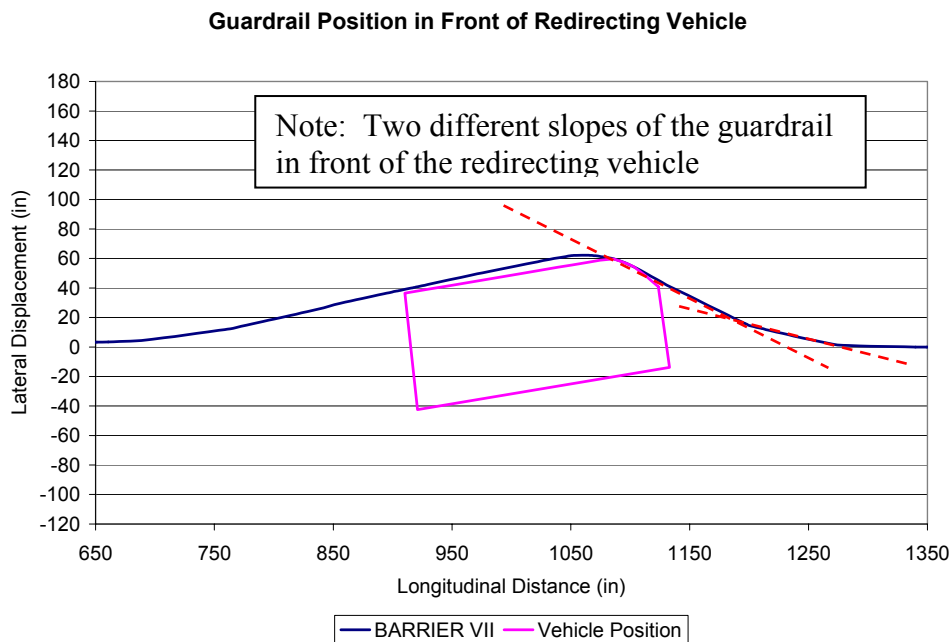


**Figure 32. Critical Position of Guardrail in Front of the Redirecting Vehicle**

In addition, during full-scale vehicle crash test 22-14MG-1, a maximum rail deflection of 1448 mm (57 in.) was observed during the successful redirection. However, post-test system damage showed that tears started to form in the guardrail due to improperly cut post bolt slots. Therefore, the 1626 mm (64 in.) limit seemed reasonable.

### 5.2.3. Maximum Rail Tension Forces

The maximum rail tension force for each simulation will be examined. The potential for problems will be addressed according to the criteria previously discussed in section 4.1.5.

### 5.2.4. Vehicle Pocketing

The maximum rail slope for each simulation will be examined. The potential for problems will be addressed according to the maximum allowable rail slope previously discussed in section 4.1.5. However, the method of determining the maximum rail slope was improved with the development of a computer program using the method of least squares, using 3 nodes and 5 nodes; both which are listed in the CIP evaluation table.

The method of least squares allows the calculation of a line through the data, with a slope and intercept. The rail slope is the desired measurement and was calculated by the following equation:

$$\text{Rail Slope} = \frac{n \sum x_i y_i - \sum x_i \sum y_i}{n \sum x_i^2 - (\sum x_i)^2}$$

where,

n = the number of experimental observations

$x_i, y_i$  = are the measured values

Note that the maximum rail slope is actually the minimum rail slope (i.e., most negative) due to the direction of impact in the BARRIER VII model.

### 5.2.5. Wheel Snag

Wheel snag was believed to be a significant concern with the increase in impact angle. Each simulation will be examined and according to the criteria previously discussed in section

4.1.5, the potential for problems will be addressed. In addition, vaulting was also believed to be a significant concern with the increase in impact angle, probably more so than wheel snag, as the two are closely related. Based upon engineering judgment, an impact with moderate wheel snag potential will be believed to provide a good test case. It was also believed the potential for vaulting is significantly increased during modified G4(1S) simulations due to its lower rail mounting height.

### 5.3. MGS Baseline Post Property CIP Simulation Results

Results were obtained by running the MGS baseline post property model with the increased impact angles at each of the impact nodes previously discussed; no other alterations to the model were made. Parallel time, maximum rail deflection, maximum rail tension, vehicle pocketing, and wheel snag results for each flare rate are listed in Table 19 through Table 28.

**Table 19. MGS Baseline Post Property – 6:1 Flare Rate CIP Results**

Impact Node	Impact Location	Parallel Time	Max. Deflection	Max. Tension	Pocketing Analysis		Snag Analysis		
					3 Node	5 Node	node	snag	dy
(no.)	(from post 12)	(s)	(in.)	(kips)	(rail slope)		(no.)	(in.)	(in.)
56	37.5" u.s.	0.5312	80.75	66.12	-0.3197	-0.3103	none	none	none
57	28.125" u.s.	0.5392	81.24	66.88	-0.3204	-0.3131	none	none	none
58	18.75" u.s.	0.5368	80.95	71.61	-0.3197	-0.3131	none	none	none
59	9.375" u.s.	0.5432	81.10	68.30	-0.3189	-0.3125	none	none	none
60	at post 12	0.5388	81.10	66.64	-0.3203	-0.3096	none	none	none
61	9.375" d.s.	0.5204	79.11	67.30	-0.3182	-0.3065	69	6.06	14.84
62	18.75" d.s.	0.5618	78.94	67.65	-0.3189	-0.3034	69	3.54	12.66
63	28.125" d.s.	0.5618	79.12	68.80	-0.3133	-0.3015	69	0.43	9.87
64	37.5" d.s.	0.5152	78.95	69.72	-0.3126	-0.3039	none	none	none

**Table 20. MGS Baseline Post Property – 7:1 Flare Rate CIP Results**

Impact Node	Impact Location	Parallel Time	Max. Deflection	Max. Tension	Pocketing Analysis		Snag Analysis		
					3 Node	5 Node	node	snag	dy
(no.)	(from post 12)	(s)	(in.)	(kips)	(rail slope)		(no.)	(in.)	(in.)
56	37.5" u.s.	0.4744	73.79	64.00	-0.3133	-0.3056	none	none	none
57	28.125" u.s.	0.4836	73.74	67.31	-0.3133	-0.3046	none	none	none
58	18.75" u.s.	0.4912	73.91	68.96	-0.3189	-0.3087	none	none	none
59	9.375" u.s.	0.4836	72.62	69.40	-0.3188	-0.3068	none	none	none
60	at post 12	0.478	72.38	67.95	-0.3132	-0.3041	none	none	none
61	9.375" d.s.	0.4684	72.32	66.22	-0.3133	-0.3037	69	5.26	14.14
62	18.75" d.s.	0.472	73.08	68.08	-0.3127	-0.2976	69	2.44	11.56
63	28.125" d.s.	0.4624	72.40	68.93	-0.3077	-0.2969	none	none	none
64	37.5" d.s.	0.4536	70.45	69.76	-0.3070	-0.2966	none	none	none

**Table 21. MGS Baseline Post Property – 8:1 Flare Rate CIP Results**

Impact Node	Impact Location	Parallel Time	Max. Deflection	Max. Tension	Pocketing Analysis		Snag Analysis		
					3 Node	5 Node	node	snag	dy
(no.)	(from post 12)	(s)	(in.)	(kips)	(rail slope)		(no.)	(in.)	(in.)
56	37.5" u.s.	0.4444	67.77	64.72	-0.3076	-0.3007	none	none	none
57	28.125" u.s.	0.4464	68.02	68.22	-0.3132	-0.3009	none	none	none
58	18.75" u.s.	0.4476	68.13	68.33	-0.3133	-0.3040	none	none	none
59	9.375" u.s.	0.4524	68.10	69.61	-0.3133	-0.3062	none	none	none
60	at post 12	0.4532	68.18	67.66	-0.3133	-0.3033	none	none	none
61	9.375" d.s.	0.4468	68.03	66.36	-0.3076	-0.2982	69	4.29	13.11
62	18.75" d.s.	0.4408	67.60	68.31	-0.3076	-0.2936	69	2.00	11.10
63	28.125" d.s.	0.4284	66.06	69.47	-0.3021	-0.2986	none	none	none
64	37.5" d.s.	0.4304	66.23	69.31	-0.3006	-0.2928	none	none	none

**Table 22. MGS Baseline Post Property – 9:1 Flare Rate CIP Results**

Impact Node	Impact Location	Parallel Time	Max. Deflection	Max. Tension	Pocketing Analysis		Snag Analysis		
					3 Node	5 Node	node	snag	dy
(no.)	(from post 12)	(s)	(in.)	(kips)	(rail slope)		(no.)	(in.)	(in.)
56	37.5" u.s.	0.4260	64.51	65.90	-0.3070	-0.2973	none	none	none
57	28.125" u.s.	0.4260	64.30	67.06	-0.3070	-0.2978	none	none	none
58	18.75" u.s.	0.4272	64.22	71.07	-0.3077	-0.3012	none	none	none
59	9.375" u.s.	0.4256	63.90	67.63	-0.3077	-0.3012	105	0.56	14.54
60	at post 12	0.4248	64.32	68.84	-0.3077	-0.2984	69	5.89	14.61
61	9.375" d.s.	0.4120	62.18	68.82	-0.3070	-0.2946	69	4.03	12.57
							105	1.39	15.01
62	18.75" d.s.	0.4164	62.90	68.05	-0.3077	-0.2922	69	1.23	10.27
63	28.125" d.s.	0.4144	63.11	69.93	-0.3015	-0.2903	none	none	none
64	37.5" d.s.	0.4148	63.15	68.85	-0.2994	-0.2864	none	none	none

**Table 23. MGS Baseline Post Property – 10:1 Flare Rate CIP Results**

MGS Baseline Post Property - 10:1 Flare Rate									
Impact Node	Impact Location	Parallel Time	Max. Deflection	Max. Tension	Pocketing Analysis		Snag Analysis		
					3 Node	5 Node	node	snag	dy
(no.)	(from post 12)	(s)	(in.)	(kips)	(rail slope)		(no.)	(in.)	(in.)
56	37.5" u.s.	0.4100	61.46	66.23	-0.3006	-0.2924	none	none	none
57	28.125" u.s.	0.4120	61.52	68.75	-0.3076	-0.2976	none	none	none
58	18.75" u.s.	0.4124	61.53	69.90	-0.3077	-0.3004	none	none	none
59	9.375" u.s.	0.4144	61.32	67.29	-0.3076	-0.3006	none	none	none
60	at post 12	0.4032	59.74	67.67	-0.3070	-0.2967	69	5.54	14.16
61	9.375" d.s.	0.4016	59.88	68.72	-0.3056	-0.2933	69	3.37	11.73
62	18.75" d.s.	0.3976	59.93	68.40	-0.3000	-0.2862	69	1.05	9.85
63	28.125" d.s.	0.3996	60.93	70.09	-0.3000	-0.2862	none	none	none
64	37.5" d.s.	0.4008	60.54	68.63	-0.3000	-0.2862	none	none	none

**Table 24. MGS Baseline Post Property – 11:1 Flare Rate CIP Results**

Impact Node	Impact Location	Parallel Time	Max. Deflection	Max. Tension	Pocketing Analysis		Snag Analysis		
					3 Node	5 Node	node	snag	dy
(no.)	(from post 12)	(s)	(in.)	(kips)	(rail slope)		(no.)	(in.)	(in.)
56	37.5" u.s.	0.3968	59.27	66.75	-0.2951	-0.2903	none	none	none
57	28.125" u.s.	0.4000	59.32	71.07	-0.3021	-0.2939	none	none	none
58	18.75" u.s.	0.4008	59.02	69.58	-0.3062	-0.2983	none	none	none
59	9.375" u.s.	0.3956	57.67	66.99	-0.3076	-0.2978	none	none	none
60	at post 12	0.3928	57.77	68.81	-0.3049	-0.2946	69	5.11	13.89
61	9.375" d.s.	0.3928	57.93	68.47	-0.3007	-0.2916	69	3.05	11.45
62	18.75" d.s.	0.3900	58.26	68.45	-0.3015	-0.2889	69 105	0.55 1.41	9.85 14.59
63	28.125" d.s.	0.3880	58.59	69.45	-0.2951	-0.2836	none	none	none
64	37.5" d.s.	0.3916	58.64	68.69	-0.2950	-0.2845	none	none	none

**Table 25. MGS Baseline Post Property – 12:1 Flare Rate CIP Results**

Impact Node	Impact Location	Parallel Time	Max. Deflection	Max. Tension	Pocketing Analysis		Snag Analysis		
					3 Node	5 Node	node	snag	dy
(no.)	(from post 12)	(s)	(in.)	(kips)	(rail slope)		(no.)	(in.)	(in.)
56	37.5" u.s.	0.3820	57.44	67.11	-0.2951	-0.2890	none	none	none
57	28.125" u.s.	0.3860	57.15	70.02	-0.3021	-0.2942	none	none	none
58	18.75" u.s.	0.3840	55.86	68.95	-0.3062	-0.2965	none	none	none
59	9.375" u.s.	0.3880	56.02	68.56	-0.3077	-0.2982	69	6.57	14.73
60	at post 12	0.3856	56.11	68.23	-0.3021	-0.2932	69	4.77	13.03
61	9.375" d.s.	0.3852	56.29	68.58	-0.3015	-0.2890	69 105	2.81 0.01	11.29 13.09
62	18.75" d.s.	0.3816	56.26	69.35	-0.3000	-0.2856	69 105	0.45 1.25	9.55 13.95
63	28.125" d.s.	0.3800	56.77	68.98	-0.2950	-0.2822	105	2.41	14.89
64	37.5" d.s.	0.3788	56.55	68.48	-0.2950	-0.2814	none	none	none

**Table 26. MGS Baseline Post Property – 13:1 Flare Rate CIP Results**

Impact Node	Impact Location	Parallel Time	Max. Deflection	Max. Tension	Pocketing Analysis		Snag Analysis		
					3 Node	5 Node	node	snag	dy
(no.)	(from post 12)	(s)	(in.)	(kips)	(rail slope)		(no.)	(in.)	(in.)
56	37.5" u.s.	0.3808	55.89	71.04	-0.2938	-0.2858	none	none	none
57	28.125" u.s.	0.3736	54.40	70.11	-0.3006	-0.2924	none	none	none
58	18.75" u.s.	0.3752	54.74	68.01	-0.3070	-0.2967	none	none	none
59	9.375" u.s.	0.3820	54.89	68.72	-0.3055	-0.2967	69	6.29	14.51
60	at post 12	0.3792	54.63	67.89	-0.3000	-0.2924	69	4.53	12.77
61	9.375" d.s.	0.3784	54.78	68.79	-0.3014	-0.2882	69	2.62	11.08
62	18.75" d.s.	0.3780	55.43	68.56	-0.3000	-0.2856	69	0.10	9.60
							105	0.52	13.58
63	28.125" d.s.	0.3748	55.38	68.86	-0.2950	-0.2817	105	1.95	14.45
64	37.5" d.s.	0.3612	52.12	71.99	-0.2950	-0.2798	105	0.32	13.08

**Table 27. MGS Baseline Post Property – 14:1 Flare Rate CIP Results**

Impact Node	Impact Location	Parallel Time	Max. Deflection	Max. Tension	Pocketing Analysis		Snag Analysis		
					3 Node	5 Node	node	snag	dy
(no.)	(from post 12)	(s)	(in.)	(kips)	(rail slope)		(no.)	(in.)	(in.)
56	37.5" u.s.	0.3668	52.76	71.26	-0.2950	-0.2849	none	none	none
57	28.125" u.s.	0.3696	53.41	69.84	-0.3000	-0.2913	none	none	none
58	18.75" u.s.	0.3708	53.71	67.63	-0.3006	-0.2954	none	none	none
59	9.375" u.s.	0.3768	54.01	68.25	-0.3006	-0.2978	69	5.84	14.46
60	at post 12	0.3744	53.48	68.12	-0.2993	-0.2914	69	4.36	12.54
61	9.375" d.s.	0.3748	53.94	68.49	-0.3000	-0.2865	69	2.24	11.06
62	18.75" d.s.	0.3712	53.89	68.85	-0.2950	-0.2833	69	0.05	9.35
							105	0.32	13.08
63	28.125" d.s.	0.3692	54.01	68.41	-0.2938	-0.2798	105	1.36	13.94
64	37.5" d.s.	0.3580	51.28	71.61	-0.2945	-0.2784	none	none	none

**Table 28. MGS Baseline Post Property – 15:1 Flare Rate CIP Results**

Impact Node	Impact Location	Parallel Time	Max. Deflection	Max. Tension	Pocketing Analysis		Snag Analysis		
					3 Node	5 Node	node	snag	dy
(no.)	(from post 12)	(s)	(in.)	(kips)	(rail slope)		(no.)	(in.)	(in.)
56	37.5" u.s.	0.3632	51.88	71.45	-0.2889	-0.2858	96	1.45	13.25
57	28.125" u.s.	0.3648	52.33	69.00	-0.2951	-0.2910	96	2.82	14.38
58	18.75" u.s.	0.3668	52.62	67.47	-0.3021	-0.2944	none	none	none
59	9.375" u.s.	0.3672	52.61	67.25	-0.3006	-0.2946	69	5.80	14.10
60	at post 12	0.3704	52.70	68.53	-0.3006	-0.2921	69	4.14	12.46
61	9.375" d.s.	0.3688	52.55	68.56	-0.2951	-0.2855	69	2.15	10.85
62	18.75" d.s.	0.3660	52.69	68.81	-0.2950	-0.2825	none	none	none
63	28.125" d.s.	0.3640	52.79	67.61	-0.2950	-0.2792	105	1.15	13.45
64	37.5" d.s.	0.3548	50.42	71.26	-0.2945	-0.2766	none	none	none

#### 5.4. MGS Early Post Release Property CIP Simulation Results

Results were obtained by running the MGS early post release property model with the increased impact angles at each of the impact nodes previously discussed; no other alterations to the model were made. Parallel time, maximum rail deflection, maximum rail tension, vehicle pocketing, and wheel snag results for each flare rate are listed in Table 29 through Table 32. Higher flare rates resulted in anchorage failure and thus are not presented.

**Table 29. MGS Early Post Release Property – 12:1 Flare Rate CIP Results**

Impact Node	Impact Location	Parallel Time	Max. Deflection	Max. Tension	Pocketing Analysis		Snag Analysis		
					3 Node	5 Node	node	snag	dy
(no.)	(from post 12)	(s)	(in.)	(kips)	(rail slope)		(no.)	(in.)	(in.)
56	37.5" u.s.	0.4776	79.48	66.59	-0.4970	-0.4922	none	none	none
57	28.125" u.s.	0.4292	74.47	68.81	-0.5858	-0.5715	105	2.45	12.43
58	18.75" u.s.	0.4308	64.65	68.95	-0.5119	-0.5023	105	2.16	10.64
59	9.375" u.s.	0.4296	64.96	65.77	-0.5004	-0.4656	69	6.57	14.73
							105	5.02	13.68
60	at post 12	0.4284	65.20	66.42	-0.4920	-0.4773	69	4.77	13.03
61	9.375" d.s.	0.4296	65.22	66.29	-0.5399	-0.5224	69	2.81	11.29
62	18.75" d.s.	0.4224	64.29	68.94	-0.5232	-0.5075	69	0.45	9.55
63	28.125" d.s.	0.4196	64.45	65.94	-0.5239	-0.5135	none	none	none
64	37.5" d.s.	0.4132	63.18	68.48	-0.4970	-0.4727	none	none	none

**Table 30. MGS Early Post Release Property – 13:1 Flare Rate CIP Results**

Impact Node	Impact Location	Parallel Time	Max. Deflection	Max. Tension	Pocketing Analysis		Snag Analysis		
					3 Node	5 Node	node	snag	dy
(no.)	(from post 12)	(s)	(in.)	(kips)	(rail slope)		(no.)	(in.)	(in.)
56	37.5" u.s.	0.4150	63.48	67.32	-0.5017	-0.4896	none	none	none
57	28.125" u.s.	0.4168	62.28	70.11	-0.5352	-0.5273	none	none	none
58	18.75" u.s.	0.4219	62.99	68.31	-0.5004	-0.4877	105	1.72	10.48
59	9.375" u.s.	0.4224	63.31	65.39	-0.4897	-0.4762	69	6.29	14.51
							105	3.82	12.58
60	at post 12	0.4147	62.91	64.97	-0.4798	-0.4466	69	4.53	12.77
							105	6.18	14.62
61	9.375" d.s.	0.4152	62.50	66.55	-0.4809	-0.4646	69	2.62	11.08
62	18.75" d.s.	0.4154	62.91	66.83	-0.5119	-0.4947	69	0.10	9.60
63	28.125" d.s.	0.4059	61.67	67.17	-0.4928	-0.4797	none	none	none
64*	37.5" d.s.	0.3772	55.05	71.99	-0.3821	-0.3719	105	5.30	15.10

\* The early release behavior was not observed during this simulation

**Table 31. MGS Early Post Release Property – 14:1 Flare Rate CIP Results**

Impact Node	Impact Location	Parallel Time	Max. Deflection	Max. Tension	Pocketing Analysis		Snag Analysis		
					3 Node	5 Node	node	snag	dy
(no.)	(from post 12)	(s)	(in.)	(kips)	(rail slope)		(no.)	(in.)	(in.)
56	37.5" u.s.	0.4004	58.91	68.16	-0.4968	-0.4913	none	none	none
57	28.125" u.s.	0.4080	60.66	69.84	-0.5145	-0.5046	none	none	none
58	18.75" u.s.	0.4120	61.34	67.33	-0.4873	-0.4721	105	1.59	10.31
59	9.375" u.s.	0.4156	61.95	67.02	-0.4858	-0.4813	69	5.84	14.46
							105	3.11	11.99
60	at post 12	0.4060	61.12	66.99	-0.4786	-0.4545	69	4.36	12.54
							105	4.56	13.54
61	9.375" d.s.	0.4076	60.91	65.68	-0.4381	-0.4264	69	2.24	11.06
62	18.75" d.s.	0.3960	59.89	66.31	-0.4461	-0.4355	69	0.05	9.35
63	28.125" d.s.	0.3908	59.12	68.41	-0.4501	-0.4364	none	none	none
64*	37.5" d.s.	0.3584	51.37	71.61	-0.2945	-0.2784	105	0.04	12.76

\* The early release behavior was not observed during this simulation

**Table 32. MGS Early Post Release Property – 15:1 Flare Rate CIP Results**

Impact Node	Impact Location	Parallel Time	Max. Deflection	Max. Tension	Pocketing Analysis		Snag Analysis		
					3 Node	5 Node	node	snag	dy
(no.)	(from post 12)	(s)	(in.)	(kips)	(rail slope)		(no.)	(in.)	(in.)
56	37.5" u.s.	0.3936	57.63	69.14	-0.4725	-0.4648	none	none	none
57	28.125" u.s.	0.3980	58.89	69.00	-0.4868	-0.4790	none	none	none
58	18.75" u.s.	0.4028	59.56	67.25	-0.4664	-0.4600	105	0.95	9.95
59	9.375" u.s.	0.4028	59.66	66.79	-0.4727	-0.4575	69	5.80	14.10
							105	2.71	11.59
60	at post 12	0.3988	59.49	67.11	-0.4739	-0.4698	69	4.14	12.46
							105	3.68	13.52
61	9.375" d.s.	0.3888	58.06	66.86	-0.4440	-0.4097	69	2.15	10.85
							105	3.68	13.52
62	18.75" d.s.	0.3828	57.42	68.81	-0.4426	-0.4127	105	4.56	14.24
63	28.125" d.s.	0.3804	57.05	67.61	-0.4451	-0.4186	none	none	none
64*	37.5" d.s.	0.3548	50.42	71.26	-0.2945	-0.2766	none	none	none

\* The early release behavior was not observed during this simulation

### 5.5. Modified G4(1S) CIP Simulation Results

Results were obtained by running the modified G4(1S) model with the increased impact angles at each of the impact nodes previously discussed; no other alterations to the model were made. Parallel time, maximum rail deflection, maximum rail tension, vehicle pocketing, and

wheel snag results for each flare rate are listed in Table 33 through Table 40. Higher flare rates resulted in anchorage failure and thus are not presented.

**Table 33. Modified G4(1S) – 8:1 Flare Rate CIP Results**

Impact Node	Impact Location	Parallel Time	Max. Deflection	Max. Tension	Pocketing Analysis		Snag Analysis		
					3 Node	5 Node	node	snag	dy
(no.)	(from post 12)	(s)	(in.)	(kips)	(rail slope)		(no.)	(in.)	(in.)
57	37.5" u.s.	0.4524	66.39	64.69	-0.3906	-0.3833	none	none	none
58	28.125" u.s.	0.434	62.90	64.84	-0.3689	-0.3642	none	none	none
59	18.75" u.s.	0.4424	63.77	67.96	-0.3694	-0.3635	none	none	none
60	9.375" u.s.	0.4448	64.00	73.34	-0.3855	-0.3785	none	none	none
62	at post 12	0.4452	64.28	70.19	-0.4098	-0.3988	none	none	none
64	9.375" d.s.	0.4448	63.46	70.42	-0.3666	-0.3512	71	7.75	13.45
							107	4.72	14.08
65	18.75" d.s.	0.4444	63.76	67.98	-0.3634	-0.3548	71	5.60	11.40
66	28.125" d.s.	0.4332	62.89	68.43	-0.3634	-0.3505	71	3.27	9.13
67	37.5" d.s.	0.4304	62.41	71.16	-0.3559	-0.3433	71	0.23	6.37

**Table 34. Modified G4(1S) – 9:1 Flare Rate CIP Results**

Impact Node	Impact Location	Parallel Time	Max. Deflection	Max. Tension	Pocketing Analysis		Snag Analysis		
					3 Node	5 Node	node	snag	dy
(no.)	(from post 12)	(s)	(in.)	(kips)	(rail slope)		(no.)	(in.)	(in.)
57	37.5" u.s.	0.4120	59.15	63.84	-0.3698	-0.3616	none	none	none
58	28.125" u.s.	0.4180	60.08	64.59	-0.3698	-0.3624	none	none	none
59	18.75" u.s.	0.4252	60.79	68.69	-0.3646	-0.3605	none	none	none
60	9.375" u.s.	0.4312	61.09	71.90	-0.3838	-0.3785	none	none	none
62	at post 12	0.4284	61.10	69.24	-0.3965	-0.3876	71	9.13	14.97
64	9.375" d.s.	0.4224	60.86	68.63	-0.3758	-0.3720	71	7.17	13.13
65	18.75" d.s.	0.4220	60.09	67.90	-0.3577	-0.3490	71	5.06	10.34
							107	5.11	14.09
66	28.125" d.s.	0.4116	58.67	67.47	-0.3510	-0.3414	71	2.73	8.17
							107	5.77	14.63
67	37.5" d.s.	0.4012	56.63	73.79	-0.3446	-0.3382	107	4.43	13.77

**Table 35. Modified G4(1S) – 10:1 Flare Rate CIP Results**

Impact Node	Impact Location	Parallel Time	Max. Deflection	Max. Tension	Pocketing Analysis		Snag Analysis		
					3 Node	5 Node	node	snag	dy
(no.)	(from post 12)	(s)	(in.)	(kips)	(rail slope)		(no.)	(in.)	(in.)
57	37.5" u.s.	0.3998	56.82	64.49	-0.3637	-0.3602	98	4.88	13.92
58	28.125" u.s.	0.4052	57.83	64.11	-0.3642	-0.3597	none	none	none
59	18.75" u.s.	0.4088	58.03	67.48	-0.3641	-0.3611	none	none	none
60	9.375" u.s.	0.4180	58.71	70.67	-0.3758	-0.3720	none	none	none
62	at post 12	0.4140	58.43	70.90	-0.3848	-0.3761	71	8.79	14.51
64	9.375" d.s.	0.4068	58.18	68.44	-0.3927	-0.3806	71	6.70	12.10
65	18.75" d.s.	0.3980	57.21	68.50	-0.3899	-0.3769	71	4.77	10.03
66	28.125" d.s.	0.3896	55.91	68.39	-0.3965	-0.3775	71	2.42	7.98
67	37.5" d.s.	0.3888	54.66	72.73	-0.3446	-0.3370	107	2.95	12.55

**Table 36. Modified G4(1S) – 11:1 Flare Rate CIP Results**

Impact Node	Impact Location	Parallel Time	Max. Deflection	Max. Tension	Pocketing Analysis		Snag Analysis		
					3 Node	5 Node	node	snag	dy
(no.)	(from post 12)	(s)	(in.)	(kips)	(rail slope)		(no.)	(in.)	(in.)
57	37.5" u.s.	0.3832	55.10	63.11	-0.3775	-0.3631	98	1.44	10.46
58	28.125" u.s.	0.3948	55.94	65.35	-0.3616	-0.3590	none	none	none
59	18.75" u.s.	0.4000	56.41	67.97	-0.3634	-0.3568	none	none	none
60	9.375" u.s.	0.4068	56.59	71.56	-0.3654	-0.3625	none	none	none
62	at post 12	0.4024	56.16	69.29	-0.3758	-0.3647	71	8.45	14.15
64	9.375" d.s.	0.3952	55.71	67.56	-0.3755	-0.3629	71	6.57	11.73
65	18.75" d.s.	0.3864	54.25	67.35	-0.3791	-0.3583	71	4.25	9.78
66	28.125" d.s.	0.3732	52.09	71.39	-0.3509	-0.3398	71	2.22	7.78
67	37.5" d.s.	0.3744	53.07	73.76	-0.3677	-0.3596	none	none	none

**Table 37. Modified G4(1S) – 12:1 Flare Rate CIP Results**

Impact Node	Impact Location	Parallel Time	Max. Deflection	Max. Tension	Pocketing Analysis		Snag Analysis		
					3 Node	5 Node	node	snag	dy
(no.)	(from post 12)	(s)	(in.)	(kips)	(rail slope)		(no.)	(in.)	(in.)
57	37.5" u.s.	0.3764	53.80	63.51	-0.3840	-0.3815	none	none	none
58	28.125" u.s.	0.3876	54.53	65.59	-0.3580	-0.3563	98	5.86	14.54
59	18.75" u.s.	0.3916	54.78	67.96	-0.3585	-0.3561	none	none	none
60	9.375" u.s.	0.3972	54.85	70.94	-0.3549	-0.3500	none	none	none
62	at post 12	0.3928	54.29	68.93	-0.3638	-0.3551	71	8.14	13.26
64	9.375" d.s.	0.3896	54.31	66.45	-0.3665	-0.3567	71	6.18	11.62
65	18.75" d.s.	0.3772	52.09	68.81	-0.3642	-0.3482	71	4.33	9.57
66	28.125" d.s.	0.368	50.84	71.13	-0.3524	-0.3350	71	2.05	7.65
67	37.5" d.s.	0.3692	51.85	74.93	-0.3651	-0.3571	none	none	none

**Table 38. Modified G4(1S) – 13:1 Flare Rate CIP Results**

Impact Node	Impact Location	Parallel Time	Max. Deflection	Max. Tension	Pocketing Analysis		Snag Analysis		
					3 Node	5 Node	node	snag	dy
(no.)	(from post 12)	(s)	(in.)	(kips)	(rail slope)		(no.)	(in.)	(in.)
57	37.5" u.s.	0.3712	52.62	62.98	-0.3783	-0.3761	none	none	none
58	28.125" u.s.	0.3788	53.10	65.50	-0.3577	-0.3540	98	5.10	13.50
59	18.75" u.s.	0.3852	53.52	67.16	-0.3577	-0.3529	none	none	none
60	9.375" u.s.	0.3900	53.50	69.75	-0.3560	-0.3465	71	9.24	14.96
62	at post 12	0.3900	53.38	68.10	-0.3671	-0.3494	71	7.71	13.19
64	9.375" d.s.	0.3816	52.40	66.45	-0.3642	-0.3501	71	6.08	11.32
65	18.75" d.s.	0.3628	48.89	68.34	-0.3316	-0.3240	71	4.20	9.40
66	28.125" d.s.	0.3632	49.81	70.95	-0.3529	-0.3348	71	1.84	7.56
67	37.5" d.s.	0.3652	50.84	74.48	-0.3577	-0.3562	none	none	none

**Table 39. Modified G4(1S) – 14:1 Flare Rate CIP Results**

Impact Node	Impact Location	Parallel Time	Max. Deflection	Max. Tension	Pocketing Analysis		Snag Analysis		
					3 Node	5 Node	node	snag	dy
(no.)	(from post 12)	(s)	(in.)	(kips)	(rail slope)		(no.)	(in.)	(in.)
57	37.5" u.s.	0.3672	51.63	63.18	-0.3774	-0.3718	none	none	none
58	28.125" u.s.	0.3740	52.30	65.89	-0.3571	-0.3537	98	4.41	12.69
59	18.75" u.s.	0.3842	52.84	68.21	-0.3585	-0.3541	none	none	none
60	9.375" u.s.	0.3848	52.37	68.97	-0.3506	-0.3435	71	9.13	14.67
62	at post 12	0.3824	51.77	68.72	-0.3560	-0.3429	71	7.54	12.96
64	9.375" d.s.	0.3744	50.66	66.17	-0.3509	-0.3394	71	5.92	11.18
65	18.75" d.s.	0.3588	47.96	69.07	-0.3324	-0.3213	71	4.05	9.25
66	28.125" d.s.	0.3600	48.90	70.25	-0.3560	-0.3306	71	1.72	7.48
67	37.5" d.s.	0.3608	49.77	73.74	-0.3574	-0.3533	none	none	none

**Table 40. Modified G4(1S) – 15:1 Flare Rate CIP Results**

Impact Node	Impact Location	Parallel Time	Max. Deflection	Max. Tension	Pocketing Analysis		Snag Analysis		
					3 Node	5 Node	node	snag	dy
(no.)	(from post 12)	(s)	(in.)	(kips)	(rail slope)		(no.)	(in.)	(in.)
57	37.5" u.s.	0.3640	50.78	64.39	-0.3755	-0.3708	none	none	none
58	28.125" u.s.	0.3664	51.47	65.53	-0.3691	-0.3545	98	1.93	10.27
59	18.75" u.s.	0.3760	51.73	67.12	-0.3576	-0.3534	98	6.49	14.71
60	9.375" u.s.	0.3788	51.27	68.90	-0.3457	-0.3417	71	8.98	14.42
62	at post 12	0.3764	50.42	68.54	-0.3468	-0.3356	71	7.44	12.76
64	9.375" d.s.	0.3672	48.57	65.58	-0.3398	-0.3229	71	5.75	11.05
65	18.75" d.s.	0.3544	46.95	68.77	-0.3260	-0.3227	71	3.98	9.12
66	28.125" d.s.	0.3552	48.04	69.93	-0.3413	-0.3293	71	1.60	7.40
67	37.5" d.s.	0.3576	49.01	73.08	-0.3539	-0.3503	none	none	none

## **5.6. CIP Simulation Conclusions**

The BARRIER VII CIP simulations have been completed and results presented for the different guardrail systems and different post property simulations. For every flare rate, a CIP has been identified. In the following two chapters these CIP simulations will serve as the basis for the identification of the critical flare rate for the Midwest Guardrail System and the modified G4(1S) guardrail system.

## **6. MGS CRITICAL FLARE RATE IDENTIFICATION**

### **6.1. Introduction**

A strategy for determining the critical flare rate was presented previously. The criteria included parallel time, maximum dynamic rail displacement, maximum rail tension forces, vehicle pocketing, and wheel snag potential. In this chapter, the Midwest Guardrail System CIP simulations for each of the different flare rates and different post property scenarios are compared, evaluated, and a critical flare rate is identified.

### **6.2. BARRIER VII Simulation Scenarios**

Previously, a tendency was shown for the guardrail in the upstream region to release prematurely away from the posts. When this behavior occurred, an increased load condition occurred on the upstream end anchorage, thus increasing the propensity for system failure. Thus, anchorage failure was determined to be one of the limiting conditions in the selection of the critical flare rate, although it has rarely occurred during full-scale vehicle crash testing. Typically, a guardrail system fails due to rail rupture at a splice location. However, rail rupture has not been very predictable in BARRIER VII to this point. Thus, all the other comparison criteria must be evaluated. As a result, two different simulation models were run at each flare rate in order to completely evaluate its safety performance: (1) one with the baseline model post properties and (2) one with early guardrail release post properties in the upstream region. The following sections discuss the evaluation criteria for each simulation scenario independently for all flare rates. Conclusions are then drawn from the results of both sections.

### 6.2.1. Baseline Post Property Simulation Scenario

The results were obtained by running the baseline model with the increased impact angle; no other alterations to the model were made. Parallel time, maximum rail deflection, maximum rail tension, vehicle pocketing and wheel snag analysis results for each simulation impacting at the CIP location are listed in Table 41. A discussion of each type of results for the simulations follows in the following sub-sections. The energy balance results comparison and discussion are presented entirely in its own sub-section.

**Table 41. Simulation Evaluation Criteria for MGS Baseline**

Flare Rate	Impact Node	Impact Location	Parallel Time	Max. Deflection	Max. Tension	Pocketing Analysis		Snag Analysis		
						3 Node	5 Node	node	snag	dy
	(no.)	(from post 12)	(s)	(in.)	(kips)	(rail slope)		(no.)	(in.)	(in.)
15:1	60	at post 12	0.3704	52.70	68.53	-0.3006	-0.2921	69	4.14	12.46
14:1	59	9.375" u.s.	0.3768	54.01	68.25	-0.3006	-0.2978	69	5.84	14.46
13:1	59	9.375" u.s.	0.3820	54.89	68.72	-0.3055	-0.2967	69	6.29	14.51
12:1	60	at post 12	0.3856	56.11	68.23	-0.3021	-0.2932	69	4.77	13.03
11:1	57	28.125" u.s.	0.4000	59.32	71.07	-0.3021	-0.2939	none	none	none
10:1	58	18.75" u.s.	0.4124	61.53	69.90	-0.3077	-0.3004	none	none	none
9:1	60	at post 12	0.4248	64.32	68.84	-0.3077	-0.2984	69	5.89	14.61
8:1	61	9.375" d.s.	0.4468	68.03	66.36	-0.3076	-0.2982	69	4.29	13.11
7:1	58	18.75" u.s.	0.4912	73.91	68.96	-0.3189	-0.3087	none	none	none
6:1	59	9.375" u.s.	0.5432	81.10	68.30	-0.3189	-0.3125	none	none	none
5:1	NA*	NA*	NA*	NA*	NA*	NA*	NA*	NA*	NA*	NA*

\* Simulation Failed due to Anchorage Failure

#### 6.2.1.1. Parallel Time

As stated previously, long vehicle-barrier interaction times may be an indicator of significant problems due to vehicle-post interaction. The parallel time versus impact angle is shown in Figure 33.

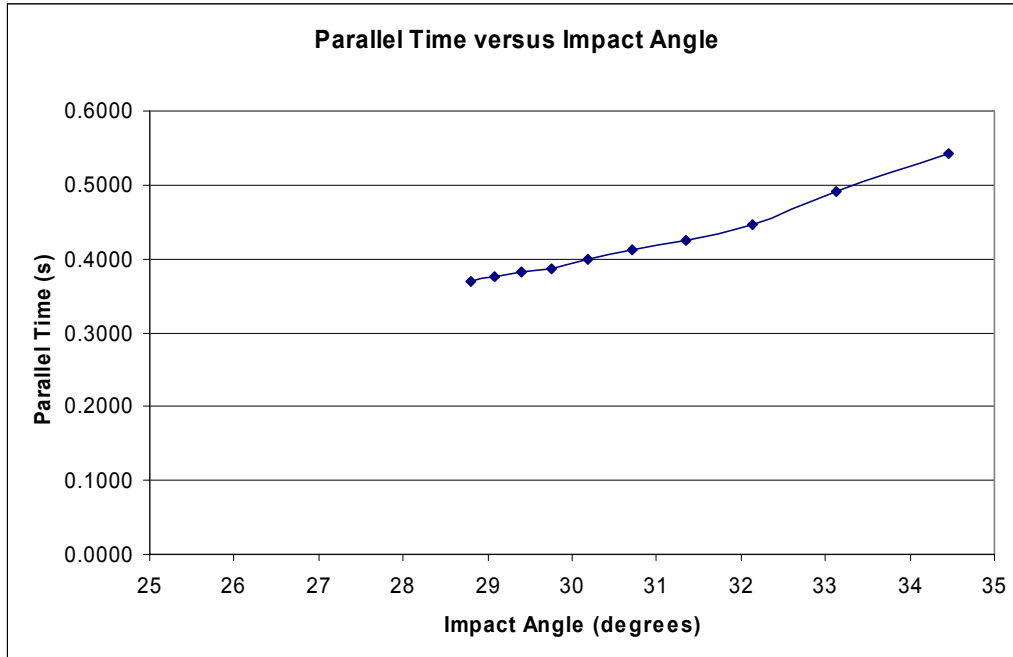


**Figure 33. Simulation Parallel Time versus Impact Angle**

The parallel time increased in a nearly linear fashion, with only a small change in slope over the entire range. As such, a specific statement regarding parallel time considerations could not be made at this time.

#### **6.2.1.2. Maximum Dynamic Rail Deflection**

Based on the maximum dynamic rail deflection criterion, researchers believed that flare rates greater than 10:1 would fail and therefore are greater than the critical flare rate.

#### **6.2.1.3. Maximum Rail Tension Forces**

The maximum rail tension force versus time for each simulation is shown in Figure 34. The maximum rail tension forces follow the same general pattern.

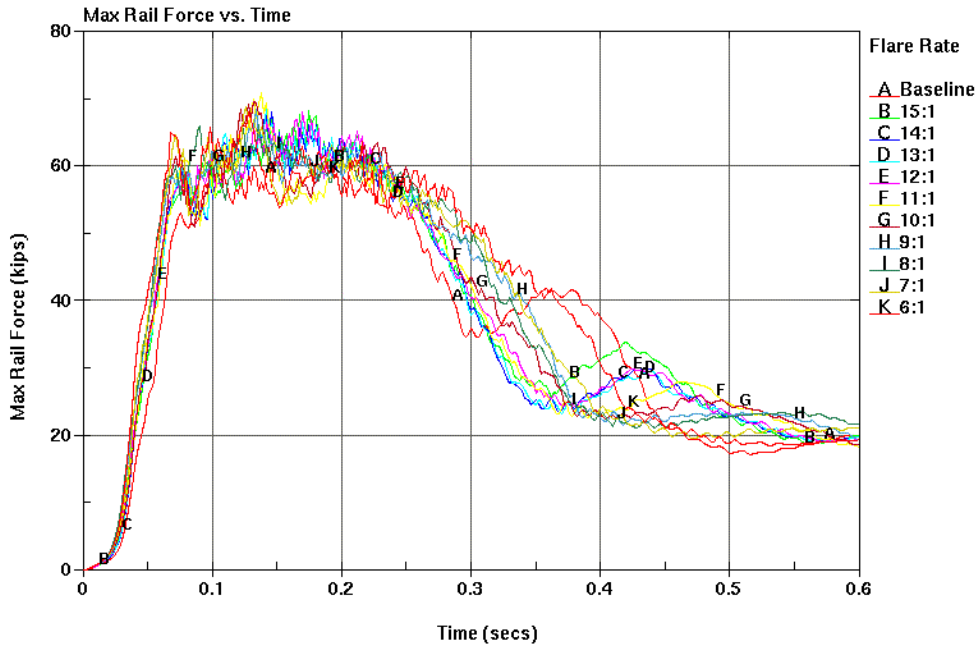


**Figure 34. Maximum Rail Tension Forces versus Time**

Tension forces in the rail remained after 600 ms, but are not shown for clarity. Upon closer examination of the information in Table 41, and Figure 34, the maximum tensile force for the flared system impacts are, on average, approximately 6% greater than the baseline impact. However, none of the maximum forces would result in a predicted failure according to the criteria previously discussed.

#### 6.2.1.4. Wheel Snag

Wheel snag was detected in the baseline simulation, along with flared simulations up to and including the 12:1 flare rate. Greater flare rates did not have wheel snag unless the CIP impact was very near the post, due to post failure. However, the vehicle was predicted to contact the posts during the impact event. As a result of this specific evaluation, wheel snag was deemed a concern for most flare rates to be full-scale vehicle crash tested. A good test case was believed

to be the 13:1 flare rate with a snag potential of 6.3 in. However, a specific statement regarding successful redirection or failure could not be made at this time.

#### **6.2.1.5. Vehicle Vaulting**

Vaulting was believed to be a significant concern with the increase in impact angle, probably more so than wheel snag, as the two are closely related. It appeared from the snag analysis and the increased rail height that the potential for a wheel to ride up a post and vault over the barrier was limited. Based upon engineering judgment, an impact with moderate wheel snag potential was believed to provide a good test case. Therefore the 13:1 flare rate impact was also selected on the potential for vehicle vaulting.

#### **6.2.1.6. Vehicle Pocketing**

Based upon the information provided in Table 41, there did not exist a potential for vehicle pocketing. The general trend showed an increased rail slope with an increased flare rate. It is important to note that the maximum rail slopes occurred between 150 and 200 ms for all of the simulations. At this time in the redirection, a large slope can lead to vehicle vaulting or vehicle roll over in a high flare rate system, and subsequent failure of the test. However, a specific statement regarding the successful redirection or failure of the flared systems could not be made at this time.

#### **6.2.1.7. Energy Balance**

According to Coon, BARRIER VII can provide energy balance results for crash reconstructions within 3% of the actual energy dissipated during a full-scale vehicle crash test

[37]. This energy evaluation potential was deemed important due to the complex energy loss events that occur during redirection, including: vehicle crush, guardrail deformation, post rotation, post deformation, post failure, friction between the vehicle and pavement, and friction between the vehicle and barrier. Examination of these different energy losses provided a basis for comparison for the baseline and flared impact events, as well as between the flared impact conditions themselves.

The energy balance results from BARRIER VII are presented as a percentage of the original kinetic energy (K.E.) of the impacting vehicle. The energy balances for the different simulations are presented in Table 42.

**Table 42. Energy Balances for MGS Baseline Post Property Simulations**

Flare Rate	Time of Energy Balance *	Type of Energy							
		Percent of Original Auto K.E.							
		Translational K.E. of Auto	Elastic Energy in Members		Inelastic Work on Members		Damping Losses	Auto - Barrier Friction Loss	Auto - Pavement Friction Loss
Beams	Posts		Beams	Posts					
Baseline	0.5090	35.9	0.1	0.5	4.6	8.9	6.9	39.1	2.6
15:1	0.7170	28.5	0.1	0.5	5.2	13.1	8.1	40.0	3.3
14:1	0.7220	27.9	0.1	0.5	5.2	13.4	8.2	40.1	3.4
13:1	0.7270	27.3	0.1	0.5	5.3	13.8	8.4	40.1	3.4
12:1	0.7670	26.5	0.1	0.5	5.4	14.3	8.6	40.1	3.4
11:1	0.7750	25.7	0.1	0.5	5.4	14.7	8.7	40.2	3.5
10:1	0.8210	24.6	0.1	0.5	5.5	15.5	8.9	40.2	3.6
9:1	0.8060	22.8	0.1	0.5	5.7	16.9	9.1	40.1	3.9
8:1	0.9620	21.3	0.1	0.5	5.7	18.3	9.3	39.9	4.1
7:1	0.9680	19.4	0.1	0.5	5.9	19.8	9.7	39.5	4.4
6:1	0.9450	16.0	0.1	0.5	6.3	22.5	10.3	39.0	5.4
5:1	2.000***	1.0	0.3	0.0	13.1	24.4	25.6	28.9	8.4

\* Time of energy balance is at the vehicle exit time.

\*\* Specific energies were omitted that had little or no effect on the total sum (Inelastic Work on Auto ~ 3.5).

\*\*\* Specified simulation end time was reached, and the simulation was terminated.

Following an analysis of the data provided in Table 42, general trends have been observed in the energy balance results. First, as the flare rate increased the exit time also increased and therefore due to the increased contact time: (1) the vehicle slows more, (2) the

damping losses increased, and (3) the auto-pavement friction losses increased. However, the auto-barrier friction loss was observed to remain relatively constant. This result was due to the fact that the vehicle exited along the barrier and thus remained in contact. However, during this time only minor contact occurred and negligible lateral force between the barrier and vehicle was detected, which was used to calculate the friction losses. Another trend was the increase in inelastic work (plastic deformation) on members as the flare rate increased. Logically, this made sense due to the increased impact severity, which resulted in more barrier damage. The inelastic energy on the vehicle remained relatively constant due to the simplified vehicle model used in BARRIER VII that limits the magnitude of deformation due to the simplified vehicle model that is used in BARRIER VII simulation. From the energy balance, it was shown that increased flare rates resulted in greater system damage.

### **6.2.2. Early Release Post Property Simulation Scenario**

The following results were obtained by running the baseline model with the 22-14MG-1 early post release properties and with the increased impact angle, discussed previously. No other alterations to the model were made. Parallel time, maximum rail deflection, maximum rail tension, vehicle pocketing and wheel snag analysis results for each simulation impacting at the CIP location are listed in Table 43. A discussion of each type of results for the simulations follows in the following sub-sections. The energy balance results comparison and discussion are presented entirely in its own sub-section.

**Table 43. Simulation Evaluation Criteria for MGS Early Release Posts**

Flare Rate	Impact Node	Impact Location	Parallel Time	Max. Deflection	Max. Tension	Pocketing Analysis		Snag Analysis		
						3 Node	5 Node	node	snag	dy
	(no.)	(from post 12)	(s)	(in.)	(kips)	(rail slope)		(no.)	(in.)	(in.)
15:1	59	9.375" u.s.	0.4028	59.66	66.79	-0.4727	-0.4575	69	5.80	14.10
								105	2.71	11.59
14:1	59	9.375" u.s.	0.4156	61.95	67.02	-0.4858	-0.4813	69	5.84	14.46
								105	3.11	11.99
13:1	59	9.375" u.s.	0.4224	63.31	65.39	-0.4897	-0.4762	69	6.29	14.51
								105	3.82	12.58
12:1	60	at post 12	0.4284	65.20	66.42	-0.4920	-0.4773	69	4.77	13.03
11:1	NA*	NA*	NA*	NA*	NA*	NA*	NA*	NA*	NA*	NA*

\* Simulation Failed due to Anchorage Failure

### 6.2.2.1. Parallel Time

Once again, the parallel times were observed to increase with an increase in impact angles. However, no specific change in the parallel time was noticed. As such, no specific comment about the parallel time was made.

### 6.2.2.2. Maximum Rail Deflection

Based on the maximum deflection limit set previously, simulations with an early release and flare rates steeper than 13:1 were predicted to fail. The 13:1 flare rate was very close to the maximum deflection limit and thus may be the critical flare rate. This conclusion assumed that the early release phenomena will again be observed in full-scale vehicle crash testing using a sever impact condition similar to test no. 22-14MG-1.

### 6.2.2.3. Maximum Rail Tension Forces

The maximum rail tension force versus time for each simulation is shown in Figure 35. The tension forces remained higher for a longer duration in the baseline simulation than observed

in the flared impact events. The baseline simulation with early post release properties did not result the early post release behavior as the impact severity was not enough to induce such an event, thus typical of the tension forces are observed. For the flared impacts, the maximum tension forces sharply decreased shortly after 150 ms. As the flare rate increased, the maximum tension force decreased more quickly, by a few milliseconds. Also, the 11:1 flare rate simulation failed due to end anchorage failure, as observed by the loss of tension force in the rail. Based on the maximum rail tension listed in Table 43, none of the simulations would result in a failed situation according to the criteria previously discussed.

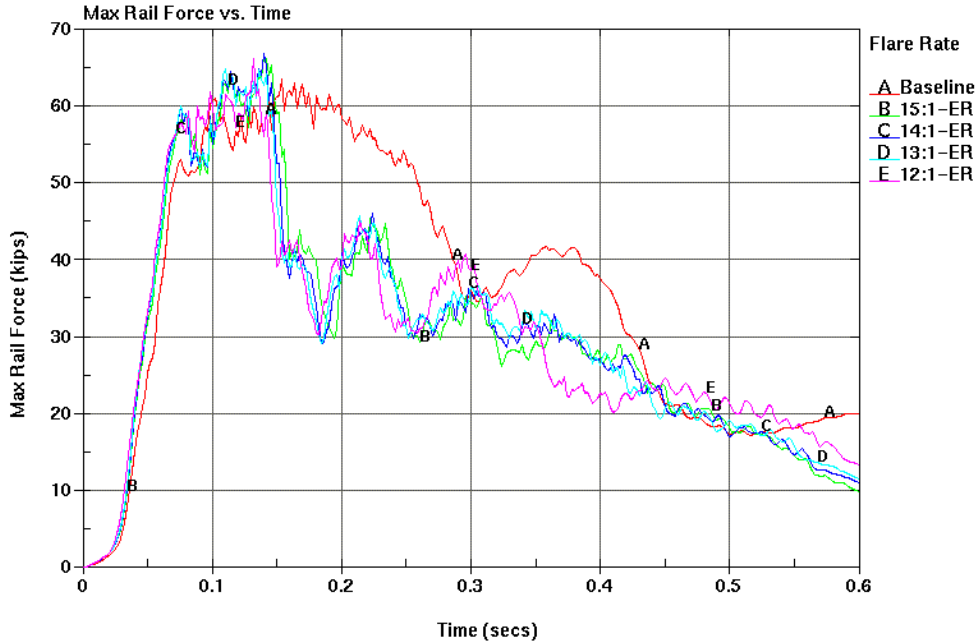


**Figure 35. Maximum Rail Tension Forces versus Time**

#### 6.2.2.4. Wheel Snag

As before, wheel snag was believed to be a concern for all flare rates to be tested. Again, the 13:1 flare rate presented itself as a good test case with a predicted snag of 6.3 in. However, a specific statement regarding successful redirection or failure could not be made at this time.

#### **6.2.2.5. Vehicle Vaulting**

As before, vaulting was believed to be a significant concern with the increase in impact angle, probably more so than wheel snag, as the two are closely related. It appeared from the snag analysis and the increased rail height that the potential for a wheel to ride up a post and vault over the barrier was limited. Based upon engineering judgment, an impact with moderate wheel snag potential was believed to provide a good test case. Therefore, the 13:1 flare rate impact was selected based on the potential for vehicle vaulting.

#### **6.2.2.6. Vehicle Pocketing**

The previously stated criteria noted that rail slopes greater than 0.4250 may result in vehicle pocketing. All the flare rates with early post release behavior result in maximum rail slopes exceeding this condition and are observed to increase with increasing impact angle. Thus, all of the flare rates simulated show potential for concern.

#### **6.2.2.7. Energy Balance**

An energy balance comparison provides as an important evaluation criterion as it provides an indication of the energy distribution in the different simulations. As before, the energy balance is presented as a percentage of the original kinetic energy of the impacting vehicle. The energy balances for the different simulations are presented in Table 44

**Table 44. Energy Balances for MGS Early Release Post Property Simulations**

Flare Rate	Time of Energy Balance*	Type of Energy							
		Percent of Original Auto K.E.							
		Translational K.E. of Auto	Elastic Energy in Members		Inelastic Work on Members		Damping Losses	Auto - Barrier Friction Loss	Auto - Pavement Friction Loss
Beams	Posts		Beams	Posts					
Baseline	0.5190	35.9	0.1	0.5	4.6	8.9	6.9	39.1	2.6
15:1	0.9160	20.2	0.1	0.2	6.8	16.2	10.3	42.0	4.3
14:1	0.9180	19.1	0.1	0.2	6.9	16.6	10.6	42.3	4.5
13:1	0.9780	17.6	0.1	0.2	7.1	16.9	10.9	42.8	5.0
12:1	0.7220	16.9	0.1	0.2	7.4	17.5	11.1	42.4	4.1

\* Time of energy balance is at the vehicle exit time.

\*\* Specific energies were omitted that had little or no effect on the total sum (Inelastic Work on Auto ~ 3.5).

As before, different conclusions can be made from the energy balances. The most significant loss of energy is again due to auto-barrier friction loss, increasing by approximately 10% between the baseline and flared impact conditions and for reasons discussed previously. The amount of energy lost to inelastic work on members (or plastic deformation) increased by approximately 100% between the baseline and flared impact conditions. The most significant difference was in the inelastic work on the posts in the system, a result of the early release post properties and increased impact severity, resulting in more post deformation and failure. There are other energy losses in the system due to damping and auto-pavement friction losses. These losses also increased during the flared impact conditions, likely due to the increased time of energy balance.

### 6.3. Conclusions

Based on (1) maximum deflection, rail slope and wheel snag results from BARRIER VII simulation; (2) potential for early release of the rail-to-post connections; (3) crash test 22-14MG-1; and (4) MwRSF researchers experience with guardrail testing, the 13:1 flare rate impacted 9.375 in. upstream of post no. 12 is recommended as the critical flare rate for the MGS.

## 7. MODIFIED G4(1S) CRITICAL FLARE RATE IDENTIFICATION

### 7.1. Introduction

A strategy for determining the critical flare rate was presented previously. The criteria included parallel time, maximum dynamic rail displacement, maximum rail tension forces, vehicle pocketing, and wheel snag potential. In this chapter, the Modified G4(1S) Guardrail System CIP simulations for each of the different flare rates are compared, evaluated, and a critical flare rate is identified.

### 7.2. Modified G4(1S) CIP Simulation Comparison

The following results were obtained by running the Modified G4(1S) baseline model with the increased impact angle, discussed previously. No other alterations to the model were made. Parallel time, maximum rail deflection, maximum rail tension, vehicle pocketing and wheel snag analysis results for each simulation impacting at the CIP location are listed in Table 45. A discussion of each type of results for the simulations follows in the following sub-sections. The energy balance results comparison and discussion are presented entirely in its own sub-section.

**Table 45. Simulation Evaluation Criteria for Modified G4(1S)**

Flare Rate	Impact Node	Impact Location	Parallel Time	Max. Deflection	Max. Tension	Pocketing Analysis		Snag Analysis		
						3 Node	5 Node	node	snag	dy
	(no.)	(from post 12)	(ms)	(in.)	(kips)	(rail slope)		(no.)	(in.)	(in.)
15:1	60	9.375" u.s.	0.3788	51.27	68.90	-0.3457	-0.3417	71	8.98	14.42
14:1	60	9.375" u.s.	0.3848	52.37	68.97	-0.3506	-0.3435	71	9.13	14.67
13:1	60	9.375" u.s.	0.3900	53.50	69.75	-0.3560	-0.3465	71	9.24	14.96
12:1	62	at post 12	0.3928	54.29	68.93	-0.3638	-0.3551	71	8.14	13.26
11:1	62	at post 12	0.4024	56.16	69.29	-0.3758	-0.3647	71	8.45	14.15
10:1	62	at post 12	0.4140	58.43	70.90	-0.3848	-0.3761	71	8.79	14.51
9:1	62	at post 12	0.4284	61.10	69.24	-0.3965	-0.3876	71	9.13	14.97
8:1	64	9.375" d.s.	0.4448	63.46	70.42	-0.3666	-0.3512	71	7.75	13.45
								107	4.72	14.08
7:1	NA*	NA*	NA*	NA*	NA*	NA*	NA*	NA*	NA*	NA*

\* Simulation Failed due to Anchorage Failure

### **7.2.1. Parallel Time**

The parallel times were observed to increase with an increase in impact angles, as shown in Table 45. However, no specific change in the parallel time was noticed. As such, no specific comment about the parallel time was made.

### **7.2.2. Maximum Rail Deflection**

Based on the 64 in. (1626 mm) maximum deflection limit, discussed previously, all applicable flare rates for the modified G4(1S) pass the maximum deflection criteria.

However, because of the lower rail height of the modified G4(1S) compared to the MGS, 21.65 in. compared to 24.875 in. at center rail mounting height, and because of the stronger posts between the modified G4(1S) and the MGS, approximately 10% stronger, it was believed that the maximum rail deflection limit for the modified G4(1S) should be 80 - 85% of the maximum allowable dynamic rail deflection limit used for the MGS. Thus, the maximum deflection limit of concern for the modified G4(1S) is between 51.2 in. and 54.4 in. (1300 mm and 1382 mm). Justification for this modification was as follows.

As a vehicle penetrates into a guardrail system during redirection, the rail has a tendency to rotate back and towards the ground. This "rotation" is enhanced as the rail is lowered and the blockout depth decreased. Additionally, the lower the rail the less interaction the rail has with the vehicle sheet metal. Instead, at low rail heights, the majority of vehicle capture is guardrail wrapping around the tires. Finally, with stiffer posts, fewer upstream and downstream posts will rotate back, which results in a more local rail deformation during redirection. Thus, higher local rail deformation for the same maximum rail deflection was considered a far more severe case and the maximum allowable dynamic rail deflection limit was decreased.

Based on this modified criteria, it is suggested that the 13:1 flare rate is a strong candidate for the critical flare rate for the modified G4(1S).

### 7.2.3. Maximum Rail Tension Forces

The maximum rail tension force versus time for each simulation is shown in Figure 36. The maximum rail tension forces follow the same general pattern.

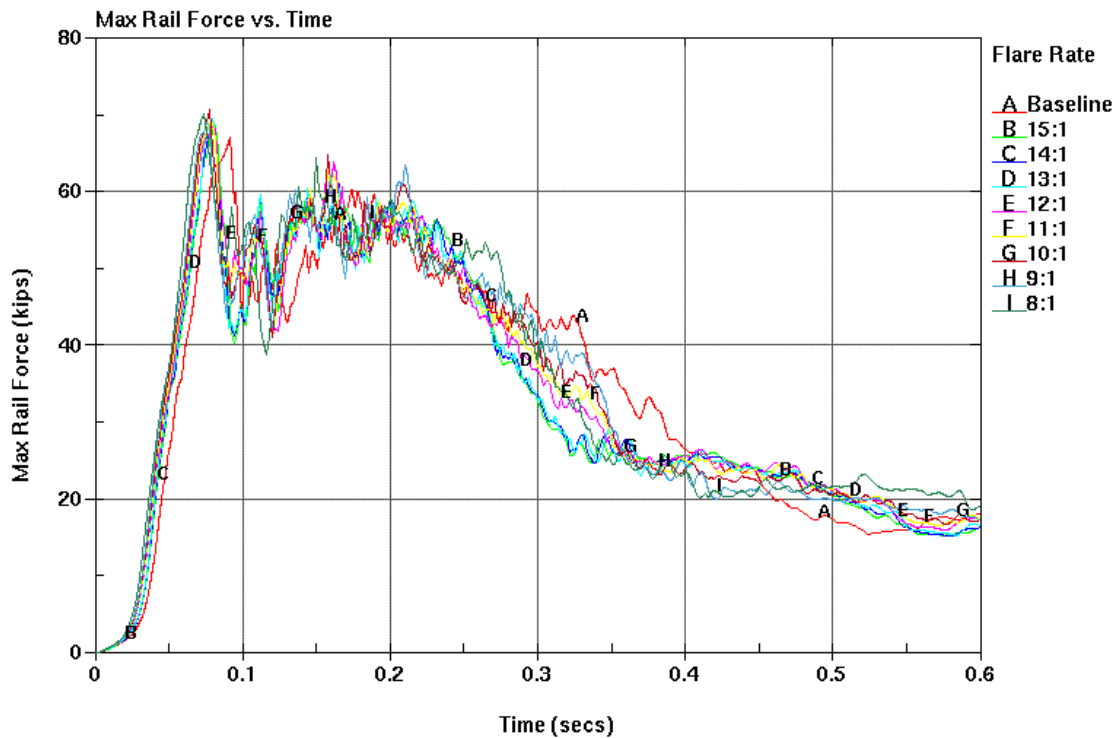


**Figure 36. Maximum Rail Tension Forces versus Time**

Tension forces in the rail remained after 600 ms, but are not shown for clarity. Upon closer examination of the information in Table 45, and Figure 36, the maximum tensile force for the flared system impacts are, on average, approximately 6% greater than the baseline impact. None of the maximum forces would result in a predicted failure according to the criteria previously discussed.

However, during test no. 22-14WB-1, conducted on the modified G4(1S) system, the guardrail was observed to rupture at a splice location. Test 22-14WB-1 had an impact severity of 156 kJ; while the impact severity of a 2000 kg pickup at 100 km/h using a 15:1 flared impact is 178.8 kJ. Therefore, the tensile capacity of the guardrail on the modified G4(1S) will likely be severely tested on flared impacts; with the 13:1 presenting itself as a good test case.

#### **7.2.4. Wheel Snag**

Wheel snag was believed to be a concern for all flare rates to be tested; with over 9 in. for several cases.

#### **7.2.5. Vehicle Vaulting**

Vehicle vaulting was believed to be a significant concern with the increase in impact angle, as the two are closely related. It appeared from the snag analysis that the potential for a wheel to ride up a post and vault over the barrier may be possible when considering the height of the barrier. The 13:1 flare rate had the highest wheel snag at 9.24 in.; while the 15:1 flare was not far behind with 9 in. of wheel snag.

#### **7.2.6. Vehicle Pocketing**

Based upon the information provided in Table 45, there did not exist a potential for vehicle pocketing. The general trend showed an increased rail slope with an increase flare rate. As such, no specific comment about vehicle pocketing was made.

### 7.2.7. Energy Balance

An energy balance comparison provides as an important evaluation criterion as it provides an indication of the energy distribution in the different simulations. As before, the energy balance is presented as a percentage of the original kinetic energy of the impacting vehicle. The energy balances for the different simulations are presented in Table 46.

**Table 46. Energy Balances for Modified G4(1S) Property Simulations**

Flare Rate	Time of Energy Balance*	Type of Energy							
		Percent of Original Auto K.E.							
		Translational K.E. of Auto	Elastic Energy in Members		Inelastic Work on Members		Damping Losses	Auto - Barrier Friction Loss	Auto - Pavement Friction Loss
Beams	Posts		Beams	Posts					
Baseline	0.5220	32.5	0.1	0.4	5.4	9.7	8.2	39.4	2.6
15:1	0.8140	23.4	0.1	0.5	6.2	13.4	9.6	41.7	4.0
14:1	0.8180	22.6	0.1	0.5	6.2	13.8	9.7	41.9	4.0
13:1	0.8240	21.9	0.1	0.5	6.3	14.2	9.9	41.9	4.1
12:1	0.8400	21.3	0.1	0.5	6.4	14.5	9.9	41.9	4.2
11:1	0.8360	20.2	0.1	0.5	6.5	15.1	10.2	42.0	4.4
10:1	0.8360	18.8	0.1	0.5	6.7	15.8	10.6	42.0	4.5
9:1	0.8320	17.3	0.1	0.5	6.9	16.8	11.0	41.9	4.8
8:1	0.8860	17.6	0.1	0.5	6.7	18.0	10.7	40.9	4.5

\* Time of energy balance is at the vehicle exit time.

\*\* Specific energies were omitted that had little or no effect on the total sum (Inelastic Work on Auto ~ 4.2).

As before, different conclusions can be made from the energy balances. The most significant loss of energy is again due to auto-barrier friction loss, increasing by approximately 10% between the baseline and flared impact conditions and for reasons discussed previously. The amount of energy lost to inelastic work on members (or plastic deformation) increased between the baseline and flared impact conditions. The most significant difference was in the inelastic work on the posts in the system, a result of the early release post properties and increased impact severity, resulting in more post deformation and failure. There are other energy losses in the system due to damping and auto-pavement friction losses. These losses also increased during the flared impact conditions, likely due to the increased time of energy balance.

### **7.3. Conclusions**

Based on the maximum deflection, wheel snag and vehicle vaulting concerns, the 13:1 flare rate is chosen as the critical flare rate for the modified G4(1S) guardrail system. However, in light of (1) recent crash testing of the G4(1S), (2) the fact that the G4(1S) has never been tested at the installation rate of 15:1, and (3) simulation results of the 15:1 flare rate were not significantly better than the 13:1 flare rate, engineering judgment will have to be used to pick which flare rate to full-scale vehicle crash test if the G4(1S) is the system selected to be tested during Phase 1 – Part 2 of the overall flare rate project.

## **8. ADDITIONAL SIMULATION USING LS-DYNA**

### **8.1. Introduction**

Finally, an initial look at detailed 3-D non-linear, finite element analysis using LS-DYNA [30] was performed. Although this simulation work is not officially part of this NCHRP project, it does provide the reader with a more complete background of efforts related to the flare rate study. LS-DYNA modeling concentrates on the MGS; but the work done on the post in soil component model is applicable to other guardrail systems as well.

The modeling process began with a standard height, strong-post, W-beam guardrail system obtained from the National Crash Analysis Center. Modeling changes were completed iteratively to develop a baseline model of the Midwest Guardrail System (MGS): including increasing the rail mounting height, decreasing the post embedment depth, increasing the blockout depth, and relocating the splice connections to mid-span locations.

A summary of the changes and resulting behaviors are listed in Table 47. Note that not all simulation runs are listed due to negligible knowledge gained.

**Table 47. Modeling Changes for NPG-4 Simulation**

Run	Changes from Original Model	Discussion of Results
1	- raised the rail & posts to MGS height	
2	- used new truck model (DB)	- simulation looks good
	- updated c2500 files for new truck	
	- set end time = 0 ms (initial position check)	
4	- created new file for c2500 and guardrail contacts	- error termination due to fender snagging on guardrail
	- include c2500-ground.k	
5	- changed truck-guardrail contact to: AUTOMATIC_SINGLE_SURFACE	- rear bumper snagged on rail
6	- removed bumper from truck-guardrail contact	- successful redirection
7	- updated soil properties from post-in-soil study (run 6)	- successful redirection
	- added cross-sections through rail	
8	- updated model with increased blackout depth	- poor HyperMesh work, needs remeshing
	- eliminated shells covering soil and blockouts	
	- set end time = 0 ms (initial check)	
12	- updated contact definition for anchorage posts/soil	- core dump at 70 ms (not sure why)
13a	- set end time for 70 ms to find problem with run 12	- simulation looks good to this point
13b	- set end time for 80 ms, d3plot = 1.0 ms	- core dump due to negative volume (contact problem)
14	- changed contact for bolt, nuts, and rail null to soft = 2	- fixed problem
17	- preload post and splice bolts	- simulation works fine
	- set end time for 10 ms	- post bolt force goes to near 0 after correctly loading?
18	- remeshed guardrail to MGS condition	- problems with overlapping elements
	- set end time = 0 ms (initial check)	
19	- removed overlapping elements	- simulation looks good
20	- set end time = 650 ms	- simulation captured and redirected vehicle
21	- changes to soil model (run 21)	- core dump at 200 ms (not sure why)
22	- switch back to old soil (run 6), add non-reflecting b.c.	- core dump at 200 ms (not sure why)

## 8.2. Baseline Model Development

The simulation process began by performing a simulation of test NPG-4 for validation purposes. For test NPG-4, a 2,000 kg pickup truck impacted the system at 98.17 km/h and 25.6 degrees. The data acquired during test NPG-4 from high-speed film was used to calibrate the model to the physical test. A graphical comparison of the simulated and actual barrier displacements for test NPG-4 is provided in Figure 37.

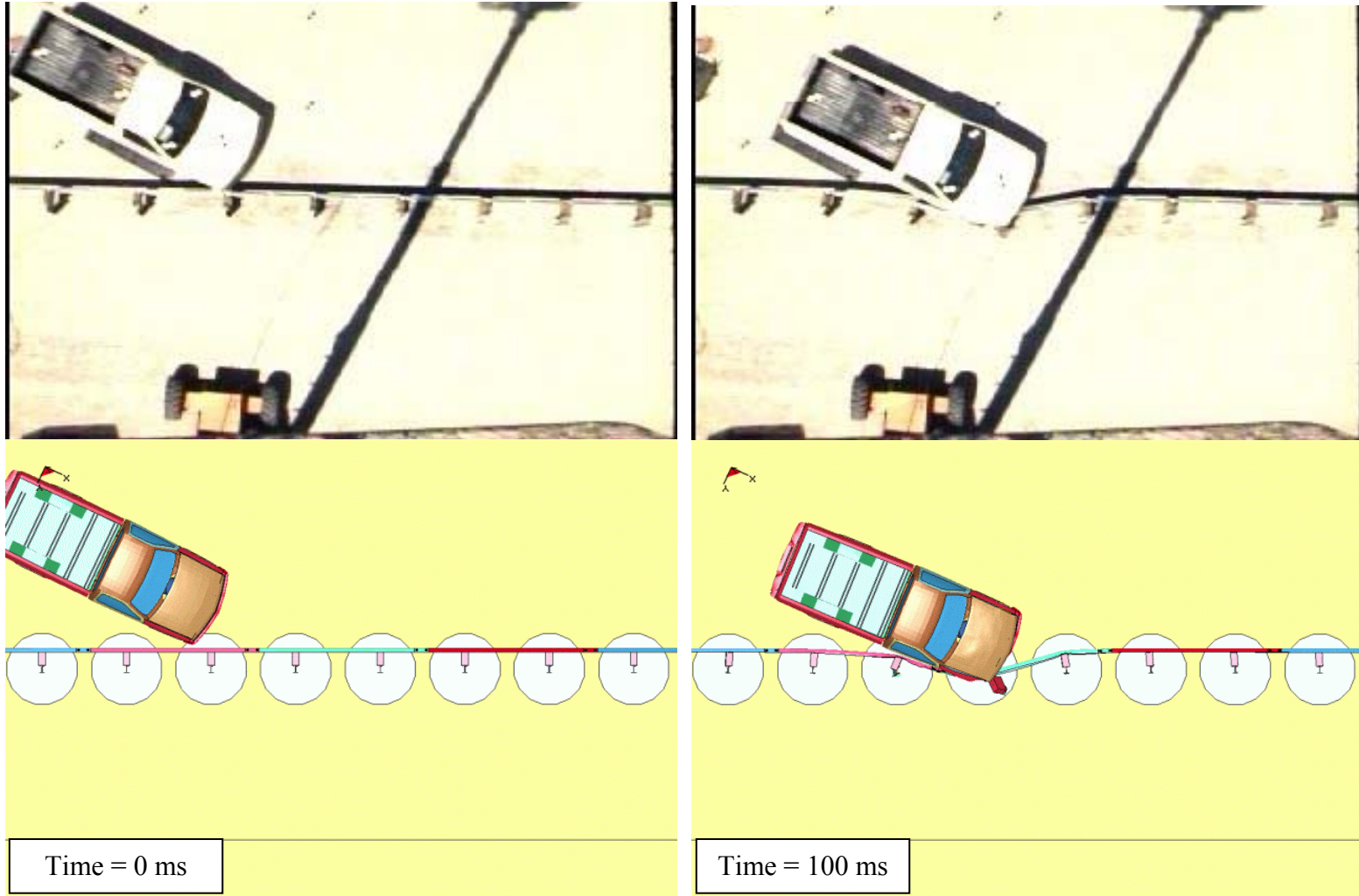


**Figure 37. Sequential Figures from LS-DYNA Simulation of NPG-4**

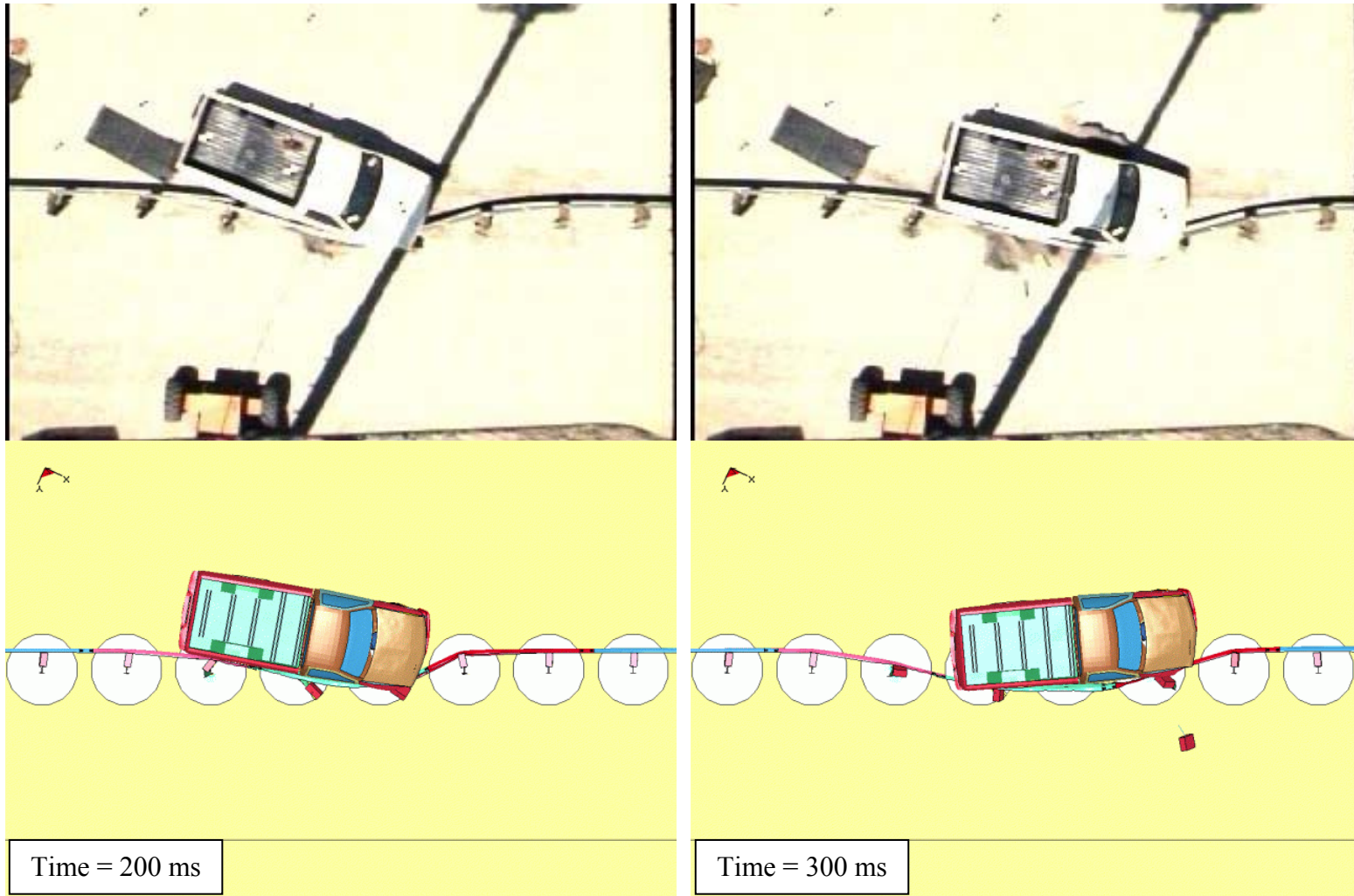


**Figure 37 (continued). Sequential Figures from LS-DYNA Simulation of NPG-4**

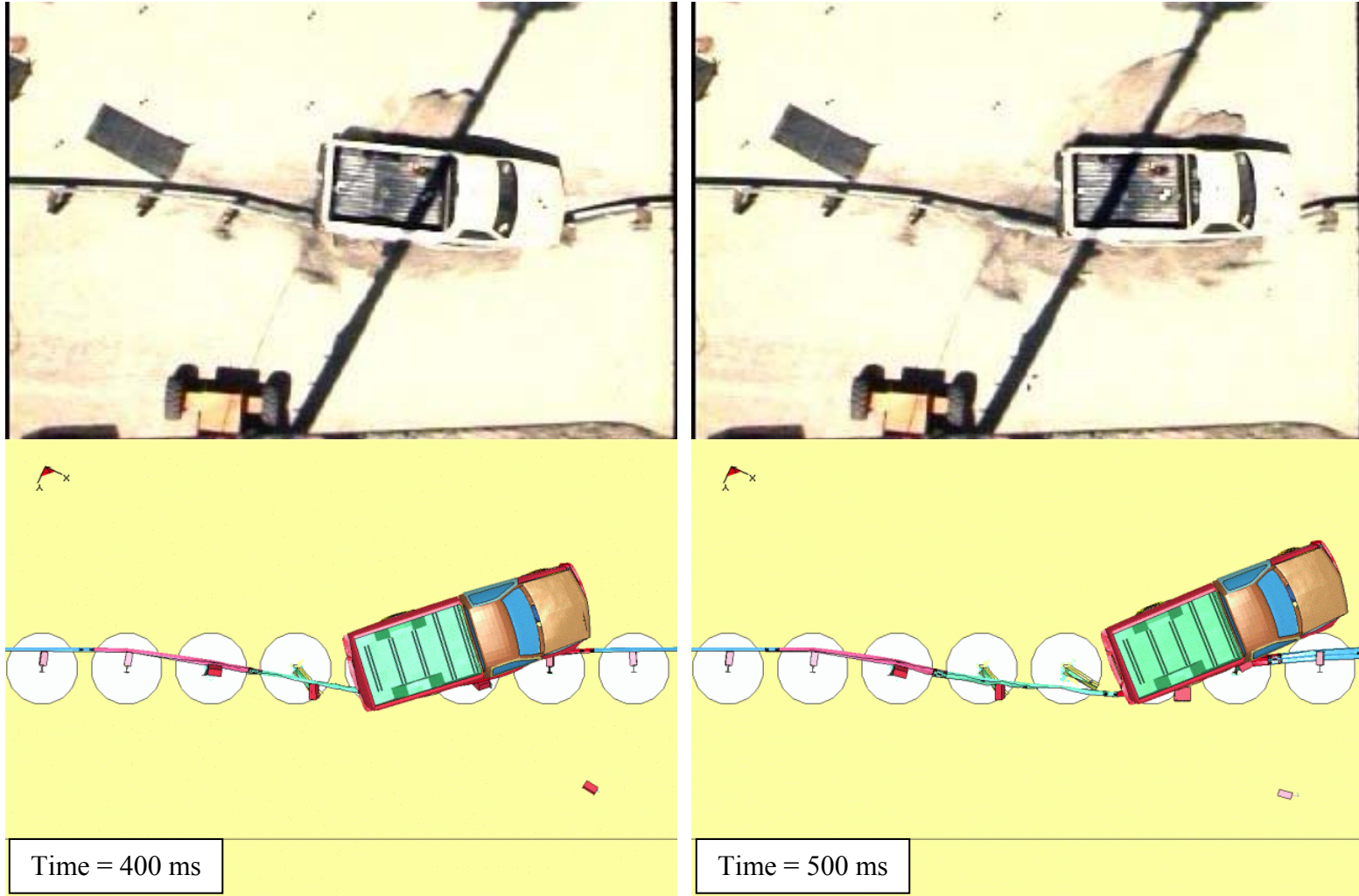
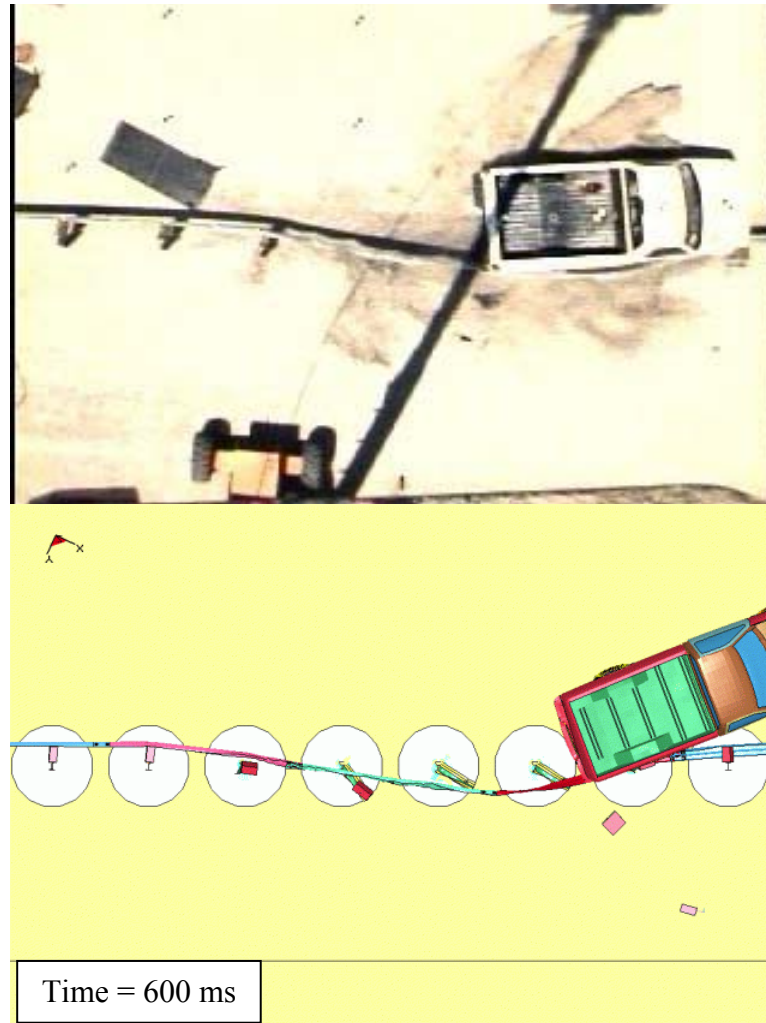


Figure 37 (continued). Sequential Figures from LS-DYNA Simulation of NPG-4



**Figure 37 (continued). Sequential Figures from LS-DYNA Simulation of NPG-4**

The LS-DYNA simulation showed a limitation into the amount of barrier penetration, as compared to that observed during the physical test. In addition, the barrier shape downstream of the maximum deflection did not match well with the simulation, under predicting the displacement of the guardrail in this region. Also, the vehicle was redirected quicker in the simulation than it was during the physical test. These behaviors were an indication that the soil response is too stiff, not allowing significant post rotation in the soil. However, even with this existing condition, the barrier was able to capture and redirect the impacting vehicle. The stiff soil situation resulted in higher than normal tensile loads in the rail and a greater potential to pocket the vehicle, neither of which had happened. As such, this model can be used to initially evaluate a flared impact, which is discussed in the following chapter.

In addition to the overhead graphical comparison, other film comparisons have been made, as shown in the following figures.

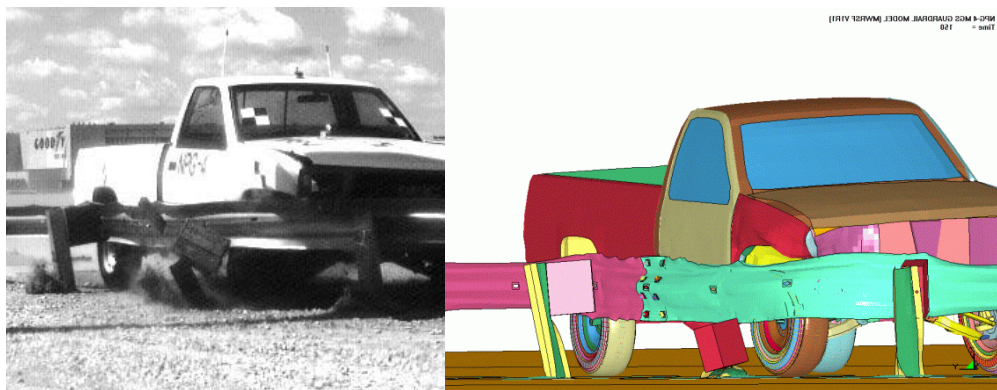


**Figure 38. Additional Graphical Comparison - Downstream Behind Rail**

Viewing the simulation at 150 ms behind the rail, just downstream of impact revealed more detail into the simulation. The first is the location of the vehicle in the frame, both being very similar. The second is the amount of deformation to the posts, again both simulations were comparable. However, the center post in the simulation was shown to be bent parallel to the ground, where this did not happen during the physical test. This was attributed to the stiff soil

response, not allowing the post to rotate through the soil before deforming. It was also interesting to note the amount of twist observed in the rightmost post. In the simulation, the post undergoes significant twisting, while this is not observed during the physical test, again attributable to the stiff soil response.

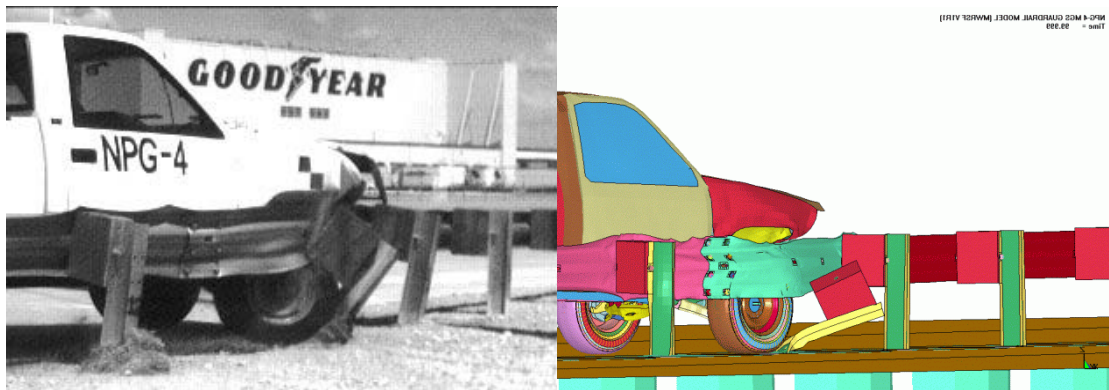


**Figure 39. Additional Graphical Comparison - Upstream Behind Rail**

Viewing the simulation at 100ms from behind the rail, just upstream of the impact also revealed more detail about differences between the simulation and physical test. This time slice showed the difference in the simulated soil behavior and the physical soil response. The behavior of the post undergoing significant displacement in both the physical test and the simulation was significantly different. This was further indication that the soil response model is critical in the proper simulation of a redirective impact. It was also important to note the similarity in the shape of the rail around the front truck for the simulation and the physical test.

As before, wheel snag was used to calibrate and evaluate the model. Wheel snag that occurred during the simulation is shown in Figure 40. The timing of the wheel snag corresponds well with what was previously reported (96 ms and 190 ms).

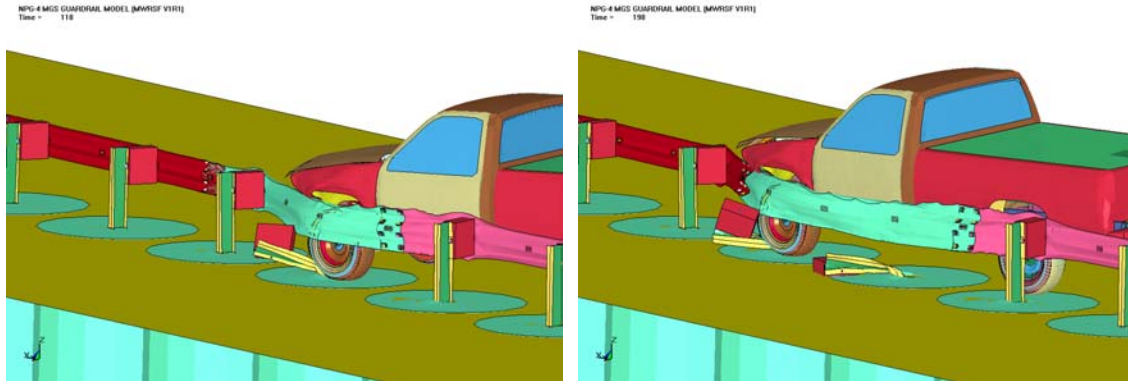


**Figure 40. Wheel Snag Observed during NPG-4 LS-DYNA Simulation**

### **8.3. Flared Impact Simulation**

With a working model for the Midwest Guardrail System, the simulation was then directed towards the evaluation of a 13:1 flared impact. As before, the flared impact was completed by increasing the impact angle in the baseline model. The simulation is shown in Figure 41.

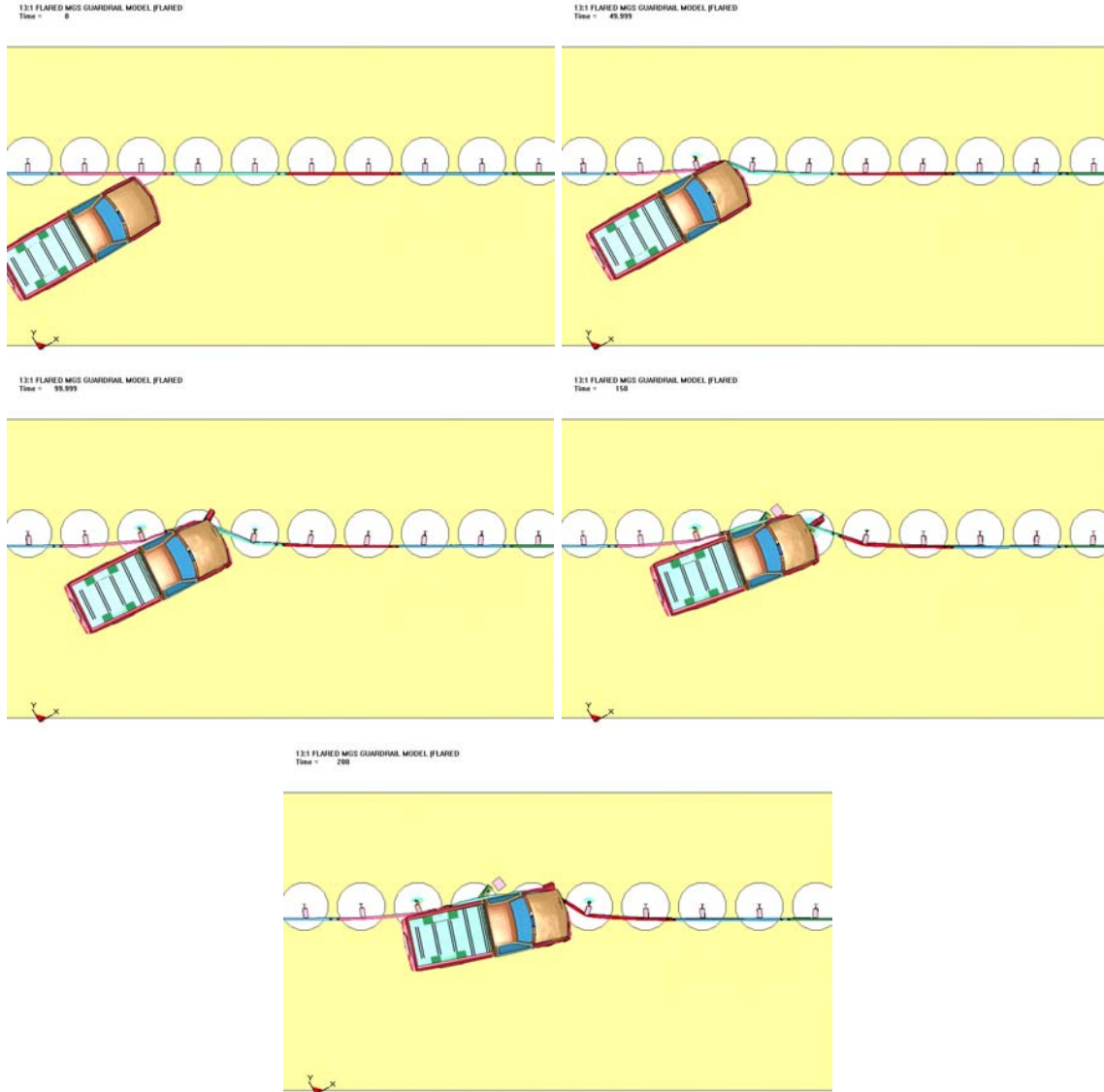


**Figure 41. Sequential Figures from 13:1 Flared Impact Simulation using LS-DYNA**

Although this simulation was still in the initial stages, there was no indication of vaulting nor the potential to pocket the vehicle. It was therefore believed that the impacting vehicle would be captured and redirected. However, it was found that severe wheel snag did occur, as shown in Figure 42, and the 13:1 flared impact is a good test case for full-scale vehicle crash testing.

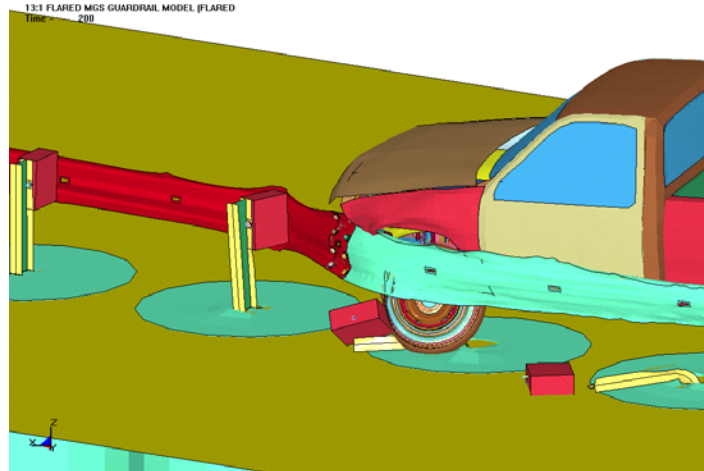


**Figure 42. Observable Wheel Snag during 13:1 Flared Simulation using LS-DYNA**

### **8.3.1. Rail Tension Forces**

Rail tension forces are an indication of potential rail rupture. Thus, cross-sections were defined in the LS-DYNA model at two locations: (1) just upstream of impact between post nos. 11 and 12 and (2) just downstream of the vehicle position near parallel time between post nos. 15 and 16. Simulations were performed for the baseline model, 13:1 flare model, and 10:1 flare model. Cross-section forces were then plotted for the two locations, as shown in Figure 43 and Figure 44.

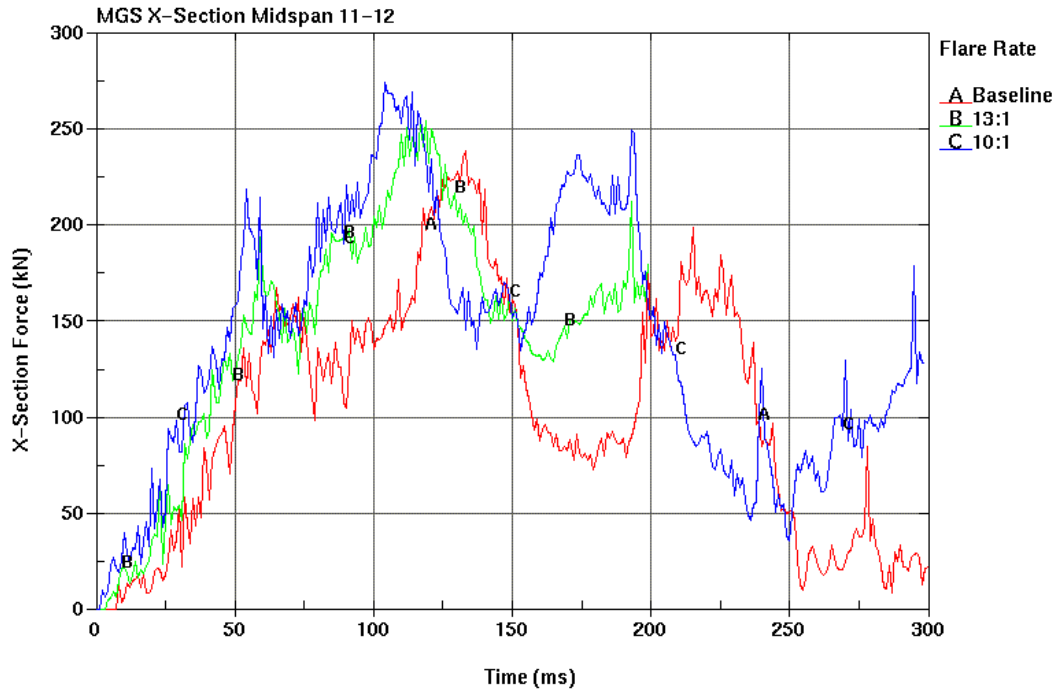


**Figure 43. Rail Tension Forces Upstream of Impact**

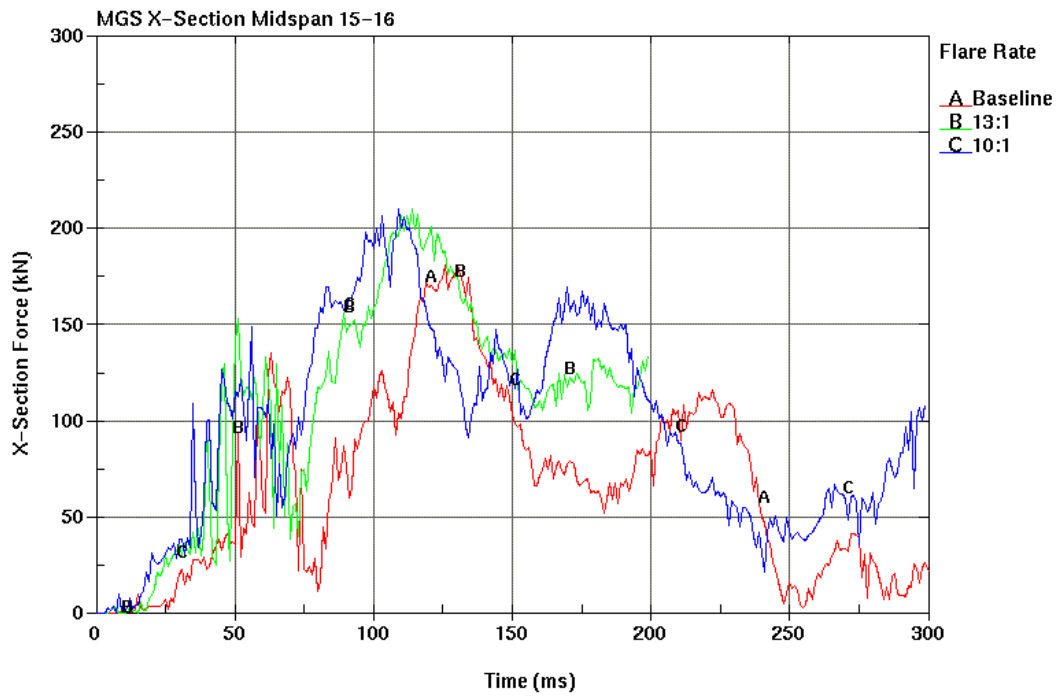


**Figure 44. Rail Tension Forces Downstream of Impact**

It was observed that as the impact angle increased, so did the rail tension forces. The maximum force observed was in the 10:1 flared impact simulation with a value of 275 kN (61.8 kips). As expected, and as seen in the physical testing, the forces in the upstream region were generally greater than in the downstream region.

An interesting feature of Figure 43 is the appearance of two distinct peaks for each of the simulation runs. The peaks are increasing as the load is being carried by the post as it rotates and plastically deforms. As the post detaches from the guardrail, the force level can be observed to drop off in the rail until the load is captured by the next post as it rotates and subsequently fails.

#### **8.4. Conclusion for LS-DYNA Simulations**

It was found that the current model does not allow for the extent of barrier penetration that was observed during the physical testing. Due to limited time and funding, and this simulation work being outside the scope of the original project, better calibration could not be completed. However, the guardrail did show the potential to capture and redirect an impacting vehicle at a 13:1 flare rate, with the potential to evaluate severe wheel snag. Thus, resulting from this simulation is a further indication that a 13:1 flare rate will serve as a good test case for evaluating the capacity of the W-beam guardrail.

## 9. SUMMARY AND FUTURE WORK

### 9.1. Summary

Past studies on strong-post, W-beam guardrail systems suggest that flaring a guardrail is generally beneficial and optimizes the guardrail installation in terms of: (1) reducing construction and maintenance costs, (2) reducing the number of impacts, and (3) reducing total accident costs, measured in terms of injuries and fatalities. Current standards suggest the use of a maximum flare rate equal to 15:1 on 110 km/h roadways. However, this flare rate has never been subjected to a capacity analysis using a 2000P crash test vehicle impacting at 100 km/h and 25 degrees. It is therefore necessary to evaluate the flare rates for: (1) determining their capacity to redirect an errant vehicle and (2) determining the potential for increased flare rates.

The analysis began by developing BARRIER VII baseline models for both a standard strong-post, W-beam system (modified G4(1S)) and the Midwest Guardrail System (MGS). The baseline models were calibrated and validated based on the relevant crash testing, including comparison of the general barrier profiles, maximum dynamic deflections, parallel times, and exit conditions.

Flared impact simulations were completed by increasing the impact angle in the baseline models. During the simulation process, it was deemed necessary to evaluate two possible scenarios based on recent testing results on the MGS system: (1) using baseline post properties and (2) using early release post properties resulting from an increased impact severity. The early release post properties were deemed to be the worst case scenario.

A critical flare rate of 13:1 was determined for both the MGS and modified G4(1) system. Barrier deflection and wheel-to-post overlap (i.e., wheel snag) were the primary criteria

used to determine the critical flare rates. For both systems, the critical impact point was determined to be 9.375 in. (238 mm) upstream of post no. 12.

3-D non-linear finite element analysis was started using LS-DYNA. A post-in-soil model was examined and improved, resulting in an initial satisfactory performance. In addition, bolted splice connections were improved, resulting in the proper pre-tension in the bolts. The component models were implemented during the development of a baseline model for the Midwest Guardrail System. A successful redirection was achieved; however, it was discovered that the soil response was too stiff. As before, flared impacts were simulated by increasing the impact angle in the baseline simulation. The simulation showed a potential for redirection at the 13:1 flare rate. However, the pickup truck was observed to snag on a post, causing an error termination when simulating the 13:1 flare rate; indicating that the 13:1 flare rate was again a critical flare rate.

## **9.2. Future Work**

Full-scale vehicle crash testing is planned based on this initial work through the Midwest States' Regional Pooled Fund Program, Project No. RPFPP-05-13. Upon completion of the full-scale crash testing, improved evaluation criteria can be developed, if necessary. Further simulation can then be completed to develop new flare rates for lower speed highways that minimize total costs while improving safety.

Further BARRIER VII analysis will be needed to address the following issues: (1) impacts just downstream of the terminals to evaluate terminal capacity at increased impact severities and (2) impacts upstream, but close to, the transition from the flared section of guardrail to tangent rail.

Improvements in LS-DYNA modeling would include better component models, with specific attention to post-soil interaction and rail-to-blockout release as the two components most in need of improvement.

## 9. REFERENCES

1. Case, H.W., Hulbert, S.F., Mount, G.E., and Brenner, R., *Effect of a Roadside Structure on Lateral Placement of Motor Vehicles*, Highway Research Board Proceedings, 1953, Vol. 32, pp 364-370.
2. Taragin, A., *Driver Behavior as Affected by Objects on Highway Shoulders*, Highway Research Board Proceedings, 1955, Vol. 34, pp 453-472.
3. Michaels, R.M., and Cozan, L.W., *Perceptual and Field Factors Causing Lateral Displacement*, Highway Research Record, 1963, No. 25, pp 1-13.
4. *Highway Guardrail-Determination of Need and Geometric Requirements with Particular Reference to Beam-Type Guardrail*, Highway Research Board Special Report 81, Highway Research Board, Washington, D.C., 1964, pp 18-22.
5. Hatton, J.H., *A Roadside Design Procedure*, Draft Report, Federal Highway Administration, Washington, D.C., January 1974, 32 p.
6. *Guide for Selecting, Locating, and Designing Traffic Barriers*, American Association of State Highway and Transportation Officials, 1997, pp 60-66.
7. Sicking, D.L., *Guidelines for Positive Barrier Use in Construction Zones*, Transportation Research Record, Issue 1035, 1985, pp 85-93.
8. Sicking, D.L., Bligh, R.P., Ross, H.E., Jr., *Optimization of Strong Post W-Beam Guardrail*, Texas Transportation Institute Research Study No. 2-8-88-1147, November 1988, pp 40-44.
9. Powell, G.H., *BARRIER VII: A Computer Program For Evaluation of Automobile Barrier Systems*, Prepared for: Federal Highway Administration, Report No. FHWA RD-73-51, April 1973.
10. *Roadside Design Guide*, Chapter 5 Roadside Barrier, Section 5.6.3 Flare Rate, American Association of State Highway and Transportation Officials (AASHTO), Washington D.C., 2002.
11. Ross, H.E., Sicking, D.L., Zimmer, R.A., and Michie, J.D., *Recommended Procedures for the Safety Performance Evaluation of Highway Features*, National Cooperative Research Program (NCHRP) Report No. 350, Transportation Research Board, Washington, D.C., 1993.
12. Mak, K.K., Bligh, R.P., Menges, W.L., *Crash Testing and Evaluation of Existing Guardrail Systems*, Research Study No. RF 471470, Sponsored by the Federal Highway Administration, Performed by Texas Transportation Institute, Texas A&M University, College Station, Texas, December 1995.

13. Buth, C.E., Menges, W.L., Ivey, D.L., and Williams, W.F., "*W-Beam Guardrail*," TRB Paper 990871, 78<sup>th</sup> Annual Meeting, Transportation Research Board, Washington, D.C., January 1999.
14. Bullard, D.L., Jr., Menges, W.L., and Alberson, D.C., *NCHRP Report 350 Compliance Test 3-11 of the Modified G4(1S) Guardrail with Timber Blockouts*, Report No. FHWA-RD-96-175, Sponsored by the Office of Safety and Traffic Operations R&D, Federal Highway Administration, Performed by Texas Transportation Institute, Texas A&M University, College Station, Texas, September 1996.
15. Sicking, D.L., Rohde, J.R., and Reid, J.D., *Development of a New Guardrail System*, Interim Report to Buffalo Specialty Products, Midwest Roadside Safety Facility, University of Nebraska-Lincoln, Lincoln, Nebraska, April 1997.
16. Polivka, K.A., Sicking, D.L., Rohde, J.R., Faller, R.K., Holloway, J.C., *Crash Testing of Michigan's Type B (W-Beam) Guardrail System – Phase II*, MwRSF Research Report No. TRP-03-104-00, Submitted to the Michigan Department of Transportation, Midwest Roadside Safety Facility, University of Nebraska-Lincoln, Lincoln, Nebraska, December 13, 2000.
17. Polivka, K.A., Faller, R.K., Sicking, D.L., Reid, J.D., Rohde, J.R., Holloway, J.C., Bielenberg, R.W., and Kuipers, B.D., *Development of the Midwest Guardrail System for Standard and Reduced Post Spacing and in Combination with Curbs*, MwRSF Research Report No. TRP-03-139-03, Draft Report to the Midwest States Regional Pooled Fund Program, Midwest Roadside Safety Facility, University of Nebraska-Lincoln, Lincoln, Nebraska, February 17, 2004.
18. Sicking, D.L., Reid, J.D., and Rohde, J.R., "Development of the Midwest Guardrail System," *Transportation Research Record 1797*, TRB, National Research Council, Washington, D.C., November 2002, pp. 44-52.
19. Faller, R.K., Polivka, K.A., Kuipers, B.D., Bielenberg, R.W., Reid, J.D., and Rohde, J.R., *Midwest Guardrail System for Standard and Special Applications*, 2004 Catalog of Practical Papers, Paper No. 04-4778, Safety, Division A – Technical Activities, Group 2 Standing Committees and Task Forces, Subject Area – Design, Transportation Research Board, Washington D.C., 2004 accepted.
20. Kuipers, B.D. and Reid, J.D., *Testing of W152x23.8 (W6x16) Steel Posts – Soil Embedment Depth Study for the Midwest Guardrail System (Non-Proprietary Guardrail System)*, MwRSF Research Report No. TRP-03-136-03, Final Report to the Midwest States' Regional Pooled Fund Program, Midwest Roadside Safety Facility, University of Nebraska-Lincoln, Lincoln, Nebraska, June 12, 2003.
21. Ray, M.H., Plaxico, C.A., and Engstrand, K.E., *Performance of W-beam Splices*, Transportation Research Record 1743, Paper No. 01-2420.

22. Buth, E.C., Zimmer, R.A., and Menges, W.L., *Testing and Evaluation of a Modified G4(1S) Guardrail with W150 x 17.0 Steel Blockouts*, Texas Transportation Institute, Texas A&M University, College Station, TX, 1996.
23. Reid, J.D., Sicking, D.L., and Bligh, R., *Critical Impact Point for Longitudinal Barriers*, Journal of Transportation Engineering, Vol. 124, No. 1, January/February 1998.
24. Tuan, C.Y., Post, E.R., Atallah, S., and Brewer, J.O., *Development of Kansas Guardrail to Bridgerail Transition Designs Using BARRIER VII*, Transportation Research Record 1743, pp. 145-154.
25. Bligh, R.P., Sicking, D.L., and Ross, H.E., *Development of a Strong Beam Guardrail/Bridge Rail Transition*, Presented at 67<sup>th</sup> Annual Meeting of the Transportation Research Board, Washington D.C., January 1988.
26. Faller, R.K., Ph.D., P.E., Personal Conversation at Midwest Roadside Safety Facility (MwRSF), May 2003.
27. Faller, R.K., Ph.D., P.E., and Polivka, K.A., M.S.M.E., E.I.T., Personal Conversation at Midwest Roadside Safety Facility (MwRSF), May 2004.
28. National Cooperative Highway Research Program Project 22-14(02), *Improved Procedures for Safety-Performance Evaluation of Roadside Features*, Principal Investigator: Dr. Dean L. Sicking, Effective Date: August 7, 2002, Completion Date: February 6, 2005. The objectives of this research are to prepare improved procedures for the safety-performance evaluation of roadside features and identify research needs for future improvements to the procedures.
29. Coon, B.A., *Development of Crash Reconstruction Procedures for Roadside Safety Appurtenances*, A Dissertation, University of Nebraska-Lincoln , August 2003.
30. Hallquist, J.O., *LS-DYNA Keyword User's Manual*, Version 970, Livermore Software Technology Corporation, Livermore, CA, April, 2003.

## APPENDIX A – MGS Calibration/Validation BARRIER VII Input Deck

```

Flare Rate Study-MGS Baseline Model mgs-bl875-calval-rcf.b7
173 71 28 1 201 73 2 0
0.0001 0.0001 2.000 2000 0 1.0 1
4 20 20 20 20 500 2
1 0.0 0.0
3 75.00 0.0
5 150.00 0.0
9 225.00 0.0
12 281.25 0.0
13 290.625 0.0
14 295.3125 0.0
15 300.00 0.0
16 304.6875 0.0
17 309.375 0.0
18 318.75 0.0
21 375.00 0.0
25 450.00 0.0
29 525.00 0.0
32 581.25 0.0
33 590.625 0.0
34 595.3125 0.0
35 600.00 0.0
36 604.6875 0.0
37 609.375 0.0
38 618.75 0.0
44 675.00 0.0
52 750.00 0.0
60 825.00 0.0
66 881.25 0.0
67 890.625 0.0
68 895.3125 0.0
69 900.00 0.0
70 904.6875 0.0
71 909.375 0.0
72 918.75 0.0
78 975.00 0.0
84 1031.25 0.0
85 1040.625 0.0
86 1045.3125 0.0
87 1050.00 0.0
88 1054.6875 0.0
89 1059.375 0.0
90 1068.75 0.0
96 1125.00 0.0
102 1181.25 0.0
103 1190.625 0.0
104 1195.3125 0.0
105 1200.00 0.0
106 1204.6875 0.0
107 1209.375 0.0
108 1218.75 0.0
114 1275.00 0.0
122 1350.00 0.0
130 1425.00 0.0
136 1481.25 0.0
137 1490.625 0.0
138 1495.3125 0.0
139 1500.00 0.0
140 1504.6875 0.0
141 1509.375 0.0
142 1518.75 0.0
145 1575.00 0.0
149 1650.00 0.0
153 1725.00 0.0
156 1781.25 0.0
157 1790.625 0.0
158 1795.3125 0.0
159 1800.00 0.0

```



14	14	15			104	0.0	0.0	0.0		
15	15	16			104	0.0	0.0	0.0		
16	16	17			104	0.0	0.0	0.0		
17	17	18			103	0.0	0.0	0.0		
18	18	19	31	1	102	0.0	0.0	0.0		
32	32	33			103	0.0	0.0	0.0		
33	33	34			104	0.0	0.0	0.0		
34	34	35			104	0.0	0.0	0.0		
35	35	36			104	0.0	0.0	0.0		
36	36	37			104	0.0	0.0	0.0		
37	37	38	66	1	103	0.0	0.0	0.0		
67	67	68			104	0.0	0.0	0.0		
68	68	69			104	0.0	0.0	0.0		
69	69	70			104	0.0	0.0	0.0		
70	70	71			104	0.0	0.0	0.0		
71	71	72	84	1	103	0.0	0.0	0.0		
85	85	86			104	0.0	0.0	0.0		
86	86	87			104	0.0	0.0	0.0		
87	87	88			104	0.0	0.0	0.0		
88	88	89			104	0.0	0.0	0.0		
89	89	90	102	1	103	0.0	0.0	0.0		
103	103	104			104	0.0	0.0	0.0		
104	104	105			104	0.0	0.0	0.0		
105	105	106			104	0.0	0.0	0.0		
106	106	107			104	0.0	0.0	0.0		
107	107	108	136	1	103	0.0	0.0	0.0		
137	137	138			104	0.0	0.0	0.0		
138	138	139			104	0.0	0.0	0.0		
139	139	140			104	0.0	0.0	0.0		
140	140	141			104	0.0	0.0	0.0		
141	141	142			103	0.0	0.0	0.0		
142	142	143	155	1	102	0.0	0.0	0.0		
156	156	157			103	0.0	0.0	0.0		
157	157	158			104	0.0	0.0	0.0		
158	158	159			104	0.0	0.0	0.0		
159	159	160			104	0.0	0.0	0.0		
160	160	161			104	0.0	0.0	0.0		
161	161	162			103	0.0	0.0	0.0		
162	162	163	168	1	102	0.0	0.0	0.0		
169	169	170	172	1	101	0.0	0.0	0.0		
173	1				301	0.0	0.0	0.0	0.0	0.0
174	3				302	0.0	0.0	0.0	0.0	0.0
175	5				303	0.0	0.0	0.0	0.0	0.0
176	9				303	0.0	0.0	0.0	0.0	0.0
177	15				303	0.0	0.0	0.0	0.0	0.0
178	21				303	0.0	0.0	0.0	0.0	0.0
179	25				303	0.0	0.0	0.0	0.0	0.0
180	29				303	0.0	0.0	0.0	0.0	0.0
181	35				303	0.0	0.0	0.0	0.0	0.0
182	44				303	0.0	0.0	0.0	0.0	0.0
183	52				303	0.0	0.0	0.0	0.0	0.0
184	60				303	0.0	0.0	0.0	0.0	0.0
185	69				303	0.0	0.0	0.0	0.0	0.0
186	78				303	0.0	0.0	0.0	0.0	0.0
187	87				303	0.0	0.0	0.0	0.0	0.0
188	96				303	0.0	0.0	0.0	0.0	0.0
189	105				303	0.0	0.0	0.0	0.0	0.0
190	114				303	0.0	0.0	0.0	0.0	0.0
191	122				303	0.0	0.0	0.0	0.0	0.0
192	130				303	0.0	0.0	0.0	0.0	0.0
193	139				303	0.0	0.0	0.0	0.0	0.0
194	145				303	0.0	0.0	0.0	0.0	0.0
195	149				303	0.0	0.0	0.0	0.0	0.0
196	153				303	0.0	0.0	0.0	0.0	0.0
197	159				303	0.0	0.0	0.0	0.0	0.0
198	165				303	0.0	0.0	0.0	0.0	0.0
199	169				303	0.0	0.0	0.0	0.0	0.0
200	171				302	0.0	0.0	0.0	0.0	0.0
201	173				301	0.0	0.0	0.0	0.0	0.0
4400.0	47400.0	20	6	4	0	1				
1	0.055	0.12	6.00	17.0						

2	0.057	0.15	7.00	18.0				
3	0.062	0.18	10.00	12.0				
4	0.110	0.35	12.00	6.0				
5	0.35	0.45	6.00	5.0				
6	1.45	1.50	15.00	1.0				
1	100.75	15.875	1	12.0	1	1	0	0
2	100.75	27.875	1	12.0	1	1	0	0
3	100.75	39.875	2	12.0	1	1	0	0
4	88.75	39.875	2	12.0	1	1	0	0
5	76.75	39.875	2	12.0	1	1	0	0
6	64.75	39.875	2	12.0	1	1	0	0
7	52.75	39.875	2	12.0	1	1	0	0
8	40.75	39.875	2	12.0	1	1	0	0
9	28.75	39.875	2	12.0	1	1	0	0
10	16.75	39.875	2	12.0	1	1	0	0
11	-13.25	39.875	3	12.0	1	1	0	0
12	-33.25	39.875	3	12.0	1	1	0	0
13	-53.25	39.875	3	12.0	1	1	0	0
14	-73.25	39.875	3	12.0	1	1	0	0
15	-93.25	39.875	3	12.0	1	1	0	0
16	-113.25	39.875	4	12.0	1	1	0	0
17	-113.25	-39.875	4	12.0	0	0	0	0
18	100.75	-39.875	1	12.0	0	0	0	0
19	69.25	37.75	5	1.0	1	1	0	0
20	-62.75	37.75	6	1.0	1	1	0	0
1	69.25	32.75	0.0	608.				
2	69.25	-32.75	0.0	608.				
3	-62.75	32.75	0.0	492.				
4	-62.75	-32.75	0.0	492.				
1	0.00	0.00						
3	822.00	0.0	25.6	60.98	0.0	0.0	1.0	

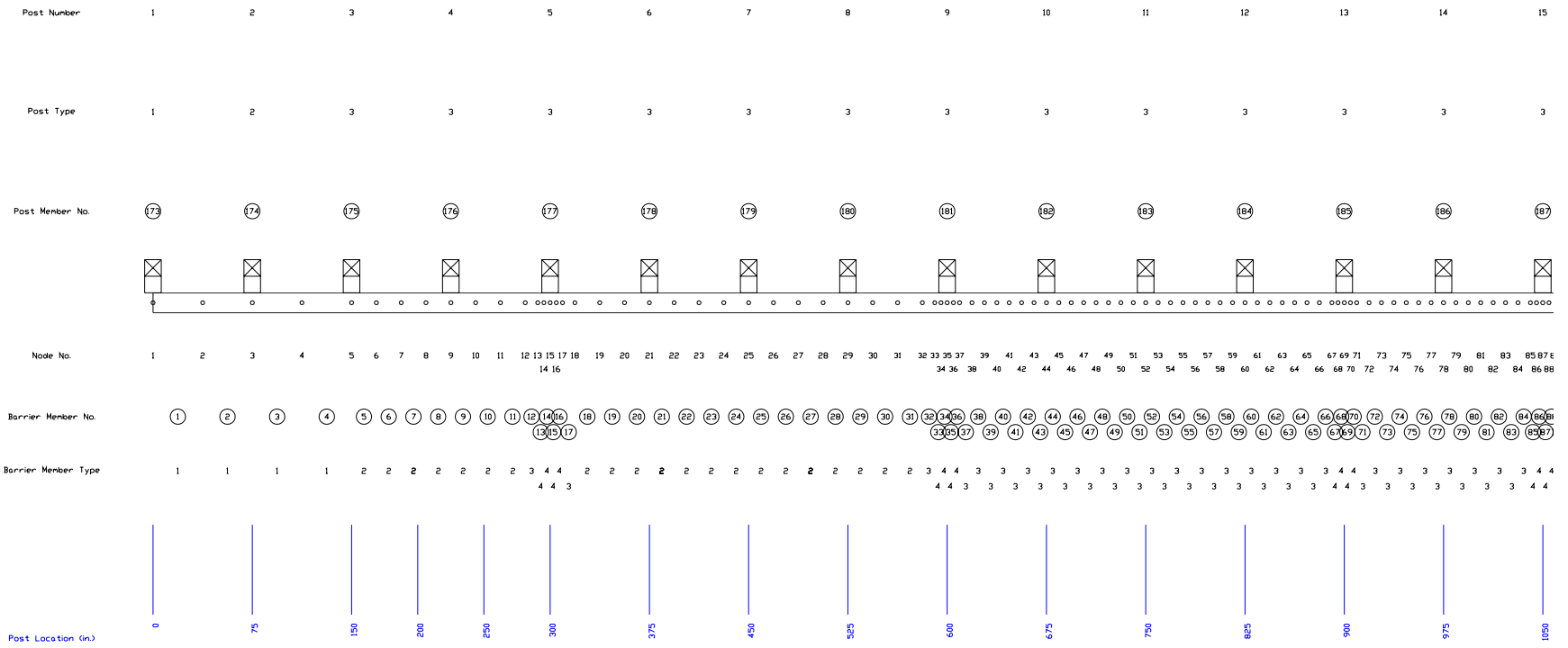


**Figure 45. Midwest Guardrail System BARRIER VII Model Details**

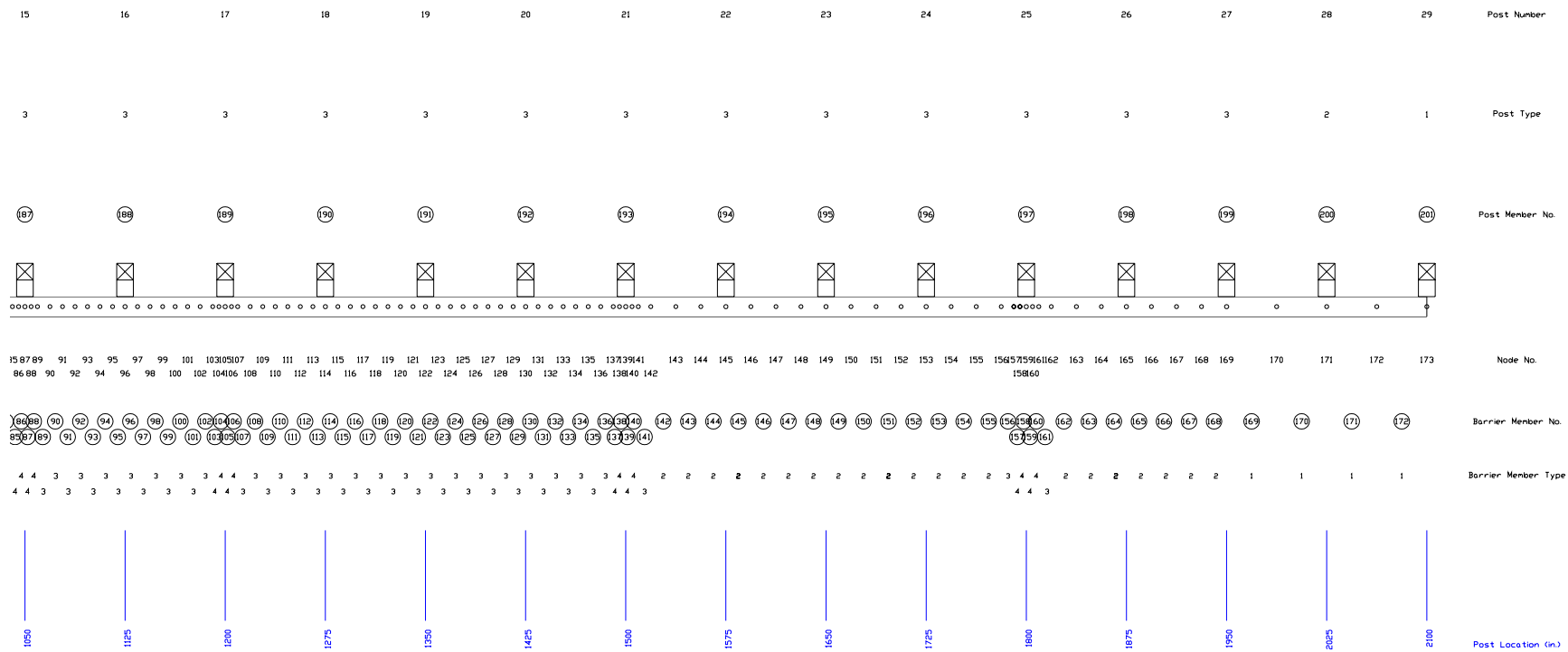


Figure 45 (continued). Midwest Guardrail System BARRIER VII Model Details

## APPENDIX B– G4(1S) Calibration/Validation BARRIER VII Input Deck

Flare Rate Study-TTI Calibration Model TTI-cal-val.b7 (calibrate to TTI test 405421-1)

191	70	51	1	220	73	2	0		
	0.0001		0.0001		1.000	3000	0	1.0	1
2	10	10	10	10	10	1			
1		0.000		0.0					
3		75.000		0.0					
4		112.500		0.0					
5		140.625		0.0					
7		150.000		0.0					
9		159.375		0.0					
10		175.000		0.0					
11		200.000		0.0					
13		250.000		0.0					
14		275.000		0.0					
15		290.625		0.0					
17		300.000		0.0					
19		309.375		0.0					
20		318.750		0.0					
23		375.000		0.0					
26		431.250		0.0					
27		440.625		0.0					
29		450.000		0.0					
31		459.375		0.0					
32		468.750		0.0					
35		525.000		0.0					
42		590.625		0.0					
44		600.000		0.0					
46		609.375		0.0					
53		675.000		0.0					
60		740.625		0.0					
62		750.000		0.0					
64		759.375		0.0					
71		825.000		0.0					
78		890.625		0.0					
80		900.000		0.0					
82		909.375		0.0					
89		975.000		0.0					
96		1040.625		0.0					
98		1050.000		0.0					
100		1059.375		0.0					
107		1125.000		0.0					
114		1190.625		0.0					
116		1200.000		0.0					
118		1209.375		0.0					
125		1275.000		0.0					
132		1340.625		0.0					
134		1350.000		0.0					
136		1359.375		0.0					
143		1425.000		0.0					
146		1481.250		0.0					
147		1490.625		0.0					
149		1500.000		0.0					
151		1509.375		0.0					
152		1518.750		0.0					
155		1575.000		0.0					
158		1631.250		0.0					
159		1640.625		0.0					
161		1650.000		0.0					
163		1659.375		0.0					
164		1668.750		0.0					
167		1725.000		0.0					
170		1781.250		0.0					
171		1790.625		0.0					
173		1800.000		0.0					
175		1809.375		0.0					
176		1818.750		0.0					
179		1875.000		0.0					



71	70	69	68	67	66	65	64	63	62											
61	60	59	58	57	56	55	54	53	52											
51	50	49	48	47	46	45	44	43	42											
41	40	39	38	37	36	35	34	33	32											
31	30	29	28	27	26	25	24	23	22											
21	20	19	18	17	16	15	14	13	12											
11	10	9	8	7	6	5	4	3	2											
1																				
100	7																			
1		2.29		1.99	37.5000	30000.0		6.92	99.5	68.5	0.05	12-Gauge	W-Beam							
2		2.29		1.99	28.1250	30000.0		6.92	99.5	68.5	0.05	12-Gauge	W-Beam							
3		2.29		1.99	4.6875	30000.0		6.92	99.5	68.5	0.05	12-Gauge	W-Beam							
4		2.29		1.99	15.6250	30000.0		6.92	99.5	68.5	0.05	12-Gauge	W-Beam							
5		2.29		1.99	25.0000	30000.0		6.92	99.5	68.5	0.05	12-Gauge	W-Beam							
6		2.29		1.99	9.3750	30000.0		6.92	99.5	68.5	0.05	12-Gauge	W-Beam							
7		2.29		1.99	18.7500	30000.0		6.92	99.5	68.5	0.05	12-Gauge	W-Beam							
300	7																			
1		21.65		0.00	6.0	6.0	100.0	675.00	675.00	0.05	Simulated	MELT								
Anchor Post 1																				
100.0		100.0		15.0	15.0															
2		21.65		0.00	3.0	3.0	100.0	150.00	225.00	0.05	Simulated	MELT								
Anchor Post 2																				
50.0		50.0		15.0	15.0															
3		21.65		0.0	3.37	3.37	65.5	214.20	227.05	0.05	6"x8",	72" Long								
CRT Timber Post																				
6.0		15.0		5.0	8.0															
4		21.65		0.0	4.59	4.59	65.5	214.20	227.05	0.05	6"x8",	72" Long								
Timber Post																				
6.0		15.0		15.0	15.0															
5		21.65		0.0	4.00	6.03	54.0	108.84	156.17	0.05	W6x8.5,	72" Long								
Steel Post																				
6.0		15.0		14.0	14.0															
6		21.65		0.00	3.0	3.0	100.0	150.00	225.00	0.05	Simulated	BCT								
Anchor Post 2																				
50.0		50.0		15.0	15.0															
7		21.65		0.00	6.0	6.0	100.0	675.00	675.00	0.05	Simulated	BCT								
Anchor Post 1																				
100.0		100.0		15.0	15.0															
1	1	2	3	1	101	0.0	0.0	0.0	0.0											
4	4	5			102	0.0	0.0	0.0	0.0											
5	5	6	8	1	103	0.0	0.0	0.0	0.0											
9	9	10			104	0.0	0.0	0.0	0.0											
10	10	11	13	1	105	0.0	0.0	0.0	0.0											
14	14	15			104	0.0	0.0	0.0	0.0											
15	15	16	18	1	103	0.0	0.0	0.0	0.0											
19	19	20			106	0.0	0.0	0.0	0.0											
20	20	21	25	1	107	0.0	0.0	0.0	0.0											
26	26	27			106	0.0	0.0	0.0	0.0											
27	27	28	30	1	103	0.0	0.0	0.0	0.0											
31	31	32			106	0.0	0.0	0.0	0.0											
32	32	33	34	1	107	0.0	0.0	0.0	0.0											
35	35	36	41	1	106	0.0	0.0	0.0	0.0											
42	42	43	45	1	103	0.0	0.0	0.0	0.0											
46	46	47	59	1	106	0.0	0.0	0.0	0.0											
60	60	61	63	1	103	0.0	0.0	0.0	0.0											
64	64	65	77	1	106	0.0	0.0	0.0	0.0											
78	78	79	81	1	103	0.0	0.0	0.0	0.0											
82	82	83	95	1	106	0.0	0.0	0.0	0.0											
96	96	97	99	1	103	0.0	0.0	0.0	0.0											
100	100	101	113	1	106	0.0	0.0	0.0	0.0											
114	114	115	117	1	103	0.0	0.0	0.0	0.0											
118	118	119	131	1	106	0.0	0.0	0.0	0.0											
132	132	133	135	1	103	0.0	0.0	0.0	0.0											
136	136	137	142	1	106	0.0	0.0	0.0	0.0											
143	143	144	145	1	107	0.0	0.0	0.0	0.0											
146	146	147			106	0.0	0.0	0.0	0.0											
147	147	148	150	1	103	0.0	0.0	0.0	0.0											
151	151	152			106	0.0	0.0	0.0	0.0											
152	152	153	157	1	107	0.0	0.0	0.0	0.0											
158	158	159			106	0.0	0.0	0.0	0.0											
159	159	160	162	1	103	0.0	0.0	0.0	0.0											

163	163	164			106	0.0	0.0	0.0		
164	164	165	169	1	107	0.0	0.0	0.0		
170	170	171			106	0.0	0.0	0.0		
171	171	172	174	1	103	0.0	0.0	0.0		
175	175	176			106	0.0	0.0	0.0		
176	176	177	181	1	107	0.0	0.0	0.0		
182	182	183			106	0.0	0.0	0.0		
183	183	184	186	1	103	0.0	0.0	0.0		
187	187	188			102	0.0	0.0	0.0		
188	188	189	190	1	101	0.0	0.0	0.0		
191	1				301	0.0	0.0	0.0	0.0	0.0
192	3				302	0.0	0.0	0.0	0.0	0.0
193	7				303	0.0	0.0	0.0	0.0	0.0
194	11				303	0.0	0.0	0.0	0.0	0.0
195	13				303	0.0	0.0	0.0	0.0	0.0
196	17				303	0.0	0.0	0.0	0.0	0.0
197	23				304	0.0	0.0	0.0	0.0	0.0
198	29				305	0.0	0.0	0.0	0.0	0.0
199	35				305	0.0	0.0	0.0	0.0	0.0
200	44				305	0.0	0.0	0.0	0.0	0.0
201	53				305	0.0	0.0	0.0	0.0	0.0
202	62				305	0.0	0.0	0.0	0.0	0.0
203	71				305	0.0	0.0	0.0	0.0	0.0
204	80				305	0.0	0.0	0.0	0.0	0.0
205	89				305	0.0	0.0	0.0	0.0	0.0
206	98				305	0.0	0.0	0.0	0.0	0.0
207	107				305	0.0	0.0	0.0	0.0	0.0
208	116				305	0.0	0.0	0.0	0.0	0.0
209	125				305	0.0	0.0	0.0	0.0	0.0
210	134				305	0.0	0.0	0.0	0.0	0.0
211	143				305	0.0	0.0	0.0	0.0	0.0
212	149				305	0.0	0.0	0.0	0.0	0.0
213	155				305	0.0	0.0	0.0	0.0	0.0
214	161				305	0.0	0.0	0.0	0.0	0.0
215	167				304	0.0	0.0	0.0	0.0	0.0
216	173				304	0.0	0.0	0.0	0.0	0.0
217	179				304	0.0	0.0	0.0	0.0	0.0
218	185				304	0.0	0.0	0.0	0.0	0.0
219	189				306	0.0	0.0	0.0	0.0	0.0
220	191				307	0.0	0.0	0.0	0.0	0.0
4576.8	47400.0	20	6	4	0	1				
1	0.055	0.12	6.00	17.0						
2	0.057	0.15	7.00	18.0						
3	0.062	0.18	10.00	12.0						
4	0.110	0.35	12.00	6.0						
5	0.35	0.45	6.00	5.0						
6	1.45	1.50	15.00	1.0						
1	100.75	15.875	1	12.0	1	1	0	0		
2	100.75	27.875	1	12.0	1	1	0	0		
3	100.75	39.875	2	12.0	1	1	0	0		
4	88.75	39.875	2	12.0	1	1	0	0		
5	76.75	39.875	2	12.0	1	1	0	0		
6	64.75	39.875	2	12.0	1	1	0	0		
7	52.75	39.875	2	12.0	1	1	0	0		
8	40.75	39.875	2	12.0	1	1	0	0		
9	28.75	39.875	2	12.0	1	1	0	0		
10	16.75	39.875	2	12.0	1	1	0	0		
11	-13.25	39.875	3	12.0	1	1	0	0		
12	-33.25	39.875	3	12.0	1	1	0	0		
13	-53.25	39.875	3	12.0	1	1	0	0		
14	-73.25	39.875	3	12.0	1	1	0	0		
15	-93.25	39.875	3	12.0	1	1	0	0		
16	-113.25	39.875	4	12.0	1	1	0	0		
17	-113.25	-39.875	4	12.0	0	0	0	0		
18	100.75	-39.875	1	12.0	0	0	0	0		
19	69.25	37.75	5	1.0	1	1	0	0		
20	-62.75	37.75	6	1.0	1	1	0	0		
1	0.0	0.0								
3	734.25	0.0	25.50	63.07	0.0	0.0	1.0			





## APPENDIX C– 22-14MG-1 Calibration/Validation BARRIER VII Input Deck

Flare	Rate	Study	2214MG-1	Model	2214MG-7.b7			
173	71	28	1	201	73	2	0	
	0.0001		0.0001		1.500	2000	0	1.0 1
2	10	10	10	10	500	1		
1		0.0		0.0				
3		75.00		0.0				
5		150.00		0.0				
9		225.00		0.0				
12		281.25		0.0				
13		290.625		0.0				
14		295.3125		0.0				
15		300.00		0.0				
16		304.6875		0.0				
17		309.375		0.0				
18		318.75		0.0				
21		375.00		0.0				
25		450.00		0.0				
29		525.00		0.0				
32		581.25		0.0				
33		590.625		0.0				
34		595.3125		0.0				
35		600.00		0.0				
36		604.6875		0.0				
37		609.375		0.0				
38		618.75		0.0				
44		675.00		0.0				
52		750.00		0.0				
60		825.00		0.0				
66		881.25		0.0				
67		890.625		0.0				
68		895.3125		0.0				
69		900.00		0.0				
70		904.6875		0.0				
71		909.375		0.0				
72		918.75		0.0				
78		975.00		0.0				
84		1031.25		0.0				
85		1040.625		0.0				
86		1045.3125		0.0				
87		1050.00		0.0				
88		1054.6875		0.0				
89		1059.375		0.0				
90		1068.75		0.0				
96		1125.00		0.0				
102		1181.25		0.0				
103		1190.625		0.0				
104		1195.3125		0.0				
105		1200.00		0.0				
106		1204.6875		0.0				
107		1209.375		0.0				
108		1218.75		0.0				
114		1275.00		0.0				
122		1350.00		0.0				
130		1425.00		0.0				
136		1481.25		0.0				
137		1490.625		0.0				
138		1495.3125		0.0				
139		1500.00		0.0				
140		1504.6875		0.0				
141		1509.375		0.0				
142		1518.75		0.0				
145		1575.00		0.0				
149		1650.00		0.0				
153		1725.00		0.0				
156		1781.25		0.0				
157		1790.625		0.0				
158		1795.3125		0.0				



1	1	2	4	1	101	0.0	0.0	0.0		
5	5	6	11	1	102	0.0	0.0	0.0		
12	12	13			103	0.0	0.0	0.0		
13	13	14			104	0.0	0.0	0.0		
14	14	15			104	0.0	0.0	0.0		
15	15	16			104	0.0	0.0	0.0		
16	16	17			104	0.0	0.0	0.0		
17	17	18			103	0.0	0.0	0.0		
18	18	19	31	1	102	0.0	0.0	0.0		
32	32	33			103	0.0	0.0	0.0		
33	33	34			104	0.0	0.0	0.0		
34	34	35			104	0.0	0.0	0.0		
35	35	36			104	0.0	0.0	0.0		
36	36	37			104	0.0	0.0	0.0		
37	37	38	66	1	103	0.0	0.0	0.0		
67	67	68			104	0.0	0.0	0.0		
68	68	69			104	0.0	0.0	0.0		
69	69	70			104	0.0	0.0	0.0		
70	70	71			104	0.0	0.0	0.0		
71	71	72	84	1	103	0.0	0.0	0.0		
85	85	86			104	0.0	0.0	0.0		
86	86	87			104	0.0	0.0	0.0		
87	87	88			104	0.0	0.0	0.0		
88	88	89			104	0.0	0.0	0.0		
89	89	90	102	1	103	0.0	0.0	0.0		
103	103	104			104	0.0	0.0	0.0		
104	104	105			104	0.0	0.0	0.0		
105	105	106			104	0.0	0.0	0.0		
106	106	107			104	0.0	0.0	0.0		
107	107	108	136	1	103	0.0	0.0	0.0		
137	137	138			104	0.0	0.0	0.0		
138	138	139			104	0.0	0.0	0.0		
139	139	140			104	0.0	0.0	0.0		
140	140	141			104	0.0	0.0	0.0		
141	141	142			103	0.0	0.0	0.0		
142	142	143	155	1	102	0.0	0.0	0.0		
156	156	157			103	0.0	0.0	0.0		
157	157	158			104	0.0	0.0	0.0		
158	158	159			104	0.0	0.0	0.0		
159	159	160			104	0.0	0.0	0.0		
160	160	161			104	0.0	0.0	0.0		
161	161	162			103	0.0	0.0	0.0		
162	162	163	168	1	102	0.0	0.0	0.0		
169	169	170	172	1	101	0.0	0.0	0.0		
173	1				301	0.0	0.0	0.0	0.0	0.0
174	3				302	0.0	0.0	0.0	0.0	0.0
175	5				304	0.0	0.0	0.0	0.0	0.0
176	9				304	0.0	0.0	0.0	0.0	0.0
177	15				304	0.0	0.0	0.0	0.0	0.0
178	21				304	0.0	0.0	0.0	0.0	0.0
179	25				304	0.0	0.0	0.0	0.0	0.0
180	29				304	0.0	0.0	0.0	0.0	0.0
181	35				304	0.0	0.0	0.0	0.0	0.0
182	44				303	0.0	0.0	0.0	0.0	0.0
183	52				303	0.0	0.0	0.0	0.0	0.0
184	60				303	0.0	0.0	0.0	0.0	0.0
185	69				303	0.0	0.0	0.0	0.0	0.0
186	78				303	0.0	0.0	0.0	0.0	0.0
187	87				303	0.0	0.0	0.0	0.0	0.0
188	96				303	0.0	0.0	0.0	0.0	0.0
189	105				303	0.0	0.0	0.0	0.0	0.0
190	114				303	0.0	0.0	0.0	0.0	0.0
191	122				303	0.0	0.0	0.0	0.0	0.0
192	130				303	0.0	0.0	0.0	0.0	0.0
193	139				303	0.0	0.0	0.0	0.0	0.0
194	145				303	0.0	0.0	0.0	0.0	0.0
195	149				303	0.0	0.0	0.0	0.0	0.0
196	153				303	0.0	0.0	0.0	0.0	0.0
197	159				303	0.0	0.0	0.0	0.0	0.0
198	165				303	0.0	0.0	0.0	0.0	0.0
199	169				303	0.0	0.0	0.0	0.0	0.0

200	171		302	0.0	0.0	0.0	0.0	0.0
201	173		301	0.0	0.0	0.0	0.0	0.0
	5000.0	47400.0	20	6	4	0	1	
1	0.055	0.12		6.00			17.0	
2	0.057	0.15		7.00			18.0	
3	0.062	0.18		10.00			12.0	
4	0.110	0.35		12.00			6.0	
5	0.35	0.45		6.00			5.0	
6	1.45	1.50		15.00			1.0	
1	100.75	15.875	1	12.0	1	1	0	0
2	100.75	27.875	1	12.0	1	1	0	0
3	100.75	39.875	2	12.0	1	1	0	0
4	88.75	39.875	2	12.0	1	1	0	0
5	76.75	39.875	2	12.0	1	1	0	0
6	64.75	39.875	2	12.0	1	1	0	0
7	52.75	39.875	2	12.0	1	1	0	0
8	40.75	39.875	2	12.0	1	1	0	0
9	28.75	39.875	2	12.0	1	1	0	0
10	16.75	39.875	2	12.0	1	1	0	0
11	-13.25	39.875	3	12.0	1	1	0	0
12	-33.25	39.875	3	12.0	1	1	0	0
13	-53.25	39.875	3	12.0	1	1	0	0
14	-73.25	39.875	3	12.0	1	1	0	0
15	-93.25	39.875	3	12.0	1	1	0	0
16	-113.25	39.875	4	12.0	1	1	0	0
17	-113.25	-39.875	4	12.0	0	0	0	0
18	100.75	-39.875	1	12.0	0	0	0	0
19	69.25	37.75	5	1.0	1	1	0	0
20	-62.75	37.75	6	1.0	1	1	0	0
1	69.25	32.75		0.0			608.	
2	69.25	-32.75		0.0			608.	
3	-62.75	32.75		0.0			492.	
4	-62.75	-32.75		0.0			492.	
1	0.0	0.0						
3	822.00	0.0	26.97	62.58	0.0	0.0	1.0	